# Mixing Assessment of Non-Cohesive Mono-disperse and Bi-disperse Particles in a Paddle Mixer – Experiments and Discrete Element Method (DEM) Application

By

Amirsalar Yaraghi, BEng

Chemical Engineering

Ryerson University, Toronto, 2013

A thesis

presented to Ryerson University

in partial fulfillment of the requirements for the degree of

Master of Applied Science

in the program of Chemical Engineering

Toronto, Ontario, Canada, 2018

## AUTHOR'S DECLARATION FOR ELECTRONIC SUBMISSION OF A THESIS

I hereby declare that I am the sole author of this thesis. This is a true copy of the thesis, including any required final revisions, as accepted by my examiners.

I authorize Ryerson University to lend this thesis to other institutions or individuals for the purpose of scholarly research.

I further authorize Ryerson University to reproduce this thesis by photocopying or by other means, in total or in part, at the request of other institutions or individuals for the purpose of scholarly research.

I understand that my thesis may be made electronically available to the public.

# ABSTRACT

**Amirsalar Yaraghi**

**Mixing Assessment of Non-Cohesive Mono-disperse and Bi-disperse Particles in a Paddle Mixer – Experiments and Discrete Element Method (DEM) Application**

**MASc, Chemical Egineering, Ryerson University, Toronto, ON, 2018**

The objective of this study was to assess the mixing performance of a horizontal paddle blender for mono-disperse and bi-disperse particles. The assessment was performed through the application of the Discrete Element Method (DEM) simulations, experiments, and Analysis of Variance (ANOVA). EDEM 2.7 commercial software was utilized for the mono-disperse simulations while LIGGGHTS(R)-PUBLIC 3.3.1, an open source software, was used for the bi-disperse simulations. DEM models were validated with experimental data. Simulations were performed to explore the effect of impeller rotational speed, vessel fill level, particle number composition, and particle loading arrangement on mixing quality defined by the Relative Standard Deviation (RSD) index. The flow pattern and mixing mechanisms were examined through granular temperature, particle diffusivity, and Peclet number. The impeller rotational speed was the most influential parameter on the mixing performance of mono-disperse particles. The particle number composition was the dominating parameter on the mixing quality of bi-disperse particles.

# Acknowledgments

I would first like to thank my supervisors Dr. Farhad Ein-Mozaffari, and Dr. Ali Lohi of the Department of Chemical Engineering at Ryerson University for their invaluable guidance, and support throughout the course of the project.

I would also like to thank Dr. Mohammadreza Ebrahimi for his endless support, patience, and encouragement. The door to Dr. Ebrahimi's office was always open whenever I ran into a trouble spot or had a question about my research or inscription. He consistently steered me in the right direction whenever he thought I needed it.

I acknowledge the assistance of the experts, peers, staff, and technologists of the Department of Chemical engineering at Ryerson University. Without their passionate participation, input, and comments the completion of this project could not have been successfully accomplished. Financial support from the Natural Science and Engineering Research Council of Canada (NSERC) is gratefully acknowledged.

Finally, I must express my very profound gratitude to my parents, and to my brother for providing me with unfailing support and continuous encouragement throughout my years of study and through the process of researching and writing this thesis. This accomplishment would not have been possible without them. Thank you.

I dedicate my thesis to my parents Ali and Nadia and also my brother Amirali for their endless love and support.

# Table of Contents

# List of Tables

# List of Figures

# Nomenclature

| | |
|---|---|
| $A$ | Impeller rotation speed parameter (-) |
| $B$ | Vessel fill level parameter (-) |
| $C$ | Particle loading arrangement parameter (-) |
| $A^2$ | Quadratic effect for impeller rotation speed parameter (-) |
| $B^2$ | Quadratic effect for vessel fill level parameter (-) |
| $AB$ | Impeller rotation speed-vessel fill level interaction parameter (-) |
| $AC$ | Impeller rotation speed-loading arrangement interaction parameter (-) |
| $BC$ | Vessel fill level-loading arrangement interaction parameter (-) |
| $ABC$ | Impeller rotation speed-vessel fill level-loading arrangement parameter (-) |
| $a$ | Parameter coefficient for $A$ (-) |
| $b$ | Parameter coefficient for $B$ (-) |
| $a^2$ | Quadratic parameter coefficient for $A$ (-) |
| $b^2$ | Quadratic parameter coefficient for $B$ (-) |
| $ab$ | Parameter coefficient for $AB$ (-) |
| $ac$ | Parameter coefficient for $AC$ (-) |
| $bc$ | Parameter coefficient for $BC$ (-) |
| $abc$ | Parameter coefficient for $ABC$ (-) |
| $D_{fg}$ | Diffusivity coefficient in the $f$ direction due to gradient in $g$ direction $\left(\frac{m^2}{s}\right)$ |
| $e$ | Coefficient of restitution (-) |
| $F_{jh}^N$ | Normal force resulting from the contact of particle $j$ with particle $h$ ($N$) |
| $F_{jh}^T$ | Tangential force resulting from the contact of particle $j$ with particle $h$ ($N$) |
| $F_j^g$ | Gravitational force for particle $j$ ($N$) |
| $G_{eq}$ | Equivalent shear modulus |
| $G_j$ | Shear modulus of particle $j$ ($Pa$) |
| $G_h$ | Shear modulus of particle $h$ ($Pa$) |

$I_j$ Moment of inertia of particle $j$ $(kg.m^2)$

$k$ Number of the model obtained for each particle loading arrangement (-)

$K$ Total number of samples (-)

$l$ Number of levels for impeller rotation speed (-)

$M_{jh}^T$ Tangential torque resulting from the contact of particle $j$ with particle $h$ $(N.m)$

$M_{jh}^r$ Rolling friction torque resulting from the contact of particle $j$ with particle $h$ $(N.m)$

$m_{eq}$ Equivalent mass $(kg)$

$m_h$ Mass of particle $h$ $(kg)$

$m_j$ Mass of particle $j$ $(kg)$

$n_i$ Number of one type of particle in *i*th sample (-)

$N_i$ Total number of particles in *i*th sample (-)

$P$ Overall proportion of one type of particle (-)

$Pe_{fg}$ Peclet number in the $f$ direction due to gradient in $g$ direction (-)

$q$ Number of levels for vessel fill level (-)

$R_{eq}$ Equivalent radius $(m)$

$R_j$ Radius of particle $j$ $(m)$

$R_h$ Radius of particle $h$ $(m)$

$RSD$ Relative standard deviation (%)

$R$ Radius of mixer $(m)$

$t$ Time $(s)$

$T$ Granular temperature $\left(\frac{m^2}{s^2}\right)$

$\Delta t$ Time step for Diffusivity calculations $(s)$

$U'$ Localized fluctuation velocity $\left(\frac{m}{s}\right)$

$U_f$ Average particle speed in the $f$ direction $\left(\frac{m}{s}\right)$

$v_j$ Velocity of particle $j$ $\left(\frac{m}{s}\right)$

$\Delta x_f$ Particle displacement in the $f$ direction relative to particle's initial position $(m)$

$\overline{\Delta x_f}$ Mean particle displacement in the $f$ direction relative to particle's initial position ($m$)

$\Delta x_g$ Particle displacement in the $g$ direction relative to particle's initial position ($m$)

$\overline{\Delta x_g}$ Mean particle displacement in the $g$ direction relative to particle's initial position ($m$)

$Y_j$ Young's modulus of particle $j$ ($Pa$)

$Y_h$ Young's modulus of particle $h$ ($Pa$)

$Y_{eq}$ Equivalent Young's modulus ($Pa$)

*Greek letters*

$\beta$ Overall average of response variable (-)

$\delta_n$ Normal overlap ($m$)

$\delta_t$ Tangential overlap ($m$)

$\varepsilon$ Error (-)

$\epsilon_h$ Poisson ratio of particle $h$ (-)

$\epsilon_j$ Poisson ratio of particle $j$ (-)

$\mu$ Overall mean concentration of one type of particle (-)

$\mu_r$ Rolling friction coefficient (-)

$\mu_s$ Sliding friction coefficient (-)

$\sigma^2$ Variance of samples (-)

$\omega_j$ Angular Velocity of particle $j$ $\left(\frac{rad}{s}\right)$

$\omega_h$ Angular Velocity of particle $h$ $\left(\frac{rad}{s}\right)$

# Chapter 1: Introduction

Powder mixing is instrumental to a variety of industries including chemicals, food, cosmetics, mining, agriculture, plastics, and pharmaceuticals [1]. Essentially in most particle processing applications, powder mixing plays a significant role in the quality of the final product [2]. In order to put this significance into perspective, one can observe the overall annual worldwide production of granules which translates to over a trillion kilograms of granular products [1]. Most of these powder based products must attain a uniform blend in order to meet quality and performance standards. Therefore, understanding the underlying principles governing the physical mechanisms of mixing and de-mixing in solid-solid systems becomes a vital objective.

The objective of this study was to extensively investigate the mixing performance of a horizontal laboratory-scale agitated paddle blender by investigating the mixing kinetics, flow pattern and segregation mechanism of mono-disperse and bi-disperse particles. This was done by implementing experiments, ANOVA technique and DEM simulations. To the best of the author's knowledge, no such comprehensive investigation has been carried out on this type of mixing system. In order to achieve this objective, initially, the DEM simulation model was validated against a set of experimental data obtained by direct sampling method. Subsequently, the influence of key operating parameters on the mixing quality was assessed by using the validated DEM model. The parameters selected include, impeller rotational speed, vessel fill level, and the particle loading arrangement of the mixing components. The overall mixing quality was evaluated by incorporating the RSD mixing index. The flow pattern for the mono-disperse system was examined through granular temperature, particle diffusivity, and Peclet number obtained from simulation results. The flow pattern for the bi-disperse system was examined by determining the particle diffusivity, Peclet number and by qualitatively assessing the mixing performance.

In Chapter two a brief review is performed on powder mixtures, mixing mechanisms, types of powder mixers, and experimental quantitative techniques utilized for the assessment of mixture quality. In this chapter, a comprehensive literature review is presented on the mixing assessment of mono-disperse and bi-disperse particles in powder blenders using DEM. Chapter three describes the design specifications and procedure of the experimental set-up used in this study. The scope, development, and application of DEM is introduced in Chapter four. Chapter four additionally, covers the specific modelling approach and computational platforms used for both the mono-disperse and bi-disperse mixing investigations. Chapter five and six summarize the results of the mixing kinetics, flow pattern of mono-disperse and bi-disperse particles in a horizontal paddle blender by using experiments and DEM simulations. Chapter seven draws conclusions and presents recommendations for future investigations based on the results obtained from Chapters five and six.

# Chapter 2: Fundamentals of powder mixing and literature review

In order to understand the behaviour of solid-solid interactions, one must first become familiar with the distinct variety of solid mixture categories and their core properties. Perfect particle mixtures are defined as assemblies which attain perfect homogeneity in terms of their particle distribution (Figure 1-a) [3, 4, 5]. In other words, taking any sample containing large number of particles from such mixture would have the same composition throughout [6]. In such mixtures, particles alternate themselves along a lattice (Figure 1-a) [1, 5]. However, this state can never be achieved. Alternatively, a random mixture (Figure 1-b) is achievable, where the particles are randomly positioned along a lattice [2].

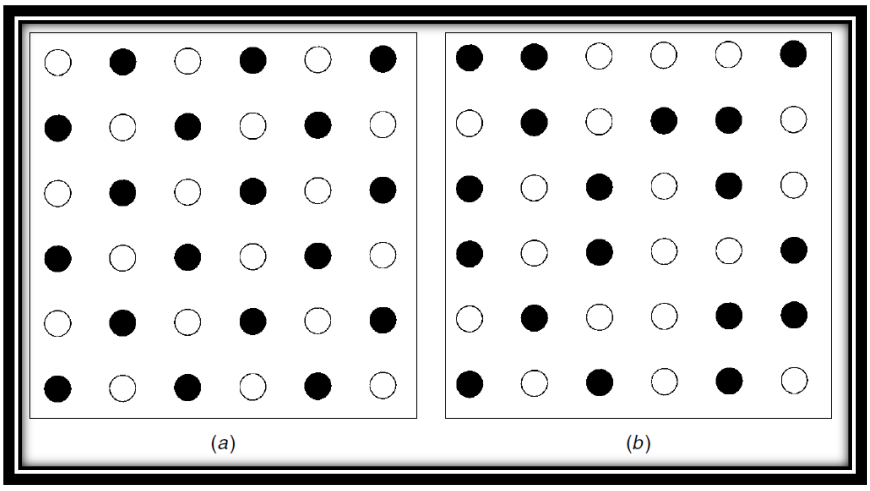


Figure 1: (a) Perfect mixture, (b) Random mixture [1].

Perhaps the most important mixture type is the segregated mixture [7]. Segregation occurs when the difference in the particle's physical and mechanical properties such as size and density causes the particles to separate into different regions within the mixture [8]. Free-flowing mixtures are more prone to segregation (Figure 2-a) as opposed to cohesive mixtures (Figure 2-b) [7]. This is

due to the fact that in cohesive systems, individual particles cannot move freely and independently with respect to the bulk mixture.

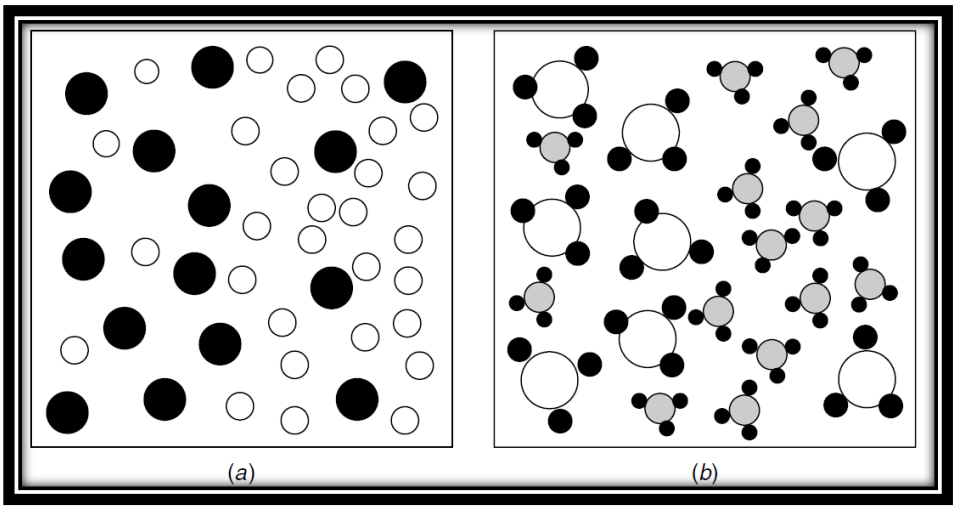


Figure 2 : (a) Segregation in free-flowing mixtures, (b) segregation in cohesive mixtures [1].

## 2.1 Mixer classification and mixing mechanisms

Powder mixers are broadly classified into batch or continuous mixers, with batch being the most commonly used system in the food and pharmaceutical industries [2-3]. Two common types of batch mixers include the tumbling and convective mixers [6, 9]. A tumbling mixer is composed of a closed vessel which rotates about its own axis [10, 11]. In this type of blender mixing is achieved predominantly by the diffusive mechanism which promotes random motion of particles down a slope surface also known as the free surface [9, 12]. Typical tumbling mixers include the Double-cone, Slanted double cone, V-type, Y-type, and Bin blender (Figure 3) [13]. A convective powder blender is composed of a stationary vessel (vertical or horizontal) and a shaft (single or twin) which has an agitating device mounted on it [14]. In this mixer category, mixing is achieved predominantly by the convective mechanism which drives the random motion of bulk mass from

one location to another. Such mixers are suitable for both cohesive and free-flowing particle applications [1, 15]. Typical convective mixers include the Paddle, Plow, Ribbon, Screw, and Sigma-blade [1]. In addition, the shear mixing mechanism typically takes place in both the convective and tumbling mixers whereby mixing is linked to internal and/or external forces applied on the system such as agitators and vessel rotation [16]. However, other varieties of batch blenders also exist which include, Gravity silo, Pneumatic, and high intensity blenders [5]. Based on the comprehensive literature review performed, the advantages and disadvantages of convective and tumbling batch mixers are summarized in Table 1.

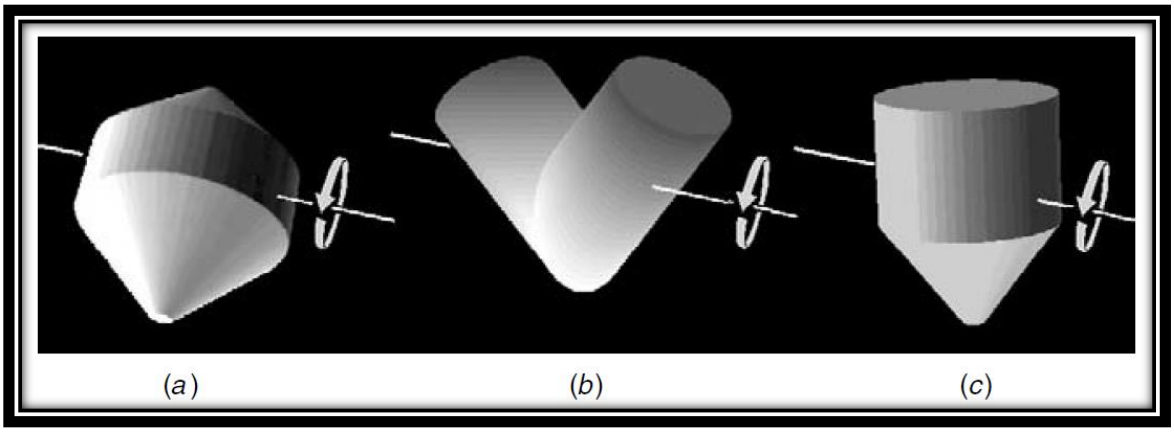


Figure 3: (a) Double-cone, (b) V-type, (c) Bin-type [1].

Table 1: Comparison between tumbling and convective batch mixers

| Mixer type | Advantages | Disadvantages |
|---|---|---|
| **Tumbling** | - Low utility and maintenance cost<br>- Detailed understanding of dynamic and performance<br>- Easy mixture analysis<br>- Simple manufacturing and optimization<br>- No attrition or shearing of particles (no impellers) | - Cannot process material prone to segregation and agglomeration<br>- Only batch<br>- Low operating capacity<br>- Mostly processes free-flowing material<br>- Axial mixing is rate limiting |
| **Convective** | - Process material prone to segregation and agglomeration<br>- Batch and continuous<br>- High operating capacity<br>- Can process free-flowing and cohesive material<br>- Axial mixing is dominant | - High utility and maintenance cost<br>- Limited understanding of dynamics and performance<br>- Difficult mixture analysis due to sampling difficulties<br>- Manufacturing and optimization<br>- Attrition and shearing is possible for sensitive material |

During a particle mixing process all mixing mechanisms mentioned earlier (convective, diffusive and shear) can occur [17]. However, one will dominate the other two depending mainly on the type of blender and the vessel and/or agitator rotational speed [6]. Reader is referred to Alexander et al. [1], Ortega-Rivas [2], Beitzel et al. [16], Van den Bergh [18], and Nakamura et al. [19] for further discussion regarding the application and mechanism of the aforementioned mixers. For this investigation the Paddle blender was selected based on the high operating capacity and broad applicability for various particle material.

### 2.1.1 Paddle and Plow mixers

This type of blender consists typically of a single or double trough vessel with an impeller, composed of either a single or twin shafts on which paddles/plows at regular intervals are mounted on [20]. In the case of the plow design (Figure 4) the particles are lifted and tossed randomly causing chaotic motion. This chaotic motion of particles can enforce shear on other particles in contact and therefore induce mixing [21]. The Paddle mixer is very similar to the plow type, however this type of blender as the name suggests consists of a paddle shaped impellers shown in Figure 5. Additionally, paddles can be arranged and positioned so as to promote lateral and axial mixing [22]. Paddle blenders are generally operated at higher rotating/tip speeds compared to the plow type [23]. However, at very high speeds segregation may take place in the mixture [24]. Table 2 presents information on the application, advantages, disadvantages, and typical operating conditions for the, Plow and Paddle powder blenders.

Table 2: Applications, advantages, disadvantages, and typical operating conditions for Plow, and Paddle mixers [1].

| Type of mixer | Particle size range | Internal configuration | Mixing time | Particle degradation | Industry application | Operational issues |
|---|---|---|---|---|---|---|
| **Plow** | ≤ 5mm free flowing | Single/double shafts, plows at even intervals | ≤ 5 min random mixing | Negligible | Food, ceramics, chemicals, plastics, pharmaceuticals | Emptying, clean up |
| **Paddle** | ≤ 5mm cohesive/free flowing | Single/double shafts, paddles | ≤ 6 min random mixing | At high speeds, attrition | Food, sewage treatment pharmaceuticals | Clean up, sampling |

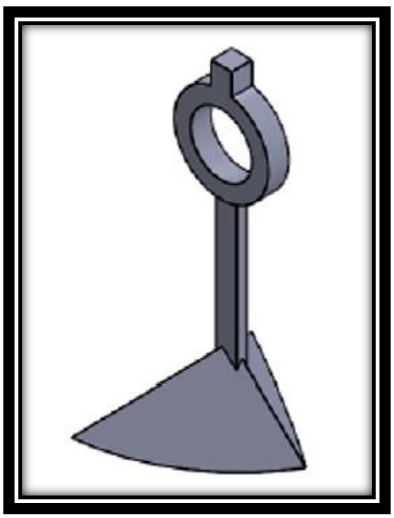

Figure 4: Plow blade [21].

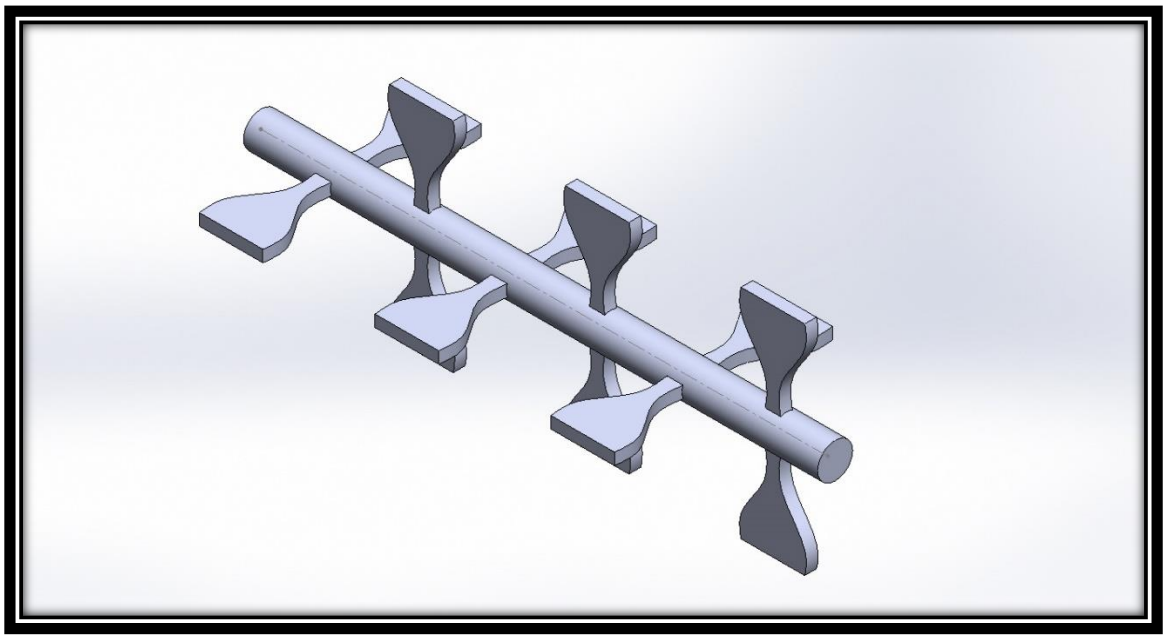

Figure 5: Paddle impeller.

The fluidizing paddle mixer or commonly known as the Forberg mixer as shown in Figure 6 is a variation of the paddle blender discussed above [23]. This type of mixer consists of paddles attached to either a single or a twin shaft in a twin trough vessel which is shown in Figure 6 [15]. The two counter rotating paddle impellers operated at high speeds scatter the particles throughout

the vessel and thus rapidly fluidizing the content [15, 23]. One of the main advantages of such blenders is that it can operate at large capacities of up to $50m^3$ [3]. On the other hand, this type of blender can induce particle breakage and attrition due to its inherently rapid impeller speeds.

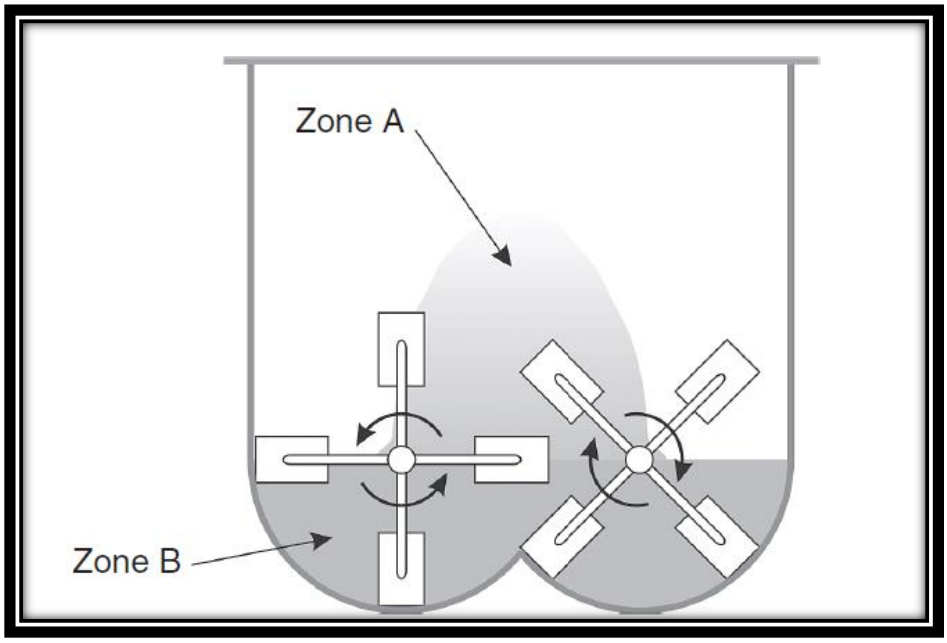


Figure 6: Forberg mixer [12].

## 2.2 Mechanism of segregation

Most mixing mechanisms in various blenders are also accompanied by some specific type of segregation as well, therefore in order to truly grasp the blending mechanisms one must also understand the dynamics involved in the segregation. As mentioned previously, segregation occurs in a blend when there is a difference in particle property of the mixture. In the following section the available segregation mechanisms for the convective blenders are presented.

Generally, there are two recognized segregation mechanisms for convective powder blenders that are referred to as momentum, and sifting/sieving [16, 25]. The main parameters, which directly

affect both segregation mechanisms, are particle size, density, and shape [3, 7]. The momentum mechanism describes the mechanism in which flowing bulk particles impact a pile formed directly below it [26]. Due to the differences in momentum between the large and small particles, the larger particles migrate towards the outer layer of the pile while the smaller particles are deposited below the point of impact [5, 27]. An example of this phenomenon can be observed when particles carried by impellers impact the previously transported pile. In addition, in this model the smaller particles tend to drop directly below the impeller while the larger particles are thrown off the impeller [25]. The sifting/sieving mechanism takes place when smaller particles sift into the gaps formed between larger particles [8]. An example of this mechanism can be observed when poly-dispersed mixing is occurring in an agitated mixer.

### 2.3 Experimental assessment of mixture quality

In the following sections, a literature review will be carried out regarding the experimental techniques utilized for the assessment of powder mixture quality. The performance of agitated powder blenders has been commonly investigated in literature both quantitatively and qualitatively through experiments [28, 29]. Numerous experimental techniques such as visual assessment, positron emission particle tracking (PEPT), radioactive particle tracking (RPT) are used by Jones and Bridgwater [30], Jones et al. [31], Laurent and Bridgwater [32], and Stewart et al. [33, 34]. Particle Image Velocimetry (PIV) by Conway et al. [35], and Remy et al. [36], and Near Infrared Spectroscopy (NIR) by Blanco et al. [37], and Berntsson et al. [38] have been previously applied in agitated blender studies. The main advantage of implementing the aforementioned types of experimental methods is the non-intrusive nature of the techniques. The mixture is not physically disturbed in order to attain information about the position and velocity of the particles. However, in PEPT and RPT a single tracer particle is incorporated within the mixer to draw specific

information however, it may not accurately represent the entirety of the mixing system. PIV and NIR on the other hand, can only provide information regarding free surface and regions close to the wall of the mixer. Mixing kinetics of particles can also be assessed through direct sampling of the mixture under investigation. In this method, samples with specific sizes are taken from various regions of the mixture as representative of the whole system. These samples are then statistically analyzed to reveal the mixing characteristics of the system [39]. The most common technique utilized for sampling is the use of a thief probe (Figure 7) [39, 40]. The main advantage of using such devices is that numerous samples of various sizes can be obtained to represent the whole mixture. However, these devices are fairly intrusive and can therefore, introduce errors in the sample composition. The samples are then statistically quantified by indices such as Lacey, Poole, and RSD, also known as the coefficient of variation (CoV). The aforementioned mixing indices are the most commonly used mixing indicators for assessing powder blends [2, 9, 39, 41-42]. These methods incorporate the lower, upper and sample variances to produce the final mixing index. However, many methods exist for quantifying mixture quality in powder blends. Reader is referred to Chapter 3 for detail definition of the RSD index.

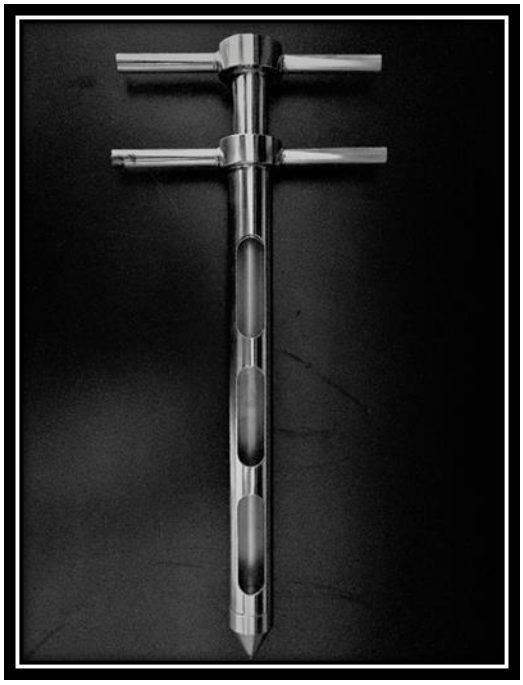

Figure 7: Three slot sampling thief.

## 2.4 Discrete Element Method (DEM)

Experimental data can only provide information regarding the general behavior of mixing and cannot fully address the underlying mixing phenomena. Numerical simulations, on the other hand, can reveal critical information about the behavior and interaction of particles which would otherwise be experimentally difficult or impossible to obtain. The accurate models, which are validated with experimental data could potentially be used to reveal critical information on both the mechanisms and kinetics of mixing within various powder blenders and perhaps initiate a platform for accurate and practical scaling procedures for the design of industrial powder mixers [43]. The granular flows are often simulated by DEM [6, 10]. DEM takes into account the discrete nature of individual particles as oppose to its continuum counterpart and is therefore able to accurately track the motion and position of each particle within a large assembly [43]. With recent

technological advancements, the computational processing capabilities have been enhanced significantly. This progress has enabled researchers to incorporate advanced modeling methods such as DEM to simulate the dynamic behavior of particles within industrially applicable devices [10, 20, 28, 43-54]. Additionally, DEM allows engineers to test and alter critical operating parameters which would experimentally be difficult to accomplish. Furthermore, the effect of the aforementioned parameters can be considered on the desired parameters such as segregation, mixing, and flow of particles in powder mixing systems.

## 2.5 Mixing assessment for mono-disperse particles using DEM

Understanding the effects of critical operating parameters such as impeller rotational speed, vessel fill level, and particle loading arrangement on the extent of mixing and particle flow behaviours is extremely critical to perform the mixing process in an optimum condition. In some research, the validated DEM models have been applied in order to investigate the influence of various operating parameters on the mixing performance. Alian et al. [21] investigated the influence of particle loading arrangement on the mixing performance of a horizontal laboratory scale plowshare mixer. They used the PEPT experimental data presented in Cleary and Sinnott [28] to validate their DEM model. The simulation results showed that the particle loading arrangement did not significantly influence the mixing quality when different particle sizes ($d_p$= 4, 7, and 11 mm) were used. Basinskas and Sakai [55] also concluded that particle loading arrangement was not a crucial parameter when assessing the mixing performance for monodisperse particles in a horizontal ribbon agitated blender. Alian et al. [21], Cleary and Sinnott [28], Basinskas and Sakai [55], Golshan et al. [56], and Sakai et al. [57] investigated the influence of various impeller rotational speeds on the mixing of monodisperse systems. All of the studies above concluded that an increase in impeller rotational speed resulted in enhancing the mixing performance. The influence of vessel

fill level on the mixing quality has also been analyzed in literature. Sakai et al. [57] found an optimum vessel fill level at which the highest mixing rate was reached in a vertical twin-screw kneader blender. Moreover, Alian et al. [21], and kaneko et al. [58] reported that an increase in vessel fill level resulted in the reduction of mixing index. Basinskas and Sakai [55] observed the opposite trend, where an increase in vessel fill level resulted in an increase in the final mixing index.

As mentioned in section 2.3, mixing indices are commonly used to assess the influence of design, operating parameters, and material properties on the mixing performance [59-60]. However, the indices cannot differentiate between the strength of each parameter in influencing of the system performance. To address this issue, Portillo et al. [61], Just et al. [62], and Pakzad et al. [63] incorporated the ANOVA technique in order to determine the significance of the main parameters and their interactions while ranking the parameters in terms of their impact.

DEM has also enabled researchers to extract key information from simulations in order to characterize the mixing mechanisms taking place within various mixers. Limited work has been reported on quantitative assessment of mixing mechanisms in common agitated blenders. During a given solid mixing process, various mixing mechanisms contribute to the promotion of particle's random motion. As a result, analyzing and quantifying the intensity of the mechanisms could reveal critical information regarding the kinetics and flow behaviour of particles within a particular system. Remy et al. [36], Golshan et al. [56], Remy et al. [59], Remy et al. [60], and Radl et al. [64] incorporated the granular temperature parameter in their investigations in order to extensively differentiate the mixing intensity in various regions of the system. Golshan et al. [56] observed higher granular temperatures near the impeller due to higher movement of particles when compared to granular temperature values calculated for regions away from the impeller and near

the wall. Remy et al. [60] obtained maximum granular temperature values near the vessel wall and the top portion of the blades when studying vertical cylindrical bladed mixers. Remy et al. [36, 60] utilized the Peclet number to quantify the intensity of the convection and diffusion mixing mechanisms taking place in the mixing system. In all simulations performed for vertical cylindrical bladed mixers, the Peclet number was considerably larger than unity showing that convection was the dominant mechanism in the process under investigation.

## 2.6 Mixing assessment for bi-disperse particles using DEM

Powder blending often involves mixing of two or more particle components to a desired degree of uniformity [65]. For example, in the pharmaceutical industry, tablets with specific compositions are produced from the mixing of particle components with distinct properties (i.e various sizes, shapes and densities) to a pre-specified degree of homogeneity to satisfy the desired product specification [66]. As mentioned in the previous sections, particle assemblies involving distinct components tend to undergo segregation due to differences in their physical properties. As a result, processes involving the mixing of particle components with different physical properties becomes a challenging endeavor [1, 66].

As mentioned in section 2.5 numerous experimental and numerical (DEM) investigations have been carried out on the mixing performance of agitated blenders containing monodispersed particle mixtures [21, 28-29, 31, 36-37, 55-57]. However, limited investigations have been reported on assessing the mixing performance of agitated blenders by examining the effects of critical operating parameters (i.e. impeller rotational speed, vessel fill level, particle loading arrangement) and flow pattern (i.e. Peclet number and diffusivity coefficient) on the degree of mixing for a bi-disperse system.

Zhou et al. [67] examined the flow and segregation of bi-disperse particles in an agitated vertical bladed mixer by using DEM simulations and experiments. The simulation results were found to be in good agreement with PEPT experimental results retrieved from a mono-disperse system. The effects of impeller rotational speed, particle size, and volume fraction and particle density on mixing kinetics and mixing quality were investigated. It was observed that the larger particles collected in the top region of the mixing bed and the smaller particles assembled in the bottom region of the bed. This trend was in agreement with the observations reported by Remy et al. [66], and Alchikh-Sulaiman et al. [68]. It was also reported that as the size or density differences between particles were reduced, the mixing performance was enhanced. In addition, it was shown that the impeller rotational speed affected the mixing kinetics where higher impeller speeds resulted in better mixing during the initial stages of the mixing process. The final mixing quality however did not change with variations in the impeller speed. Remy et al. [66] investigated the flow and segregation of bi-disperse and poly-disperse particles in an agitated vertical bladed mixer through DEM and experiments. It was reported that the binary system had the fastest segregation occurrence compared to the poly-disperse mixture. Moreover, Remy et al. [66] used the Peclet number to determine the mobility strength of particles and the dominant mixing mechanism within an agitated mixer. It was reported that regardless of the particle size used for the binary system, the dominant mixing mechanism was convection. Alchikh-Sulaiman et al. [68] studied the mixing of bi-disperse, tri-disperse, and poly-disperse particles in a double cone slanted tumbling blender via DEM and experiments. The validated model was utilized to study the effect of particle loading arrangement, particle size, vessel speed and impeller rotational speed on the mixing index. It was concluded that for the bi-disperse mixture the Top-Bottom (TB) loading arrangement, 70 % vessel fill level, and vessel rotational speed of 45 RPM yielded the highest mixing performance. Arratia

et al. [69] analyzed the effect of particle loading arrangement and vessel fill level on the mixing of bi-disperse particles in a bin blender through experiments and simulations. It was concluded that the TB loading arrangement yielded a higher mixing index than the front-back (FB) arrangement. In addition, it was reported that as the vessel fill level was increased from 40% to 80% the mixing efficiency decreased accordingly.

## 2.7 Research objectives

Based on the comprehensive literature review performed, it was revealed that there is a lack of information on the mixing kinetics, and flow pattern of mono and bi-disperse particles inside the horizontal agitated Paddle mixer. As a result, the objective of this investigation was to carry out a comprehensive mixing assessment of mono and bi-disperse particles in the horizontal Paddle blender by using experimental, simulation (DEM), and statistical (ANOVA) methods. The experimentally validated simulation models were used to study the mixing kinetics and flow pattern of mono and bi-disperse systems. This investigation implemented the use of both commercial and open source computational platforms for carrying out the required DEM simulations. The mixing kinetics were analyzed by examining the effect of impeller rotational speed, vessel fill level, particle number composition, and particle loading arrangement on the mixing quality. In addition, the flow pattern was examined by incorporating granular temperature, particle diffusivities, and Peclet number.

# Chapter 3: Specification of experimental set-up

The experimental setup for this investigation was composed of a PVC stationary cylindrical vessel with a length of 0.500 m and a diameter of 0.216 m. In addition, PVC paddle impellers were attached to a rotating shaft which was aligned along the center of the stationary vessel (Figure 8). The shaft-impeller assembly was connected to a motor with an adjustable rotational speed controller. The impeller assembly consisted of six paddle impellers. They were arranged in an alternating 90-degree pattern as seen in Figure 8. Figure 9 and Table 3 illustrate the dimensions of the agitated paddle blender in this study. The Paddle mixer was designed, developed and assembled at the Department of Chemical engineering, Ryerson University. For all experiments spherical glass beads were implemented as the particle components. The glass beads were acquired from METALFINI, located in Montreal, Canada.

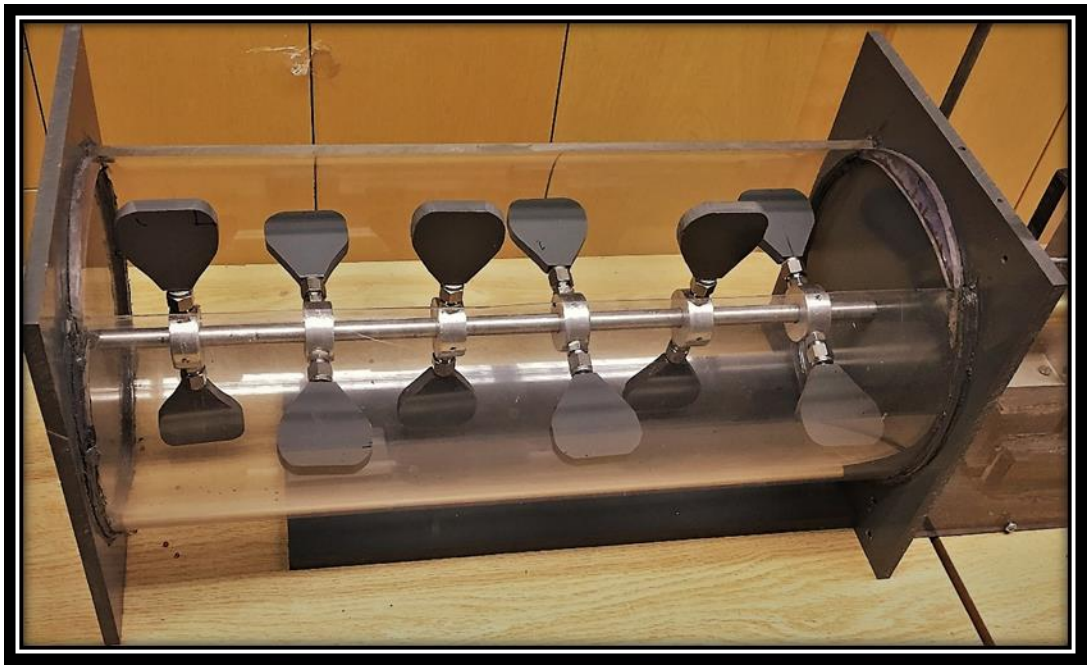

Figure 8: Paddle blender setup and initial blade position.

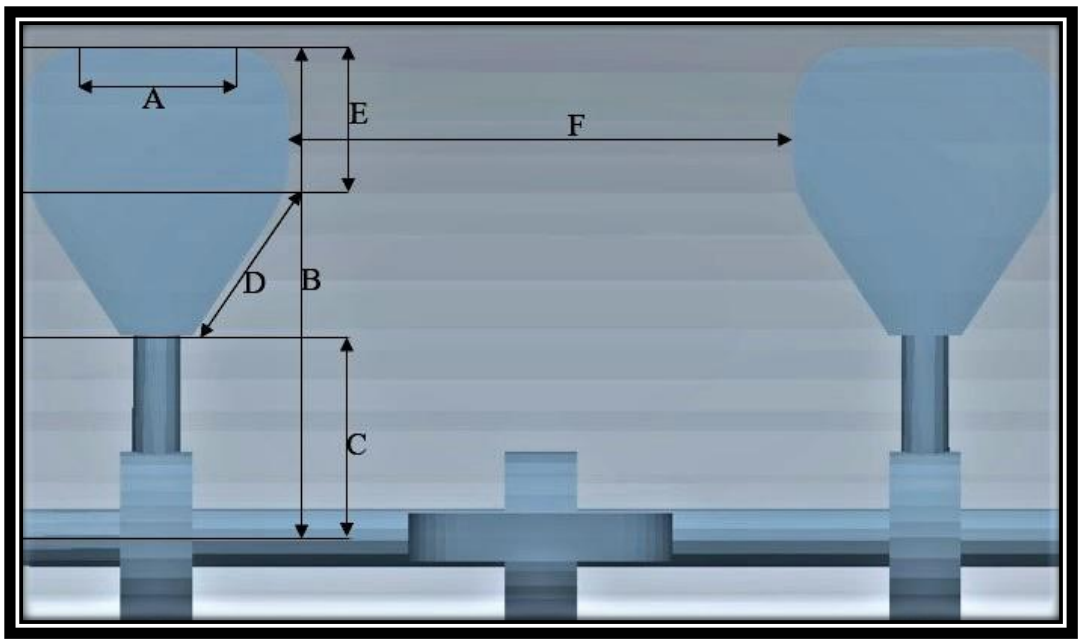


Figure 9: Paddle impeller geometry.

Table 3: Paddle mixer dimensions

| Dimension | Value (m) |
|---|---|
| **A** | 0.030 |
| **B** | 0.102 |
| **C** | 0.042 |
| **D** | 0.030 |
| **E** | 0.030 |
| **F** | 0.105 |

A three slot sampling thief illustrated in Figure 7 was utilized in order to obtain samples from the mixture for both the mono-disperse and bi-disperse investigations which in turn allowed the quantification of the mixing quality through statistical techniques. The RSD index was used for quantifying the mixing quality of samples obtained (for each of the four mixing times set out) [12, 29, 61, 70]. RSD is an indication of the extent of variability of the concentration of a specific type of particle amongst the samples obtained, relative to the overall mean concentration (number of specific particle per total number of particles) within the mixture which is defined by:

$$RSD\ \% = \frac{\sigma}{\mu} \times 100 \quad (1)$$

where $\sigma^2$ is the variance of samples gathered from the whole mixture and $\mu$ is the overall mean concentration of one type of particle within the system.

$$\sigma^2 = \frac{1}{K}\sum_{i=1}^{K}\left(\frac{n_i}{N_i} - P\right)^2 \quad (2)$$

where $P$ is the overall proportion of a specific type of particle, $K$is the total number of samples taken, $n_i$ is the number of one type of particle in $i$th sample, $N_i$ is the total number of particles in $i$th sample. For the bi-disperse investigation all RSD calculations were carried out with respect to the smaller particle.

### 3.1 Experimental method for mono-disperse investigation

In all experiments performed in this section, mono-dispersed spherical glass beads with diameter of 3 mm and density of 2500 kg/m$^3$ were used. The blender was operated at an impeller rotational speed of 40 RPM while maintaining the vessel fill level at 40 %. The particle loading arrangement was selected to be Top-Bottom. To distinguish the particles when evaluating the mixing performance, they were colored in red and black. The volume proportionality factor for both the red and black particles were set at 0.5. In all experiments, black particles were loaded at the bottom of the vessel and the red particles were loaded on top hence, creating a Top-Bottom particle loading arrangement. As stated previously, the results of this set of experiments were used in order to validate the model.

Initially, eight sample locations were selected from various positions, in order to represent the entirety of the system. Through initial screening of the experimental results it was concluded that changing the sampling locations along the length of the vessel had the most impact on the

experimental results. Therefore, to minimize disturbance induced on the particle assembly during the sampling process only four distinct locations were selected as shown in Figure 10. All four sampling locations are indicated from the front view of the blender. Each sample contained approximately 80-100 particles which were counted manually for subsequent quantitative assessment of the mixture. Sampling from the mixer was performed at four specified mixing times i.e. 5, 10, 15, 20 seconds for each experimental run. Each experimental run was replicated three times in order to ensure the reproducibility of the obtained data.

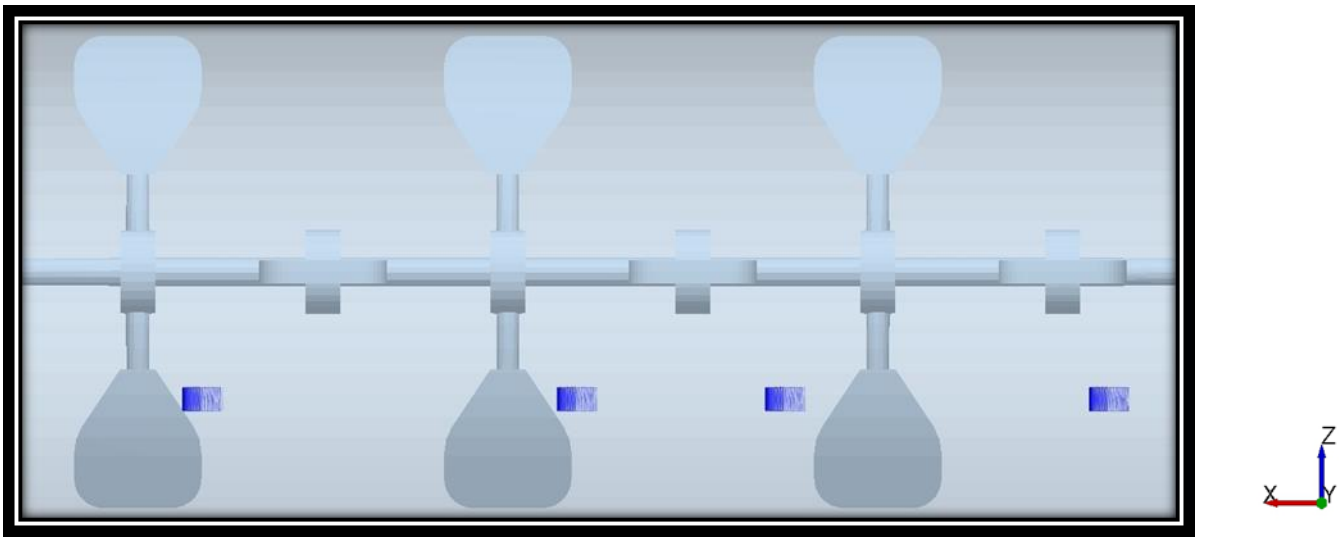


Figure 10: Sample locations (front view).

For the mono-disperse investigation a randomized experimental design was conducted to investigate the significance of each parameter i.e. impeller rotational speed, vessel fill level and particle loading arrangement and their corresponding interactions on the desired response variable (RSD). Three levels were selected for impeller rotational speed and vessel fill level variables which include, 10, 40, 70 RPM and, 40, 50, 60%, respectively and two levels for particle loading arrangement i.e. Top-Bottom, Front-Back. For this experimental design, the multifactorial Central

Composite Design (CCD) Response Surface Method (RSM) was incorporated [62-63]. The initial full statistical model constructed for the paddle blender is presented as:

$$y_{lqk} = \beta + aA_l + bB_q + cC_k + abA_lB_q + acA_lC_k + bcB_qC_k + abcABC + a^2A^2 + b^2B^2 + \varepsilon_{lqk} \quad (3)$$

where, *k, l, q* correspond to the number of levels for particle loading arrangement, impeller rotational speed, and vessel fill level, respectively. $\beta$, *A, B, C* represent the overall average of response variable, impeller rotation speed, vessel fill level, particle loading arrangement, accordingly. *AB, AC, BC, ABC,* $A^2, B^2$ indicate the impeller rotation speed- vessel fill level interaction, impeller rotation speed-loading arrangement interaction, vessel fill level-loading arrangement interaction, impeller rotation speed-vessel fill level-loading arrangement interaction, quadratic effect for *A*, quadratic effect for *B*, respectively. $\varepsilon, a, b, ab, bc, ac, abc, a^2, b^2$ correspond to the error, parameter coefficients for *A, B, AB, BC, AC, ABC* and quadratic parameter coefficients for *A, B* terms, respectively.

A hypothesis test is developed to determine which of the independent variables significantly affect the response variable and to rank the significance of each factor involved [61]. Therefore, the p-value which is an indication of significance, is acquired for each of the main effects, interactions, and curvature terms. P-values less than 0.05 indicate that the effect is significant [63]. As a result, the null hypothesis, which states that the response results for various levels of the effect are not different is rejected with a Confidence level (Cl) of 95%. Subsequently, the terms that attain a p-value greater than 0.2 are considered to be non-significant and therefore are removed from the initial model. This procedure is repeated until all terms included in the model attain p-values less than 0.05 [61]. Finally, normal probability, and response-interaction plots were constructed from

the final model in order to analyze and assess the mixing quality within the paddle blender in terms of the process parameters involved.

### 3.2 Experimental method for bi-disperse investigation

For this investigation, a bi-disperse mixture composed of 3 mm and 5 mm glass beads was used. The density of the particles was 2500 kg/m$^3$. For all experiments, the 5 mm particles were loaded at the bottom of the vessel while the 3 mm beads were loaded on top of the 5 mm particles hence creating the Top-Bottom (TB) particle loading arrangement (Figure 11). Furthermore, for each experimental run the volume proportionality factor for both types of particles were fixed at 0.5, which equivocates to a 1:1 volume scale ratio between the 3 mm and 5 mm glass beads. The operating conditions for all experiments were set at an impeller rotational speed of 40 RPM, and 40 % vessel fill level.

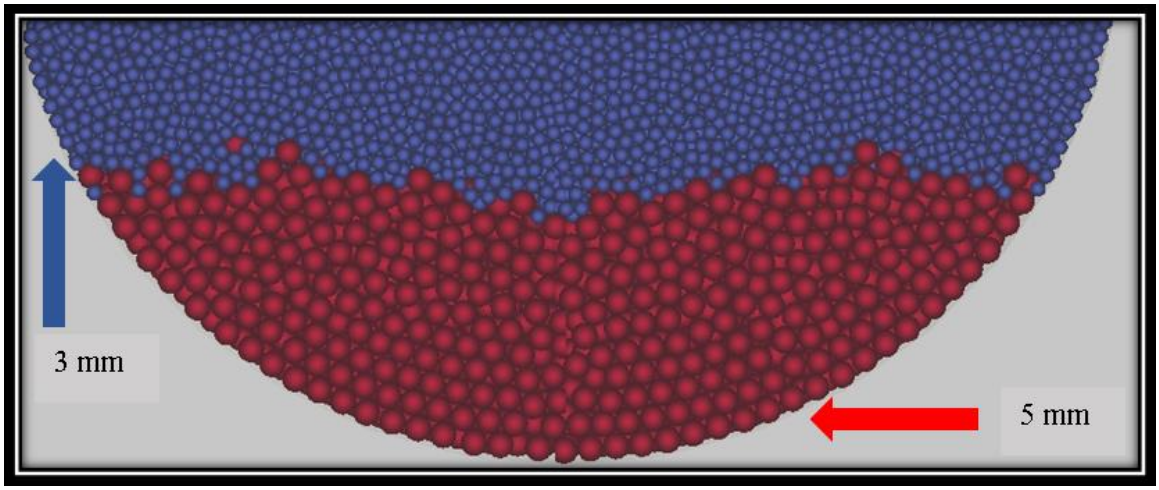


Figure 11: Initial TB particle loading arrangement (side view).

An initial analysis of the experimental data revealed that only changes in sample location along the length (*x*-direction) of the vessel had a significant influence on the experimental results obtained. To minimize disturbance induced on the particle assembly during the sampling process, six distinct sample locations were selected along the length of the vessel with each sample containing approximately 80-120 particles. The selection of these samples were based on experimental limitations (e.g. sampler and vessel geometries). The samples were cylindrical in shape with a length (*z*-direction) of 2.0 cm and a diameter (*y*-direction) of 1.7 cm. The *x*, *y*, and *z* coordinates for the origin of the 6 samples are presented in Table 4 which were taken with reference to the origin of the vessel.

Table 4: Coordinates for cylindrical shaped samples

| **Sample Coordinates** | **Sample 1** | **Sample 2** | **Sample 3** | **Sample 4** | **Sample 5** | **Sample 6** |
|---|---|---|---|---|---|---|
| ***x* (m)** | -0.240 | -0.160 | -0.080 | -0.001 | 0.080 | 0.160 |
| ***y* (m)** | 0.043 | 0.043 | 0.043 | 0.043 | 0.043 | 0.043 |
| ***z* (m)** | -0.05 | -0.05 | -0.05 | -0.05 | -0.05 | -0.05 |

These samples were retrieved at 5, 10, 15, 20 seconds of mixing, respectively, for each experimental run. Each run was replicated three times to ensure reproducibility of data. The samples were counted manually and the data was incorporated in the RSD equation to quantify the degree of mixing. As mentioned previously all RSD calculations for the bi-disperse investigation were performed with respect to the 3 mm particles.

# Chapter 4: Discrete Element Method (DEM)

DEM is a mathematical approach which models the trajectory of each individual particle defined within the system [46]. In the DEM approach, translational and rotational motion of each particle is tracked by solving Newton's equations of motion [43]. These equations can be composed of, the particle-particle, particle-wall, particle-fluid, and gravity forces as well as non-contact forces such as van der Waals, magnetic and electrostatic forces [47]. Generally, there are two models for describing the contact between particles which are defined as the soft and hard sphere models. The contact between two particles does not take place at a single point, but rather on a finite area due to the deformation of particles [46]. This concept is defined as the soft sphere model [48]. The hard sphere model on the other hand states that the contact takes places at a single point instantly without any deformation [46]. The aforementioned hard sphere model cannot be applied to dense, and long lasting contact interactions. However, the soft model translates into two rigid bodies which slightly overlap that is generally utilized for dense, long-lasting contacts, such as those observed in blenders [47]. This method incorporates small time steps and is referred to as being time-driven [47]. This small time step is therefore responsible for the long computation times associated with this specific model [46]. Newton's second law of motion for the interactions between free-flowing particles in the absence of fluids and non-contact forces is given by Zhu et al. [43], and Ketterhagen et al. [47]:

$$m_j \frac{dv_j}{dt} = \sum_h (F_{jh}^N + F_{jh}^T) + F_j^g \tag{4}$$

$$I_j \frac{d\omega_j}{dt} = \sum_h (M_{jh}^T + M_{jh}^r) \tag{5}$$

where, $m_j$, $v_j$, $I_j$, and, $\omega_j$ represent the mass, velocity, moment of inertia and angular velocity of particle $j$ respectively. $F_{jh}^N$, $F_{jh}^T$, $M_{jh}^T$, $M_{jh}^r$, correspond to the normal force, tangential force, tangential torque, and rolling resistance torque resulting from the particle-particle and particle-geometry contacts. $F_j^g$ represents the gravitational force acting on particle $j$.

Various models have been proposed to describe the contact force taking place between two particles and particle-geometry [43, 46-47]. Once the contact force, and torque are calculated based on the contact model, Eq.4 and Eq.5 can be incorporated to determine the trajectories and velocities of each particle numerically [47]. Two common contact models applied in DEM are the linear elastic and non-linear Hertz-Mindlin models. The aforementioned models have been successful in accurately predicting the behaviour of particles in various systems involving particle-particle interactions. In addition, DEM requires accurate quantities for the physical properties of the particles defined [54]. Accurate values are difficult to be determined for a specific material and therefore, causing discrepancy in the final outcome of the simulation. Table 5 presents some of the main advantages and disadvantages of applying the DEM approach for investigating the behavior and dynamic of particle assemblies.

Table 5: Advantages and disadvantages of DEM

| Advantages | Disadvantages |
|---|---|
| - Simple models are used to solve velocity and motion of particles<br>- Forces and motions of individual particles can be determined<br>- Full dynamic information<br>- Can observe the effect of parameters on particle dynamics which would be difficult to evaluate experimentally | - Limited computing capability<br>- Only applied to situations where equations for calculating inter-particle forces are well established<br>- Most models use the sphere shape model, no real particle is a perfect sphere<br>- The physical properties of particles used in the calculations are difficult to measure. |

## 4.1 Computational method for mono-disperse investigation

For the mono-disperse investigation, EDEM 2.7 commercial software was used to integrate Newton's equations of motion [56, 43]. The Hertz-Mindlin contact model was adopted to account for the particle-particle and particle-wall contact forces [13]. The normal and tangential contact forces utilized in the EDEM solver are defined as:

$$F_{jh}^{N} = -\left(\frac{4}{3}Y_{eq}\sqrt{R_{eq}}\right)\delta_n^{3/2} - \left(-\sqrt{5}\frac{\ln e}{\sqrt{\ln^2 e + \pi^2}}\sqrt{m_{eq}\left(\frac{4}{3}Y_{eq}\sqrt{R_{eq}}\right)}\right)\dot{\delta_n}\delta_n^{1/4} \quad (6)$$

$$F_{jh}^{T} = -\left(8G_{eq}\sqrt{R_{eq}}\delta_n^{\frac{1}{2}}\right)\delta_t - \left(-\sqrt{\frac{10}{3}}\frac{\ln e}{\sqrt{\ln^2 e+\pi^2}}\sqrt{m_{eq}\left(8G_{eq}\sqrt{R_{eq}}\delta_n^{\frac{1}{2}}\right)}\right)\dot{\delta_t}\delta_n^{1/4} \quad (7)$$

where $\delta_n$, $\delta_t$, and $e$ are the normal overlap, tangential overlap and coefficient of restitution, respectively. $R_{eq}$, and $Y_{eq}$ represent the equivalent radius and the equivalent Young's modulus, respectively and are defined as follows:

$$R_{eq} = \frac{R_j R_h}{R_j + R_h} \tag{8}$$

$$Y_{eq} = \frac{Y_j Y_h}{Y_j(1-\epsilon_h^2) + Y_h\left(1-\epsilon_j^2\right)} \tag{9}$$

where, $\epsilon$ is the Poisson's ratio and $m_{eq}$ is the equivalent mass which is expressed as:

$$m_{eq} = \frac{m_j m_h}{m_j + m_h} \tag{10}$$

$G_{eq}$ is the equivalent shear modulus calculated as follows:

$$\mathrm{G_{eq}} = \frac{G_j G_h}{G_j(2-\epsilon_h) + G_h\left(2-\epsilon_j\right)} \tag{11}$$

The Coulomb condition, $F_{jh}^T < \mu_s \left|F_{jh}^N\right|$ limits the tangential force obtained in Eq.7. where, $\mu_s$ is the sliding friction coefficient [59]. The tangential torque and rolling resistance torque are calculated using the following equations, respectively:

$$M_{jh}^T = n_{jh} R_j \times F_{jh}^T \tag{12}$$

$$M_{jh}^r = -\mu_r R_j \left|F_{jh}^N\right| \frac{\omega_j - \omega_h}{\left|\omega_j - \omega_h\right|} \tag{13}$$

where, $\mu_r$ represents the rolling friction coefficient. The aforementioned contact model was incorporated into EDEM. Simulation time step was calculated based on the Rayleigh time. As

suggested by Hassanpour and Pasha [71] 30% of the Rayleigh time was selected as the simulation time step.

## 4.2 Computational method for bi-disperse investigation

For the bi-disperse investigation, LIGGGHTS(R)-PUBLIC 3.3.1, an open source DEM particle simulation platform developed by Sandia National Labs was used as the numerical solver [72]. In order to post-process and visualize the simulation results, Paraview 5.0.1 was implemented. Both LIGGGHTS and Paraview were installed on Ubuntu 16.04 LTS which is an open source Linux distribution based operating system. Similar to the mon-disperse investigation the Hertz-Mindlin contact model was utilized in calculating the particle-particle and particle-wall contact forces [72]. The simulations were carried out on Dell desktop computers. The specifications for the aforementioned computers are summarized in Table 6.

Table 6: Desktop A specification

| | |
|---|---|
| **Memory** | 31.3 GB |
| **Processor** | Intel Xenon(R) CPU E5-2620 v4 @ 2.10GHz |
| **# of processors** | 32 |
| **Graphics** | GeForce 210/PCIe/SSE2 |
| **OS type** | 64-bit |
| **Disk** | 167.4 GB |

However, the tangential contact model used in LIGGGHTS differs slightly from Eq.7 utilized in EDEM. The tangential contact model used in LIGGGHTS is defined by:

$$F_{jh}^{T} = -\left(8G_{eq}\sqrt{R_{eq}}\delta_n^{\frac{1}{2}}\right)\delta_t - \left(-2\sqrt{\frac{5}{6}}\frac{\ln e}{\sqrt{\ln^2 e+\pi^2}}\sqrt{m_{eq}\left(8G_{eq}\sqrt{R_{eq}}\right)}\right)\dot{\delta}_t\delta_n^{1/4} \qquad (14)$$

# Chapter 5: Mixing assessment of non-cohesive mono-disperse particles in a paddle mixer – experiments and discrete element method (DEM) application

## 5.1 Introduction

In this section, the mixing kinetics and flow patterns of non-cohesive, monodisperse, spherical particles in a horizontal paddle blender were investigated using experiments, ANOVA, and discrete element method (DEM). Initially the simulation model was validated by a test case experiment. The validated DEM model was then utilized to examine the effects of three impeller rotational speeds i.e. 10, 40, 70 RPM, three vessel fill levels defined as the volume fraction of mixture bed to the vessel volume i.e. 40, 50, 60 %, and the particle loading arrangement of the mixing components defined as Top-Bottom and Front-Back relative to the front view of the vessel on the overall mixing quality quantified evaluated by the RSD mixing index. Particle diffusivity and Peclet number were utilized to quantify the flow pattern of particles within the system.

## 5.2 Results and discussion

### 5.2.1 Model validation

In this section, the DEM model is validated using the experimental data. As mentioned previously in the objective and experimental setup section, an initial set of experiments were performed in order to validate the DEM model. In the experimental runs, spherical glass bead particles with diameter of 3 mm were used. The impeller rotational speed, vessel fill level and particle loading arrangement were set at 40 RPM, 40% and Top-Bottom, respectively. Afterwards, the DEM model was developed in EDEM 2.7 commercial software to represent the experiment outlined above. EDEM developed by DEM Solutions Ltd. is the leading commercial software commonly used for

simulating granular flow. The simulation input parameters are listed in Table 7. These parameters were retrieved from Margio et al. [73] since the particle shape and material as well as the vessel and impeller materials utilized were found to be identical to those applied for this investigation. Margio et al. [73] mentioned that the particle's shear modulus was decreased artificially to 2.0e6 Pa to reduce the computational time. However, using the proposed shear modulus value in this study showed a significant deviation between the experimental measurements and simulation results. The implementation of a model calibration process revealed that a shear modulus value of 7.0e6 Pa could yield RSD values in close agreement with the experimental data. In simulation a total of 240,000 particles were introduced which corresponded to 40% vessel fill level. Initially 120,000 black particles were generated and allowed to settle down under gravity. Afterwards, 120,000 red particles were created on top of the red particles in order to replicate the Top-Bottom particle loading arrangement used in the experiments. When the particle's kinetic energy reached a value less than 10e-7 J, the impellers were allowed to rotate at 40 RPM for 20 seconds of simulation time. Figure 12-a and Figure 12-b show the Top-Bottom initial particle loading arrangements from the side and front views respectively. The impeller rotation direction with respect to the side view of the mixer is also shown in Figure 12-a.

The time step utilized for the simulation calculations was set at 2.886e-5 seconds which equivocates to 30 % of the Rayleigh's time. Similar to the experiments, four samples were retrieved at the end of each mixing time interval (i.e. every 5 seconds) for a total mixing time of 20 seconds and the RSD values obtained from simulations were compared against the RSDs calculated from the experimental measurements. The number of red (top) particles within each sample was extracted from the simulation results to calculate the RSD values. The RSD results obtained for both the experiment and simulation are presented in Figure 13. A very close agreement

between the simulation and experimental results is observed. Additionally, a qualitative comparison was carried out between the simulation and experiment results which is presented in Figure 14. The captured images (with reference to front view) at 5, 10, 15, and 20 seconds of mixing from both the experiment and simulation were compared. As seen, the DEM model can closely replicate the experimental observations.

Table 7: Simulation input parameters for mono-disperse investigation

| **Simulation input parameters** | **Values** |
|---|---|
| **Shear modulus for particle (*Pa*)** | 7.0e6 |
| **Shear modulus for wall (*Pa*)** | 3.0e9 |
| **Poisson's ratio for particle** | 0.3 |
| **Poisson's ratio for wall** | 0.3 |
| **Particle diameter (*mm*)** | 3 |
| **Particle density** $\left(\frac{kg}{m^3}\right)$ | 2500 |
| **Coefficient of restitution (particle-particle)** | 0.75 |
| **Coefficient of restitution (particle – wall)** | 0.75 |
| **Coefficient of static friction (particle – particle)** | 0.5 |
| **Coefficient of static friction (particle – wall)** | 0.35 |
| **Coefficient of rolling friction (particle – particle)** | 0.01 |
| **Coefficient of rolling friction (particle – particle)** | 0.005 |

(a)

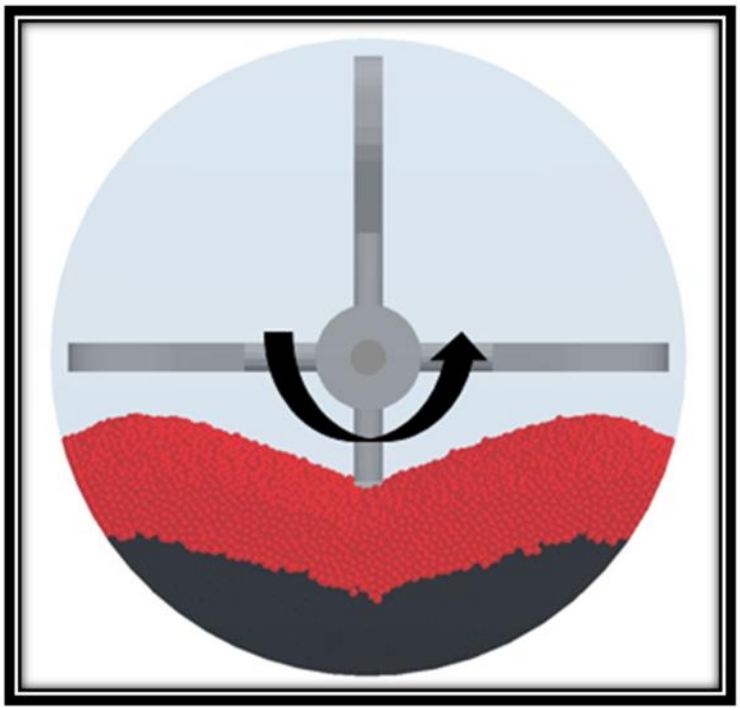

(b)

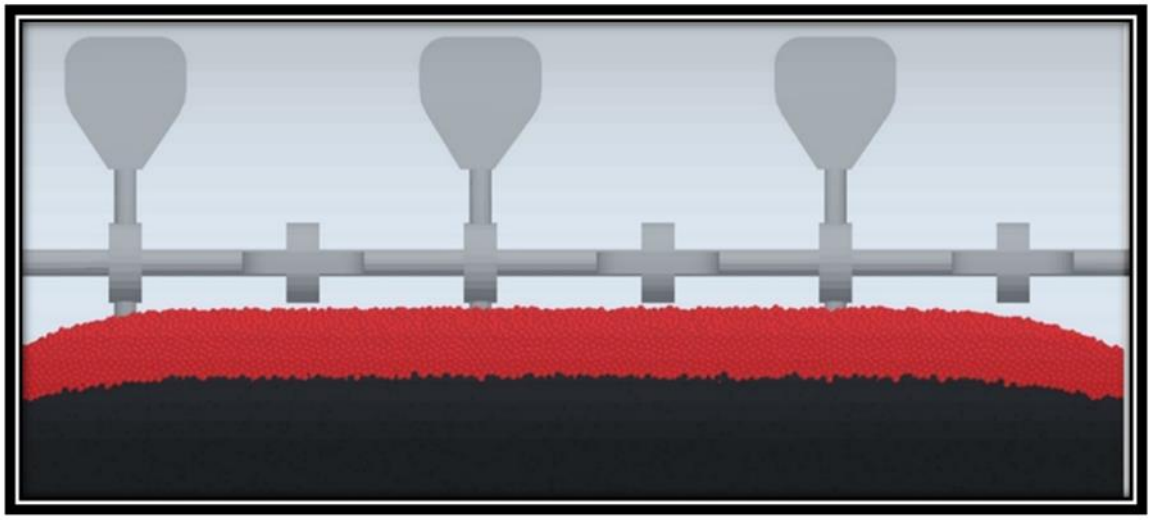


Figure 12: (a) Initial Top-Bottom particle loading arrangement (side view), (b) Initial Top-Bottom particle loading arrangement (front view).

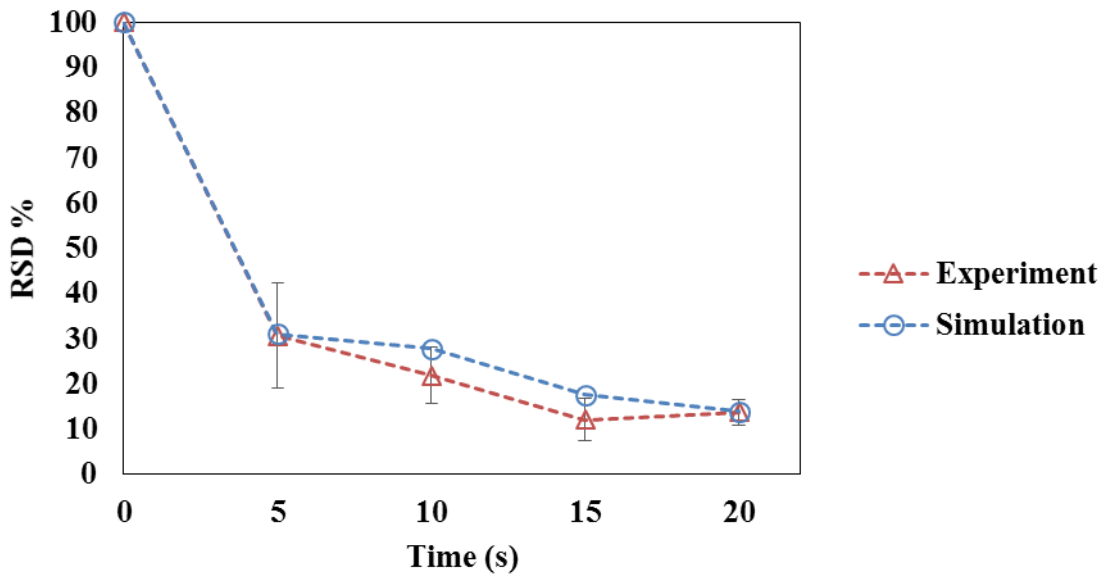


Figure 13: Model validation for 40 RPM, 40% vessel fill level, TB particle loading arrangement, 3mm spherical particles.

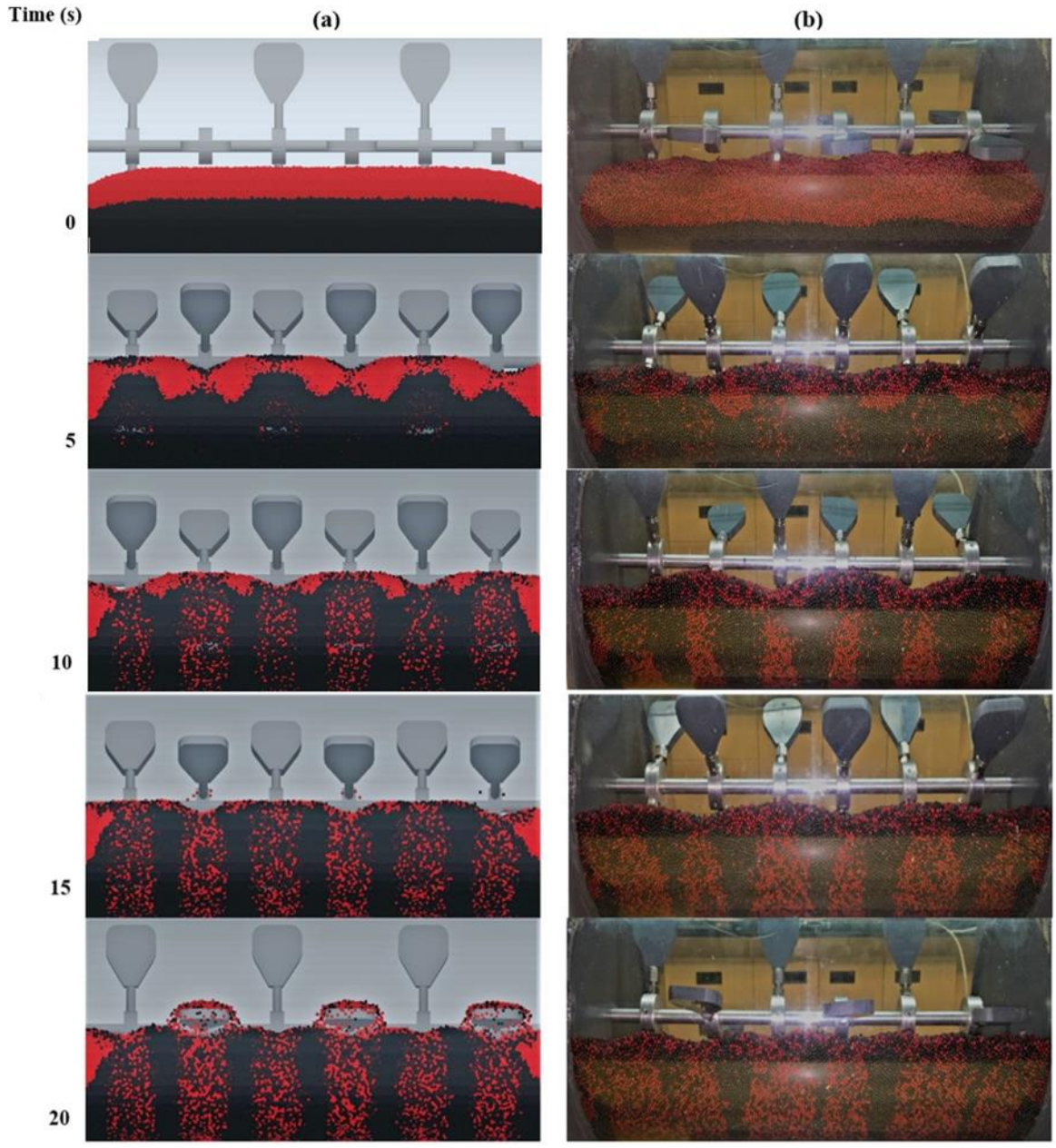


Figure 14: Qualitative comparison between simulation and experiment for 40 RPM, 40% vessel fill level, TB particle loading arrangement, 3mm spherical particles.

### 5.2.2 Mixing Kinetics: effect of operating parameters on mixing performance

In this section, 18 simulation runs (summarized in Table 8) were carried out using the validated DEM model to find the influence of the operating process parameters (i.e. impeller rotational speed, vessel fill level and particle loading arrangement) on the mixing quality. Through the application of the ANOVA technique the influential strength of each parameter and their interactions on the mixing kinetics were also investigated.

Table 8: Summary of simulation cases

| Case # | Impeller rotational speed (RPM) | Vessel fill level (%) | Particle loading arrangement |
|---|---|---|---|
| **1** | 10 | 50 | Top-Bottom |
| **2** | 10 | 40 | Top-Bottom |
| **3** | 10 | 60 | Top-Bottom |
| **4** | 10 | 40 | Front-Back |
| **5** | 10 | 50 | Front-Back |
| **6** | 10 | 60 | Front-Back |
| **7** | 40 | 50 | Front-Back |
| **8** | 40 | 60 | Front-Back |
| **9** | 40 | 50 | Top-Bottom |
| **10** | 40 | 60 | Top-Bottom |
| **11** | 40 | 40 | Top-Bottom |
| **12** | 40 | 40 | Front-Back |
| **13** | 70 | 60 | Top-Bottom |
| **14** | 70 | 40 | Front-Back |
| **15** | 70 | 60 | Front-Back |
| **16** | 70 | 40 | Top-Bottom |
| **17** | 70 | 50 | Front-Back |
| **18** | 70 | 50 | Top-Bottom |

#### *5.2.2.1 Effect of impeller rotational speed (RPM)*

Figure 15 and Figure 16 depict the influence of impeller rotational speed on RSD values. Figure 15 represents the simulation results for the TB arrangement and Figure 16 shows the simulation results for the FB arrangement at various vessel fill levels 40% (~240000 particles), 50% (~300000 particles), and 60% (~360000 particles).

The results showed that when the vessel fill level was set to 40% or 50 % regardless of the particle loading arrangement, as the impeller rotational speed was increased from 10 RPM to 70 RPM the RSD values decreased accordingly and therefore better mixing was achieved (as seen in Figure 15-a ,b, Figure 16-a, b). This observation is in agreement with Alian et al. [21], Cleary and Sinnott [28], Golshan et al. [56], and Sakai et al. [57] studies. However, when the vessel fill level was set at 60% regardless of the particle loading arrangement, increasing the impeller rotational speed from 40 to 70 RPM did not have a significant influence on the RSD values obtained as seen in Figure 15-c and Figure 16-c respectively.

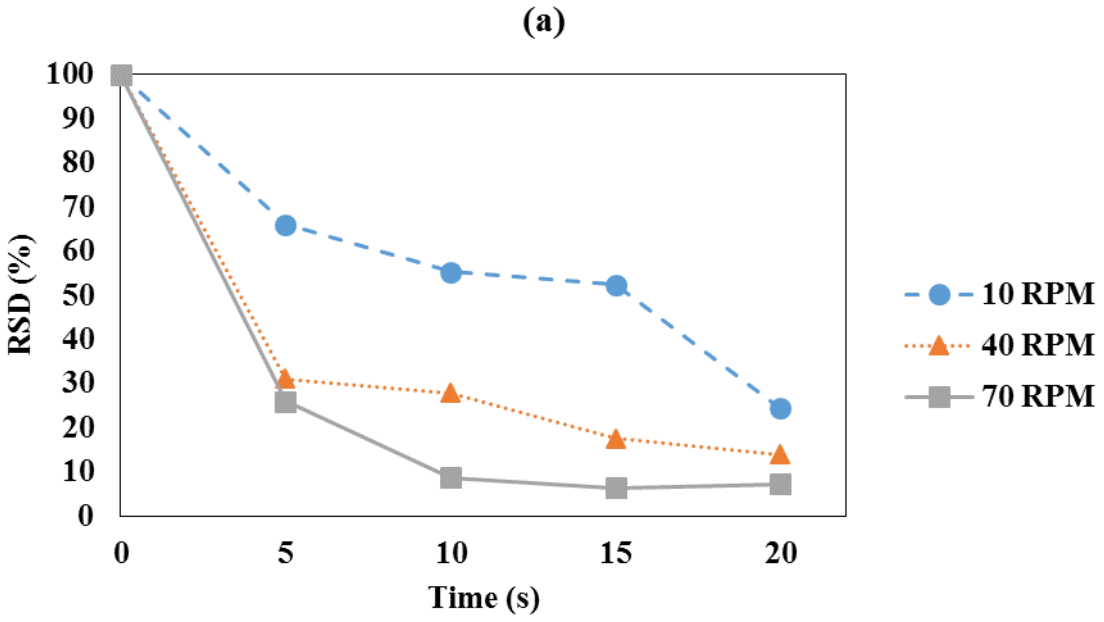

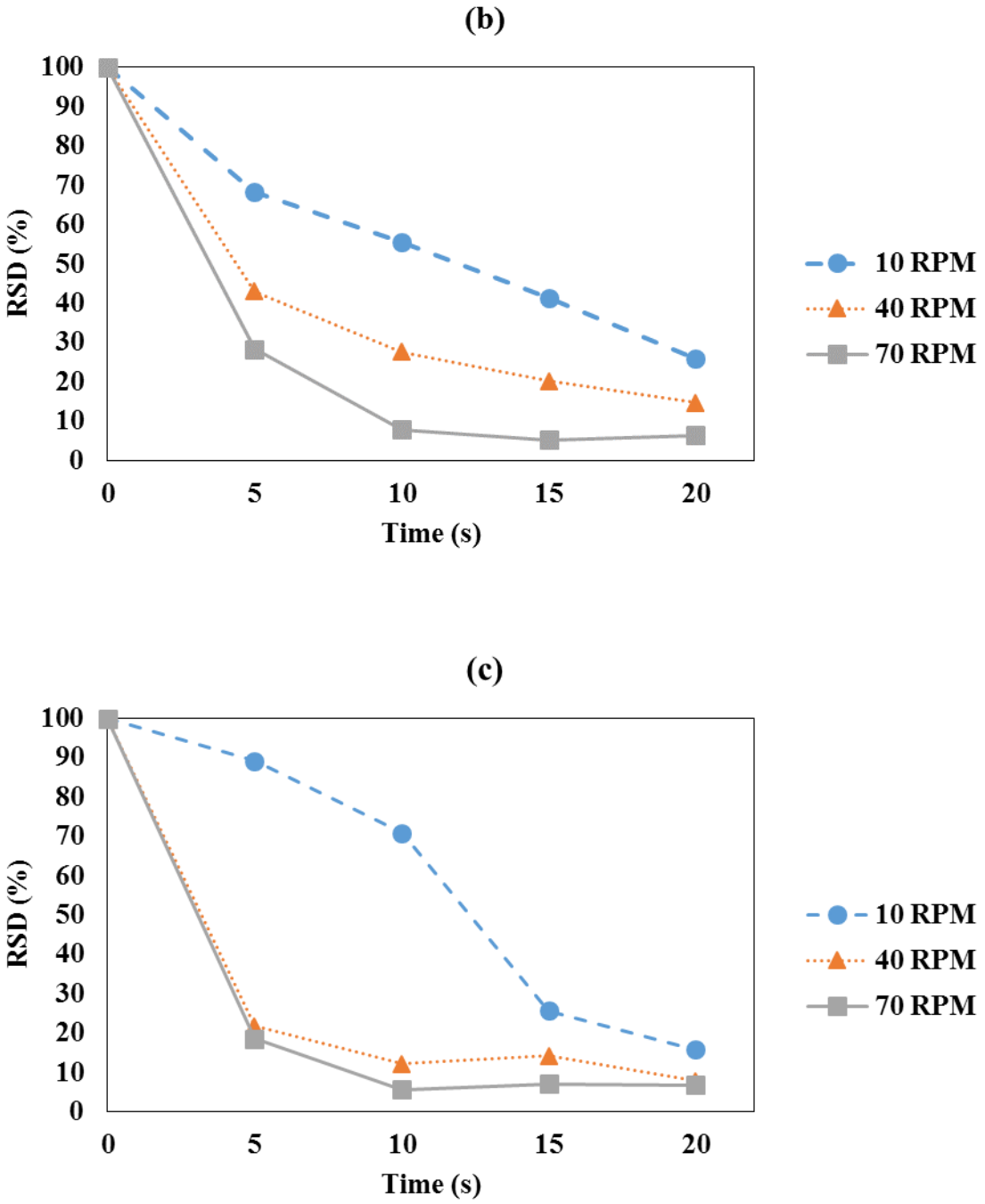


Figure 15: The effect of impeller rotation speed on RSD %, for (a) 40%, (b) 50%, (c) 60% fill level, and Top-Bottom loading arrangement.

(a)

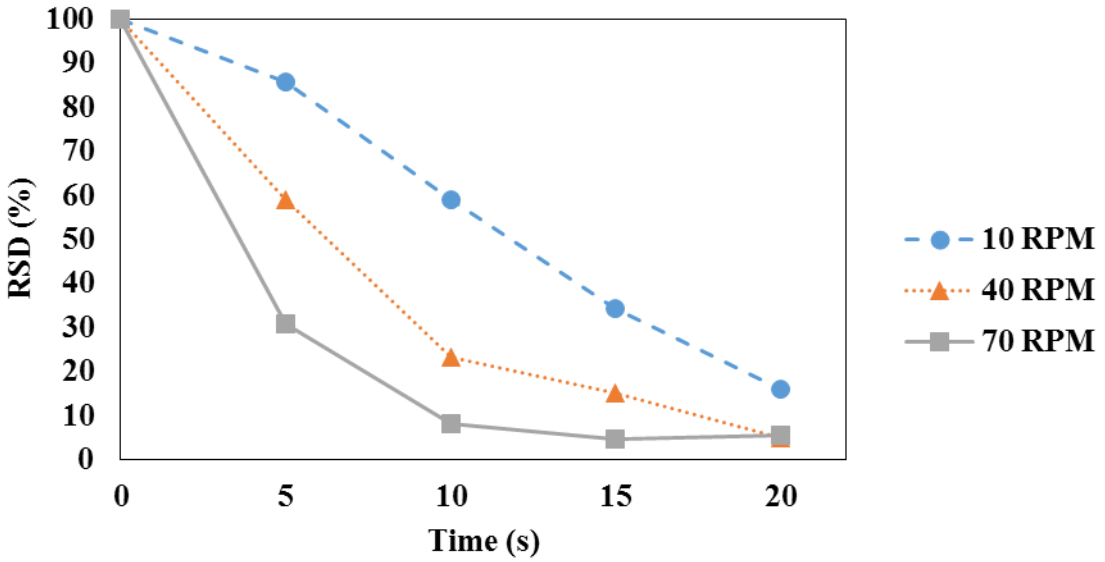
100
90
80
70
60
50
40
30
20
10
0
RSD (%)
0
5
10
15
20
Time (s)
10 RPM
40 RPM
70 RPM

(b)

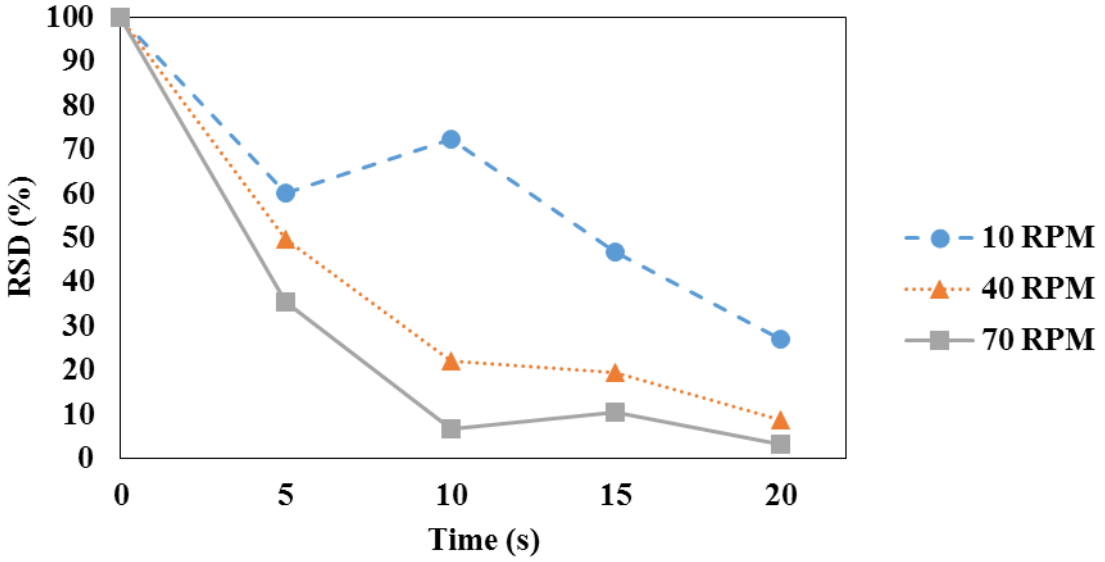
100
90
80
70
60
50
40
30
20
10
0
RSD (%)
0
5
10
15
20
Time (s)
10 RPM
40 RPM
70 RPM

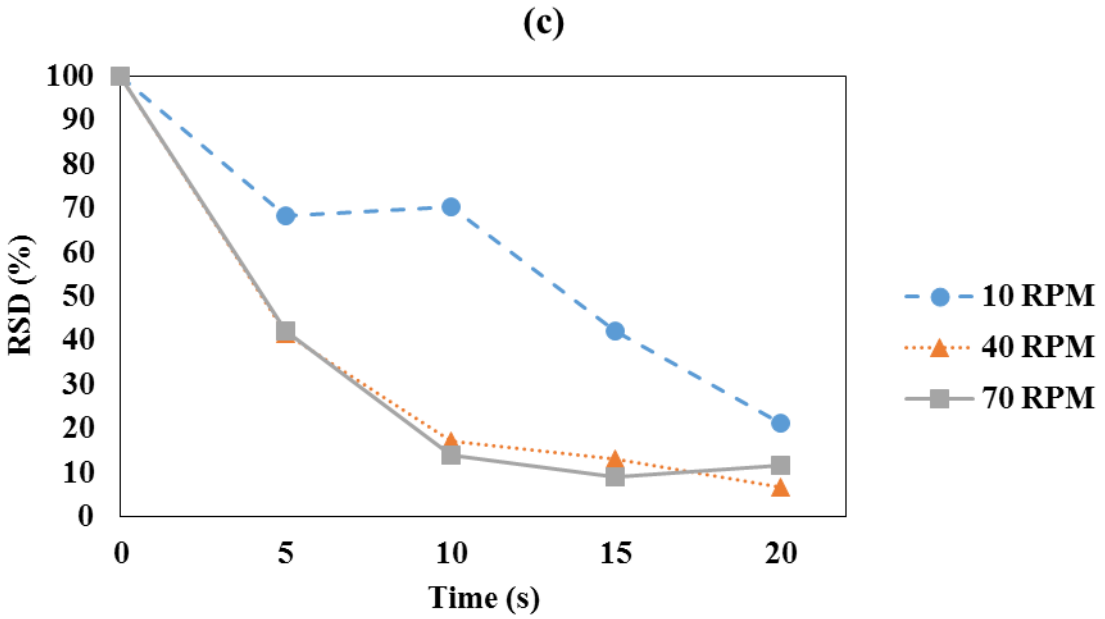


Figure 16: The effect of impeller rotation speed on RSD %, for (a) 40%, (b) 50%, and (c) 60% fill level, and Front-Back loading arrangement.

#### *5.2.2.2 Effect of vessel fill level*

In this section, the influence of vessel fill level on the extent of mixing (RSD) is analyzed. Figure 17 and Figure 18 depict the influence of vessel fill level on RSD values. Figure 17 represents the simulation results for the TB arrangement and Figure 18 shows the simulation results for the FB arrangement at various impeller rotational speeds of 10, 40 and 70 RPM.

From Figure 17 it is seen that for all impeller rotational speeds (10, 40, 70 RPM), as the fill level was increased from 40% to 50% the RSD values did not change significantly. However, for 10 RPM, as the fill level was increased to 60% the RSD values were affected significantly. At low mixing time, the simulation run with 60% vessel fill level showed a poor mixing performance compared to the simulation runs with 40% and 50% fill levels. For higher mixing times on the other hand, the mixing performance was enhanced for the simulation run with 60% vessel fill. For

40 RPM and 70 RPM it becomes clear that when the fill level was increased to 60% the RSD values decreased slightly. Therefore, one can conclude that at higher impeller rotational speeds (40, 70 RPM), and TB particle loading arrangement changes in fill level did not considerably affect the RSD values and therefore, did not influence the extent of mixing.

As seen in Figure 18-a for an impeller rotational speed of 10 RPM increasing the vessel fill level from 40% to 50% resulted in enhanced mixing performance during the initial 5 seconds of mixing. Additionally, increasing the vessel fill level from 50% to 60% showed a slight reduction in the influence on the RSD values. Similar to the conclusion drawn from the TB arrangement it is seen from Figure 18-b, and c that, for the FB arrangement, at 40 and 70 RPM the RSD values were not affected by increasing the vessel fill level from 40% to 60%.

Based on the analysis performed above (Figure 17-a and Figure 18-a) it can be concluded that for an impeller rotational speed of 10 RPM the resulting RSD profiles did not reveal any predictable and consistent trend regarding the effect of the vessel fill level on the mixing performance.

(a)

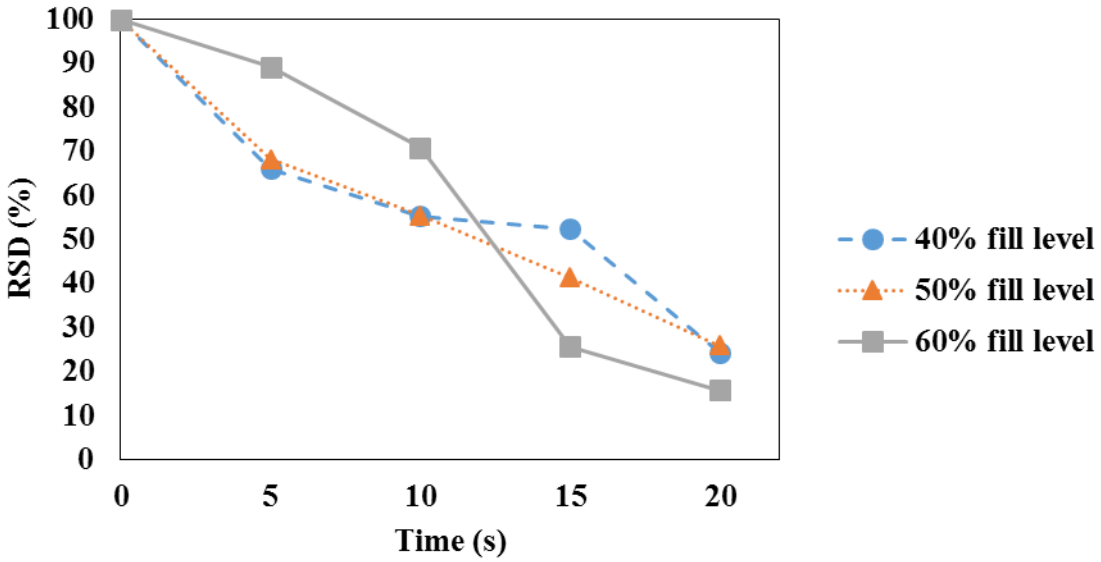
100
90
80
70
60
50
40
30
20
10
0
RSD (%)
0
5
10
15
20
Time (s)
40% fill level
50% fill level
60% fill level

(b)

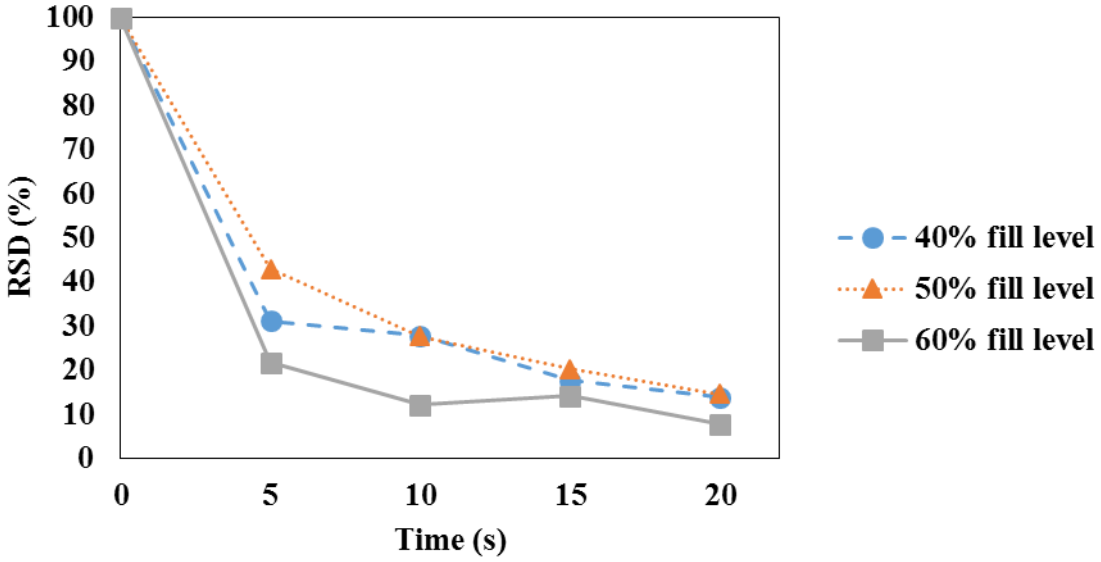
100
90
80
70
60
50
40
30
20
10
0
RSD (%)
0
5
10
15
20
Time (s)
40% fill level
50% fill level
60% fill level

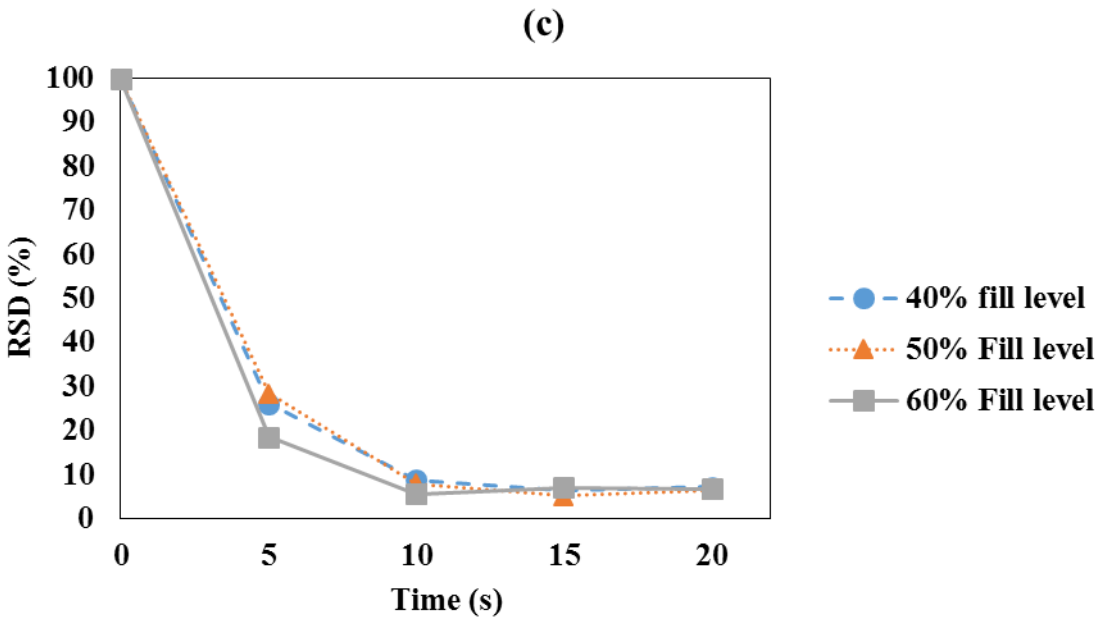


Figure 17: The effect of vessel fill level on RSD %, for (a) 10 RPM, (b) 40 RPM, (c) 70 RPM, and Top-Bottom loading arrangement.

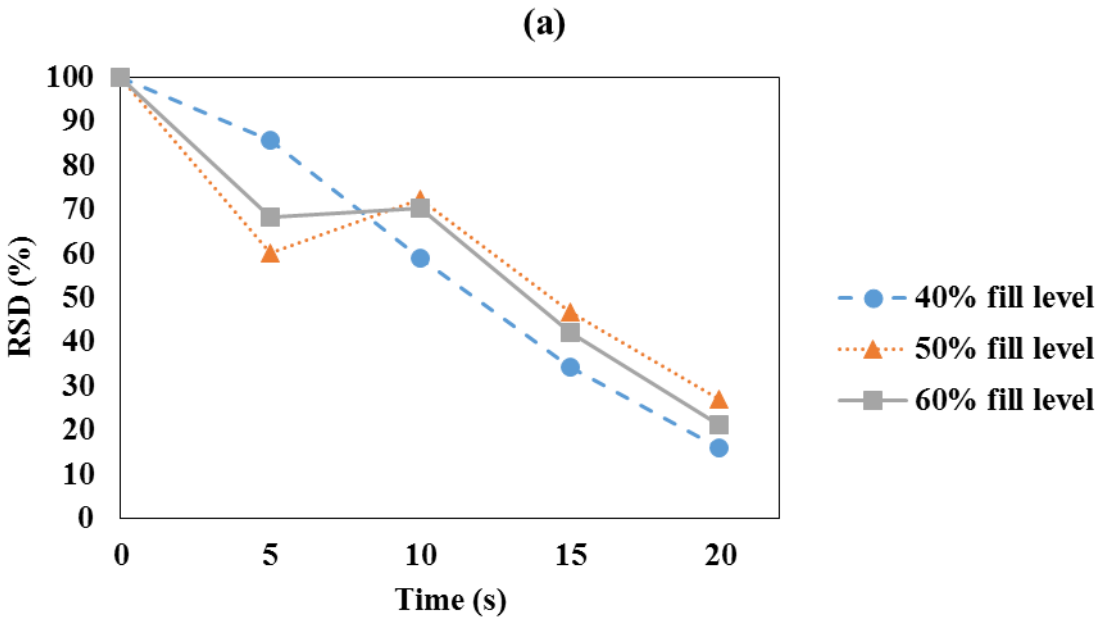

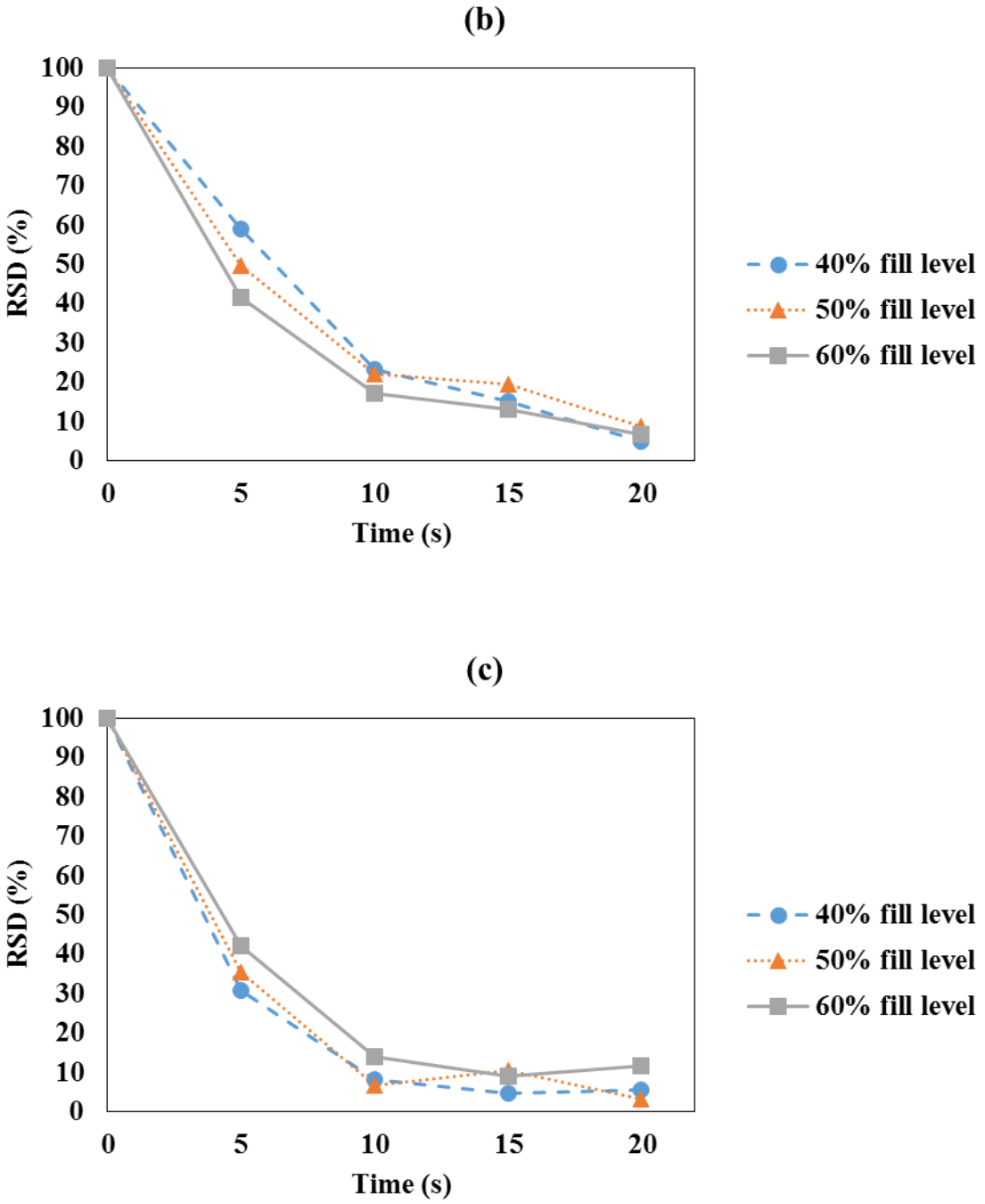


Figure 18: The effect of vessel fill level on RSD %, for (a) 10 RPM, (b) 40 RPM, (c) 70 RPM, and Front-Back loading arrangement.

#### *5.2.2.3 Effect of particle loading arrangement*

The simulation results were initially screened to assess the effect of particle loading arrangement on the mixing quality (i.e. RSD values). However, the results for each mixing time (each data point) for both the TB and FB loading arrangements did not reveal any consistent trend. Therefore, it was decided to analyze the effect of particle loading arrangement in terms of the final RSD value obtained at 20 seconds of mixing. The results are summarized in Table 9, Table 10 and Table 11 for 40%, 50% and 60 % vessel fill levels, respectively. Table 9 and Table 10 indicate that in almost all of the runs for 40 % and 50 % fill levels, lower RSD values were achieved through the implementation of the Front-Back loading arrangement. Therefore, revealing that at lower vessel fill levels the Front-Back arrangement provides higher mixing uniformity when compared to Top-Bottom loading arrangement. However, Table 11 reveals that at higher fill levels (60%), lower RSD values were obtained via the Top-Bottom arrangement indicating that better mixing was achieved through this particle loading arrangement for 60 % fill level.

Table 9: RSD results obtained for 40% vessel fill level at 20 seconds of mixing for both TB and FB loading arrangements

| **Impeller rotation speed (RPM)** | **RSD%, TB** | **RSD%, FB** |
|---|---|---|
| **10** | 24.4 | 16.10 |
| **40** | 13.9 | 5.61 |
| **70** | 7.22 | 5.61 |

Table 10: RSD results obtained for 50% vessel fill level at 20 seconds of mixing for both TB and FB loading arrangements

| **Impeller rotation speed (RPM)** | **RSD%, TB** | **RSD%, FB** |
|---|---|---|
| **10** | 25.87 | 27.12 |
| **40** | 14.64 | 8.80 |
| **70** | 6.40 | 3.27 |

Table 11: RSD results obtained for 60% vessel fill level at 20 seconds of mixing for both TB and FB loading arrangements

| Impeller rotation speed (RPM) | RSD%, TB | RSD%, FB |
|---|---|---|
| **10** | 15.82 | 21.13 |
| **40** | 6.74 | 6.56 |
| **70** | 6.74 | 11.72 |

### 5.2.3 Analysis of Variance (ANOVA)

ANOVA was carried out for examining the significance and influential strength of the parameters on the final desired response variable (RSD) obtained after 20 seconds of mixing. Table 12 and Table 13 were constructed to highlight the simulation runs in terms of the coded operating parameters under investigation. Furthermore, the statistical model representing the desired response variable (RSD) in terms of the coded parameters was obtained through Design Expert 9 by Stat-Ease Inc. which is presented by:

$$RSD = 11.54 - 7.455A - 0.2033B - 1.573C + 1.146AB + 0.1633AC + 2.325BC + 4.591A^2 - 2.764B^2 - 0.8763ABC \quad (15)$$

Table 12: Operating range and levels of the independent variables

| Variables | Symbol | -1 | 0 | 1 |
|---|---|---|---|---|
| **Impeller rotational speed (RPM)** | A | 10 | 40 | 70 |
| **Vessel fill level (%)** | B | 40 | 50 | 60 |
| **Particle loading arrangement** | C | Top-Bottom | | Front-Back |

Table 13: Design matrix in coded units

| Run # | A-impeller rotational speed (RPM) | B- vessel fill level (%) | C-particle loading arrangement |
|---|---|---|---|
| **1** | -1 | 0 | -1 |
| **2** | -1 | -1 | -1 |
| **3** | -1 | 1 | -1 |
| **4** | -1 | -1 | 1 |
| **5** | -1 | 0 | 1 |
| **6** | -1 | 1 | 1 |
| **7** | 0 | 0 | 1 |
| **8** | 0 | 1 | 1 |
| **9** | 0 | 0 | -1 |
| **10** | 0 | 1 | -1 |
| **11** | 0 | -1 | -1 |
| **12** | 0 | -1 | 1 |
| **13** | 1 | 1 | -1 |
| **14** | 1 | -1 | 1 |
| **15** | 1 | 1 | 1 |
| **16** | 1 | -1 | -1 |
| **17** | 1 | 0 | 1 |
| **18** | 1 | 0 | -1 |

The model F-value of 12.42 presented in Table 14 implies that the model was significant. Furthermore, the response model (Eq.15) attained an adjusted R-squared value of 87.47% which indicated that the model was relatively accurate in predicting RSD values with respect to operating parameters within the pre-specified range. From Table 14, it is seen that parameters A, C, and BC interaction had a significant influence on the extent of mixing. Parameter A had the most influential role, followed by BC interaction, and C respectively. Figure 19 illustrates the normal probability of the residuals. This plot was used to assess whether or not the errors were normally distributed. In addition, this tool revealed whether the error variance was homogenous or not. Thus, it becomes clear from Figure 19 that the aforementioned normality assumption was valid for the current study.

Table 14: ANOVA results for RSD response model

| Source | Degree of Freedom (DF) | Sum of Squares (SS) | Mean Square (MS) | F value | p-value |
|---|---|---|---|---|---|
| **Model** | 9 | 936.73 | 104.08 | 12.42 | 1.17E-05 |
| **A-Impeller rotation speed** | 1 | 666.92 | 666.92 | 79.58 | 1.31E-07 |
| **B-Vessel fill level** | 1 | 0.49 | 0.50 | 0.06 | 0.81 |
| **C-Particle loading arrangement** | 1 | 64.37 | 64.37 | 7.68 | 0.01 |
| **AB** | 1 | 10.51 | 10.51 | 1.25 | 0.28 |
| **AC** | 1 | 0.32 | 0.32 | 0.04 | 0.88 |
| **BC** | 1 | 64.86 | 64.87 | 7.74 | 0.01 |
| **$A^2$** | 1 | 116.45 | 116.45 | 13.89 | 0.001 |
| **$B^2$** | 1 | 42.18 | 42.19 | 5.03 | 0.04 |
| **ABC** | 1 | 6.14 | 6.14 | 0.73 | 0.40 |
| **Residual** | 16 | 134.09 | 8.38 | | |
| **Lack of Fit** | 8 | 134.09 | 16.76 | | |
| **Pure Error** | 8 | 0 | 0 | | |
| **Corr. Total** | 25 | 1070.8 | | | |

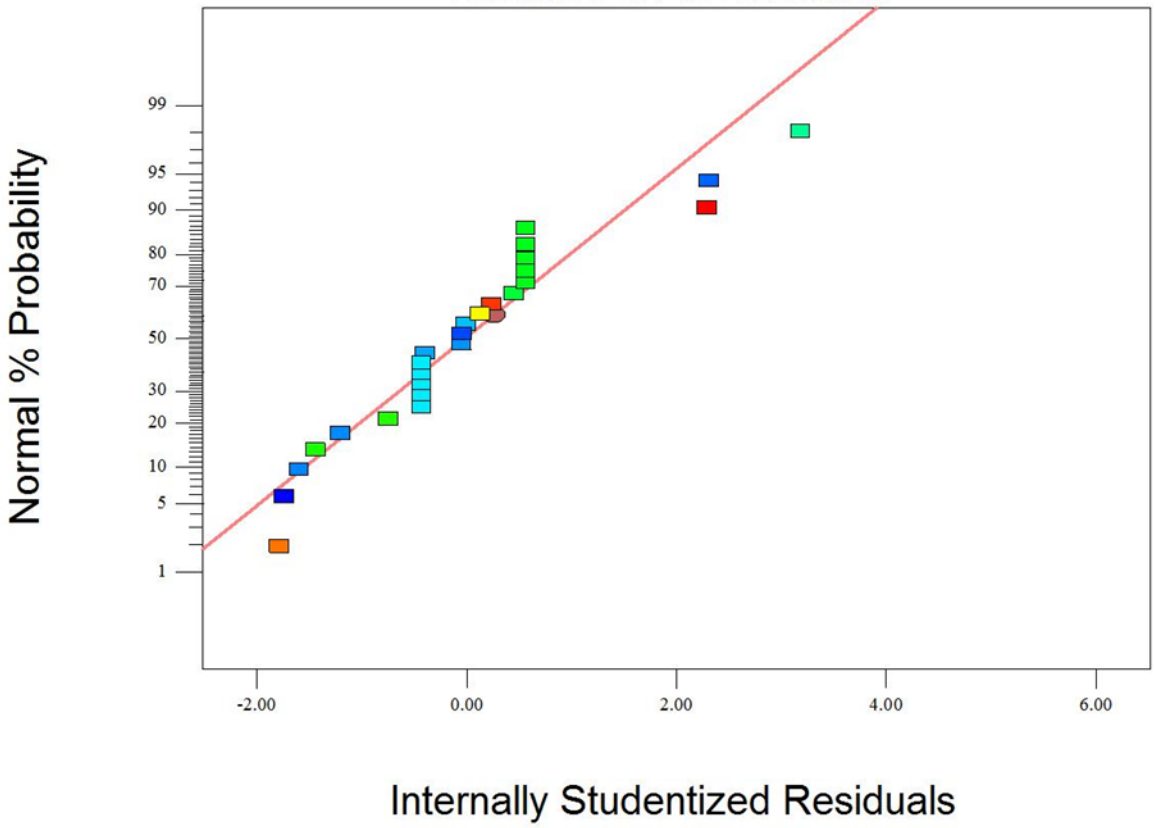


Figure 19: Normal probability plot of the internally studentized residual for RSD.

Furthermore, two interaction contour plots, were constructed in order to assess the effects of the parameters and interactions on RSD. Figure 20 and Figure 21 correspond to the Top-Bottom, and Front-Back loading arrangements respectively. In these figures, red corresponds to the lowest and navy blue to the highest RSD values respectively. It is clear in both figures that generally regardless of the changes in particle loading arrangement and vessel fill level, as the impeller rotational speed increased the RSD values decreased and as a result mixing quality was enhanced. This conclusion also confirms the results obtained in the mixing kinetics section. From Figure 20, it can be observed that for the Front-Back arrangement, variation in the fill level did not significantly affect the RSD values obtained. However, for the Top-Bottom arrangement, as the fill level was increased, better mixing was achieved. This observation confirms the ANOVA results where it was revealed that

the particle loading arrangement-vessel fill level interaction played an instrumental role in the final mixture quality. In order to further examine the impact of particle loading arrangement on RSD, one can divide both contour plots into two sections by slicing the plots horizontally from the center. It becomes clear that the Front-Back arrangement provides a more uniform mixture at lower vessel fill levels regardless of the impeller rotational speed incorporated. This result is also in good agreement with the extensive analysis performed in the mixing kinetics section presented in Table 9 and Table 10.

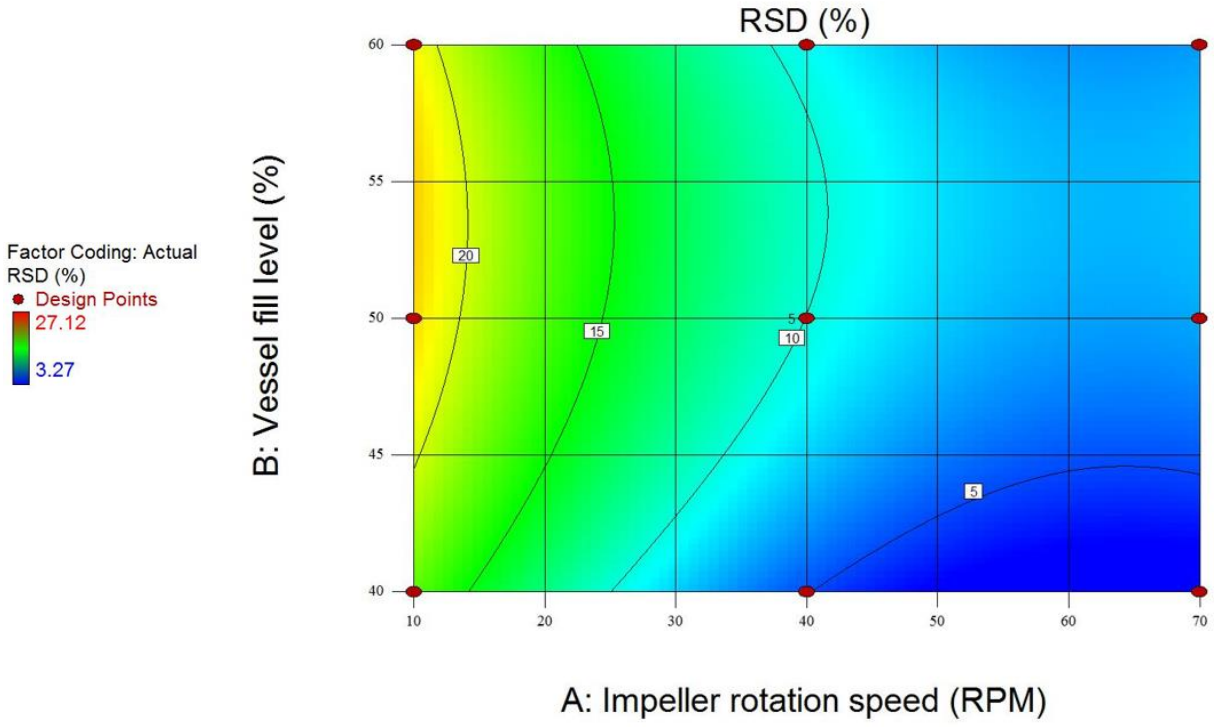


Figure 20: Contour plot showing RSD as a function of two independent variables (A and B) for the Front-Back loading arrangement.

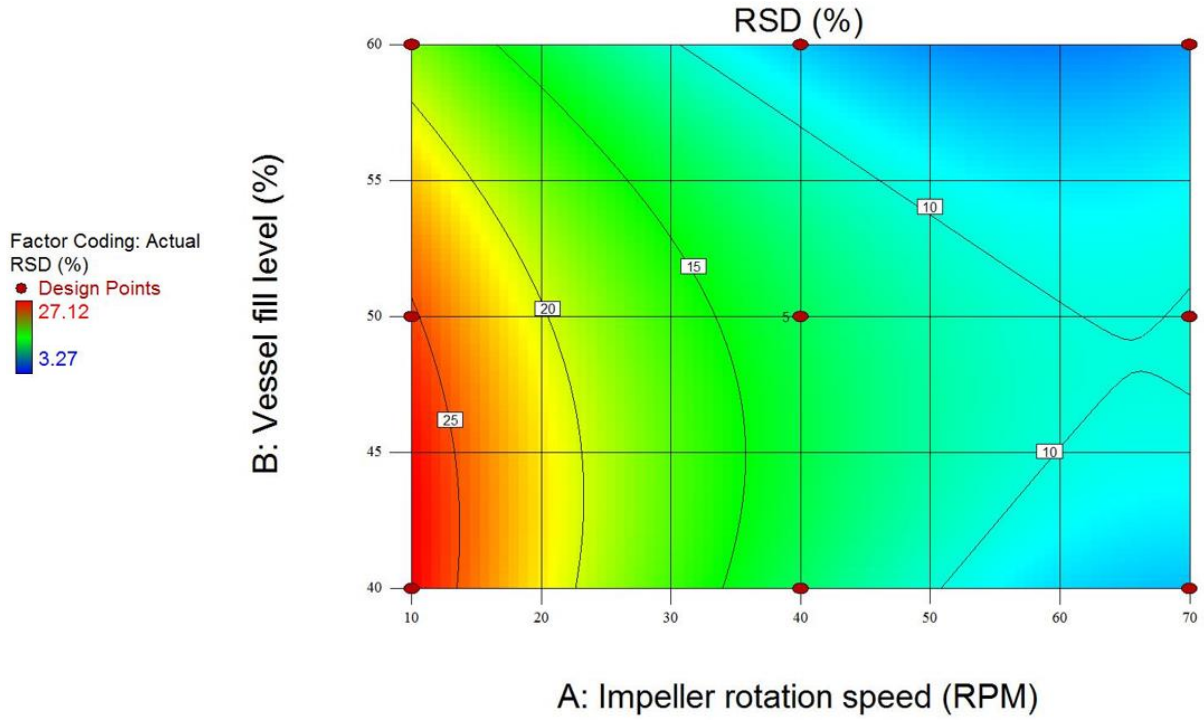


Figure 21: Contour plot showing RSD as a function of two independent variables (A and B) for the Top-Bottom loading arrangement.

### 5.2.4 Flow pattern and mixing mechanism

#### *5.2.4.1 Granular temperature*

Granular temperature is an important macroscopic property of any granular assembly since it reveals the extent of chaotic motion of particles within the system [59]. Granular temperature is defined as:

$$T = \frac{1}{2}\langle (U')^2 \rangle \tag{16}$$

where, $U'$ is the fluctuation velocity of each particle which is the instantaneous deviation from the mean velocity in a specified control volume [66]. The mean velocity is defined as the average velocity of all particles within the specified control volume at a specific time-step [60]. The < >

symbol represents the temporal averaging of $U'U'$. It is known that the granular temperature values are dependent on the size of the control volume and the time interval selected [59-60, 66]. Therefore, various control volumes and time intervals were tested in order to assess the changes that occurred in the granular temperature values obtained. It was concluded that, further reduction in control volume size less than ~4 particle diameter did not affect the granular temperature values. Moreover, it was observed that choosing the time interval smaller than 0.1s did not have a noticeable influence on the granular temperature values. Therefore, the time interval used for determining the granular temperature values was taken as 0.1s.

The control volume selected for granular temperature calculations was defined by a cube with a size of ~4 particle diameters. This selection divided the system into (39 × 17 × 17) cube bins in *x*, *y* and *z* directions accordingly (coordinate system is seen in Figure 12-b). In this study, the granular temperature was calculated for 39 bins along the *x* direction. These 39 bins were coordinated close to the center of the system in *y* direction (i.e. bin number 8) and in *z* direction these bins were located where the tip of impeller swept (i.e. bin number 2). These bins are illustrated in Figure 22.

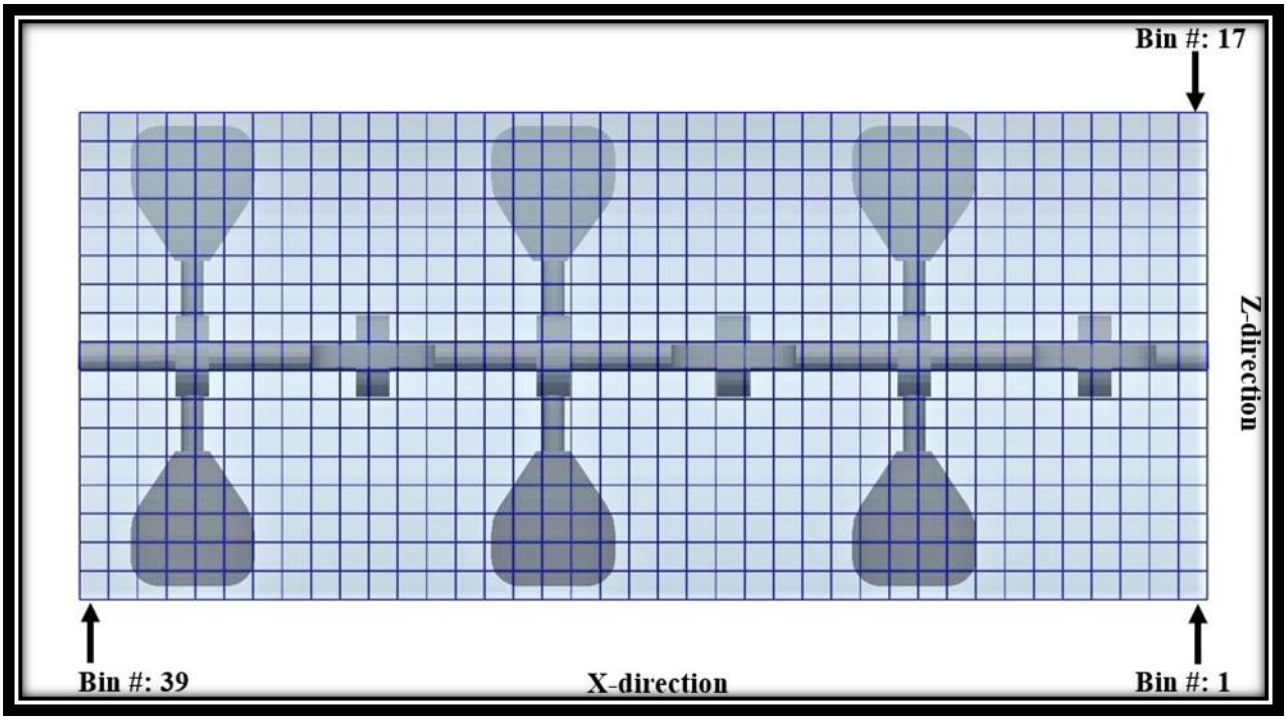


Figure 22: System bin division for granular temperature calculations.

In this section, only the effect of impeller rotational speed is studied on granular temperature. This selection was carried out based on the conclusions drawn from the ANOVA results where it was established that impeller rotational speed had the most significant impact on the mixing performance of the system. Therefore, three simulation runs were selected in which the operating parameters were set at 40% vessel fill level, Front-Back particle loading arrangement, and 10 RPM, 40 RPM, and 70 RPM impeller rotational speeds. The granular temperature results are presented in Figure 23. Figure 23 indicates that for the selected grid bins as the impeller rotational speed was increased, the granular temperatures increased accordingly since an increase in impeller rotational speed resulted in an increase in the fluctuation velocity. This conclusion is in good agreement with the results obtained in the mixing kinetic section, where an increase in impeller rotational speed resulted in higher chaotic motion of particles which in turn produced lower RSD

values (Figure 16-a) and therefore enhanced the mixing quality. In addition, it is seen that, for a given impeller rotational speed the high granular temperature values were obtained in regions that are in near proximity of the impellers. The highest granular temperature values (global) occurred at bins that match the location of the corner edges of the impellers. For example, bin# 15 and 19 match the corner edges of the tip of one of the impellers. Furthermore, the bins with lowest (global) granular temperature values corresponded to the regions between the impellers. This trend is clearer for lower impeller rotational speeds as observed in Figure 23-a, and b. However, for an impeller rotational speed of 70 RPM this trend was less obvious due to the fact that the chaotic motion of particles at both the corner edges and center of impellers did not differ significantly.

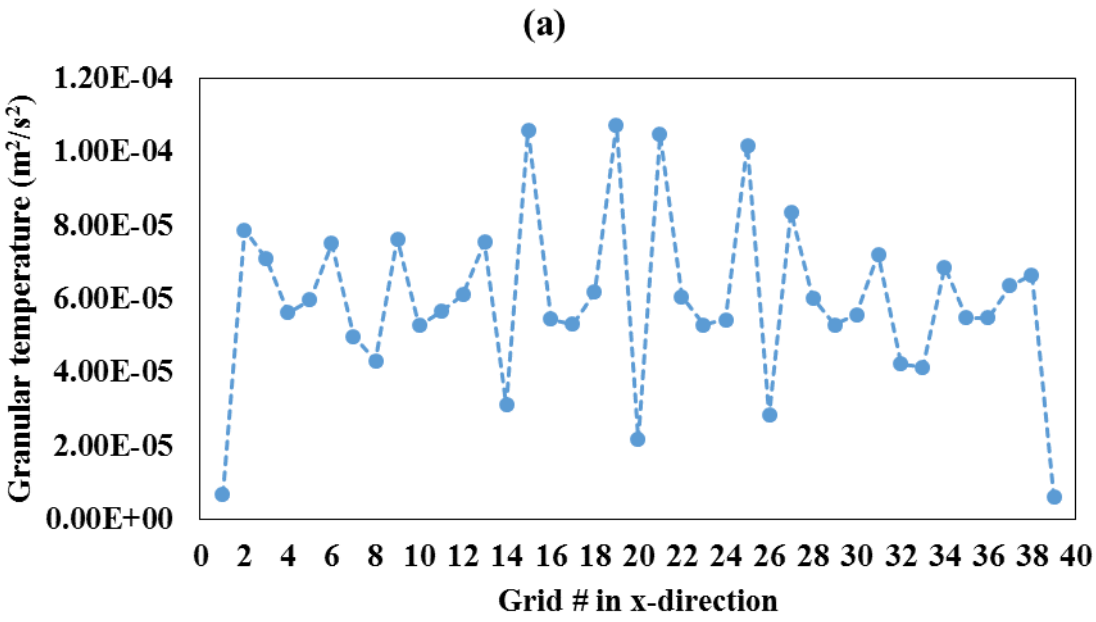

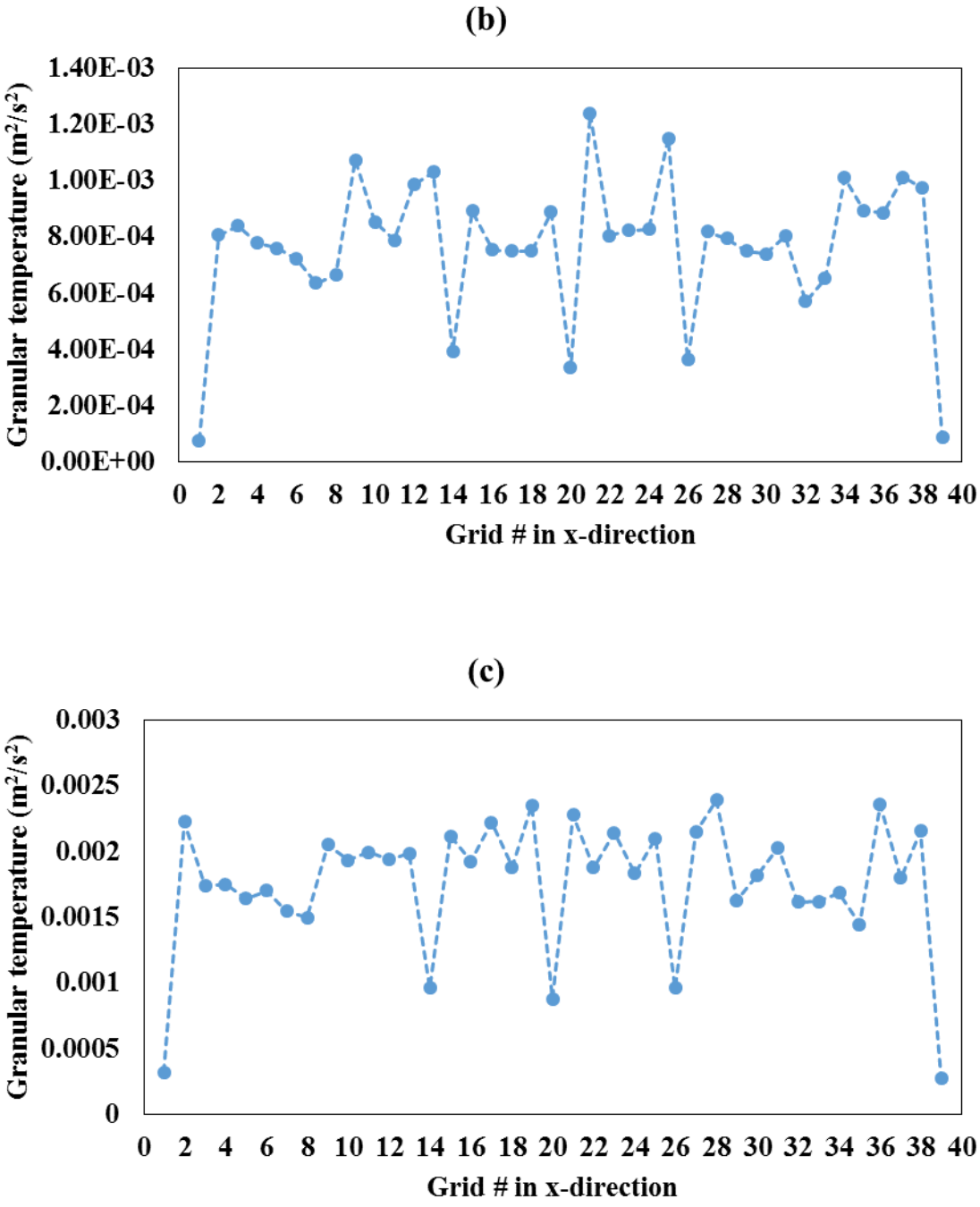


Figure 23: Granular temperature results for (a) 10 RPM, 40% vessel fill level, Front-Back, (b) 40 RPM, 40% vessel fill level, Front-Back, (c) 70 RPM, 40% vessel fill level, Front-Back.

#### *5.2.4.2 Particle diffusivity and Peclet number*

Particle diffusivity is a critical microscopic property of any granular assembly since it measures the mass flux rate due to random motion of particle [59]. Diffusivity coefficient is given by:

$$D_{fg} = \frac{\langle \left(\Delta x_f - \overline{\Delta x_f}\right)\left(\Delta x_g - \overline{\Delta x_g}\right)\rangle}{2\Delta t} \tag{17}$$

where, $\Delta x_f$ represents the particle displacement in the $f$ direction relative to particle's initial position, $\overline{\Delta x_f}$ represents the mean particle displacement of all particles in the system during Δt, and $D_{fg}$ represents the diffusivity coefficient in the *f* direction due to gradient in *g* direction [66]. Diffusivity coefficients were calculated based on a $\Delta t$ of $\frac{1}{4}$ of a revolution and were averaged over all particles within the system. This time interval was chosen by initially testing various time intervals and assessing the changes occurred on the diffusivity values obtained. It was concluded that any further reduction in the magnitude of the time interval did not change the resulting diffusivity values. The ratio between the convective and diffusive contributions to particle motion is assessed by determining the Peclet number which is given by:

$$Pe_{fg} = \frac{U_f R}{D_{fg}} \tag{18}$$

where $U_f$ is the average particle velocity in the *f* direction, and *R* is the mixer radius.

Similar to the granular temperature analysis, the effect of impeller rotational speed on the diffusivity and Peclet values was analyzed. The process conditions selected were identical to the conditions set for the granular temperature investigation. The results for the particle diffusivity and Peclet number for three simulation runs are listed in Table 15. As mentioned previously Peclet number is selected to quantify the contributions of the convective and diffusive mixing mechanisms involved. Table 15 reveals that, for any given impeller rotational speed (10 RPM, 40

RPM, 70 RPM), mixing was dominated by the diffusive mechanism in almost all directions, where most of the Peclet values were less than unity indicating the dominance of diffusive mixing over its convective counterpart. However, it can be observed that at an impeller rotational speed of 10 RPM mixing was almost equally controlled by both the convective and diffusive mechanisms in the z direction, with a slightly higher contribution from convective mixing. Moreover, Table 15 indicates that as the impeller rotational speed increased, the diffusivity coefficient increased in all directions accordingly. This result is in good agreement with the conclusions drawn from the investigations carried out in section 5.2.2.1 where increasing impeller rotational speed resulted in higher diffusivity coefficient values, which in turn produced lower RSD values and enhanced the overall mixing performance.

Table 15: Diffusivity coefficient and Peclet number results for 10 RPM, 40 RPM, and 70 RPM

| **Impeller rotational speed (RPM)** | $\boldsymbol{D_{xx}}\left(\frac{\boldsymbol{m^2}}{\boldsymbol{s}}\right)$ | $\boldsymbol{D_{yy}}\left(\frac{\boldsymbol{m^2}}{\boldsymbol{s}}\right)$ | $\boldsymbol{D_{zz}}\left(\frac{\boldsymbol{m^2}}{\boldsymbol{s}}\right)$ | $\boldsymbol{Pe_{xx}}$ | $\boldsymbol{Pe_{yy}}$ | $\boldsymbol{Pe_{zz}}$ |
|---|---|---|---|---|---|---|
| **10** | 2.8E-05 | 2.1E-04 | 1.6E-04 | 0.23 | 0.87 | 1.1 |
| **40** | 2.0E-04 | 1.1E-03 | 8.0E-04 | 0.01 | 0.04 | 0.08 |
| **70** | 6.0E-04 | 1.8E-03 | 1.8E-03 | 0.01 | 0.12 | 0.06 |

# Chapter 6: Assessment of bi-disperse solid particles mixing in a horizontal paddle mixer through experiments and discrete element method (DEM)

## 6.1 Introduction

The purpose of this section was to systematically examine the mixing performance of a horizontal agitated paddle blender for a bi-disperse system composed of particles with a diameter of 3 mm and 5 mm by using DEM simulations and experiments. For this investigation the LIGGGHTS(R)-PUBLIC 3.3.1 open source computational software was used for all simulations. The DEM model was validated by comparing the simulation results with experimental data obtained through a direct sampling method (thief probe) [39-40]. Subsequently, the validated DEM model was used to perform simulations in order to study the effect of critical operating parameters on the degree of mixing. These parameters included three impeller rotational speeds (i.e. 40, 70, 100 RPM), three vessel fill levels (i.e. 40, 50, 60 %), and particle number composition. Additionally, the influence of particle loading arrangement (i.e. TB, FB) on the RSD values were examined. The TB arrangement included two patterns based on a bi-disperse mixture of 3 mm (top/bottom) and 5 mm (top/bottom) particles. The FB arrangement was constructed by placing the 3 mm particles in front and the 5 mm particles in the back of the vessel. All of the aforementioned particle loading arrangements were defined relative to the front view of the vessel. The Relative Standard Deviation (RSD) mixing index was used to evaluate the degree of mixing. In addition, the mixing mechanisms were analyzed by using the Peclet numbers, and particle diffusivities obtained from simulations.

## 6.2 Results and discussion

### 6.2.1 Model validation

The DEM model validation using the experimental data is explained in this subsection. An initial set of experiments outlined in Section 3.2 were performed in order to validate the DEM model. As mentioned previously, the conditions selected for the experimental run consisted of spherical glass beads with diameters of 3 mm and 5 mm, impeller rotational speed of 40 RPM, vessel fill level of 40%, and the TB particle loading arrangement. LIGGGHTS-PUBLIC 3.3.1 open source software was used to develop a DEM model representing the aforementioned experimental conditions. The simulation input parameters presented in Table 16 were extracted from Margio et al. [73] since the particle, impeller, and vessel materials were found to be similar to the ones utilized for this investigation. After performing an extensive sensitivity analysis on the input parameters used for the simulation model it was concluded that the coefficient of static friction was the most sensitive parameter. Therefore, a calibration procedure was carried out on the aforementioned parameter to obtain an optimum value which would produce RSD results in close agreement with the experimental results. The optimum value for the coefficient of static friction was found to be 0.1. A summary of the procedure for setting up and executing the DEM simulation is presented in Table 17. The RSD results from the experiment and simulation are depicted in Figure 24. As seen from Figure 24, there is a very close agreement between the experimental and simulation results.

Table 16: Simulation input parameters for bi-disperse investigation

| Simulation input parameters | Values |
|---|---|
| **Shear modulus for particle (*Pa*)** | 7.0e6 |
| **Shear modulus for wall (*Pa*)** | 3.0e9 |
| **Poisson's ratio for particle** | 0.3 |
| **Poisson's ratio for wall** | 0.3 |
| **Particle diameter (*mm*)** | 3, 5 |
| **Particle density** $\left(\frac{kg}{m^3}\right)$ | 2500 |
| **Coefficient of restitution (particle-particle)** | 0.75 |
| **Coefficient of restitution (particle – wall)** | 0.75 |
| **Coefficient of static friction (particle – particle)** | 0.1 |
| **Coefficient of static friction (particle – wall)** | 0.35 |
| **Coefficient of rolling friction (particle – particle)** | 0.01 |
| **Coefficient of rolling friction (particle – particle)** | 0.005 |

Table 17: Simulation model development conditions and procedure

| | | |
|---|---|---|
| **Total number of particles** | 146,000 (40 % vessel fill level) | 120,000 (3 mm particles) ~ 80 %<br>26,000 (5 mm particles) ~ 20 % |
| **Particle loading arrangement** | TB arrangement | 5 mm particles (bottom)<br>3 mm particles (top) |
| **Impeller rotational speed** | 40 RPM | Impellers rotated for 20 seconds of simulation time. |
| **Simulation time step** | 2.886e-05 seconds | Equivalent to 30 % of Rayleigh's time. |
| **Data extraction method** | 6 samples – similar to section 2.0 | Samples extracted at the end of four mixing times (i.e. every 5 seconds) for total of 20 seconds. |
| **Mixing quantification method** | RSD | RSD values were calculated based on the number of 3 mm particles and total number of particles within each sample. |

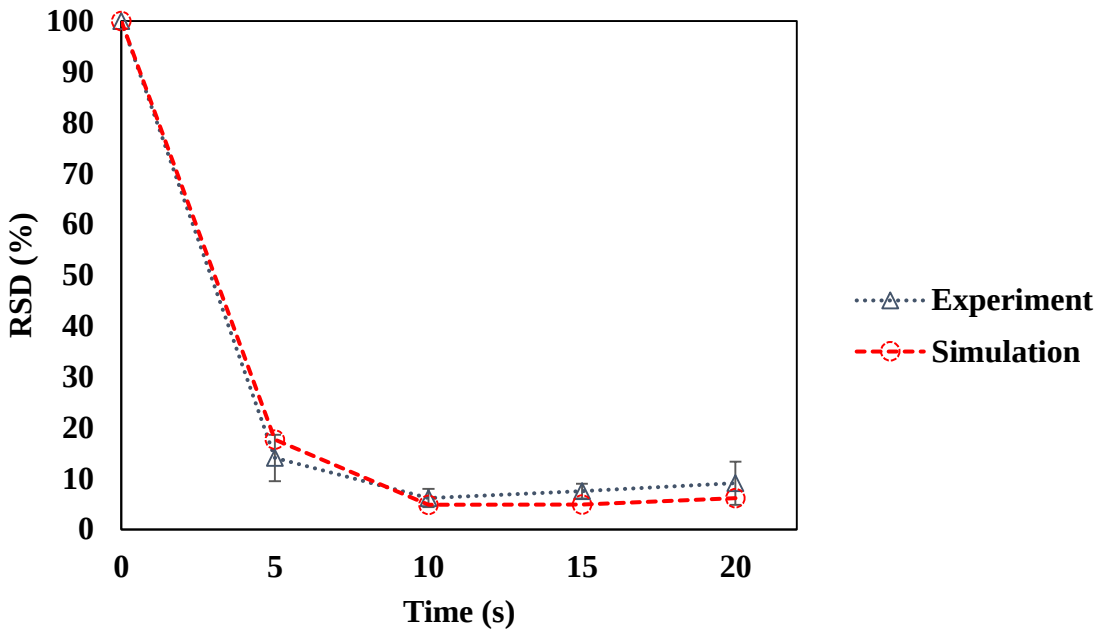


Figure 24: Model validation for 40 RPM, 40% vessel fill level, TB particle loading arrangement, 3 mm and 5 mm spherical particles.

Additionally, a comparison was made between the simulation results obtained from EDEM 2.7 and LIGGGHTS-PUBLIC 3.3.1 for the simulation case outlined above (refer to Figure 24). Figure 25 shows the RSD results obtained from EDEM and LIGGGHTS simulation software. Figure 25 indicates that there is an insignificant discrepancy between the RSD results found from LIGGGHTS and EDEM. This result shows that both computational platforms produce results in close agreement to one another. The LIGGGHTS numerical software however was selected for this section.

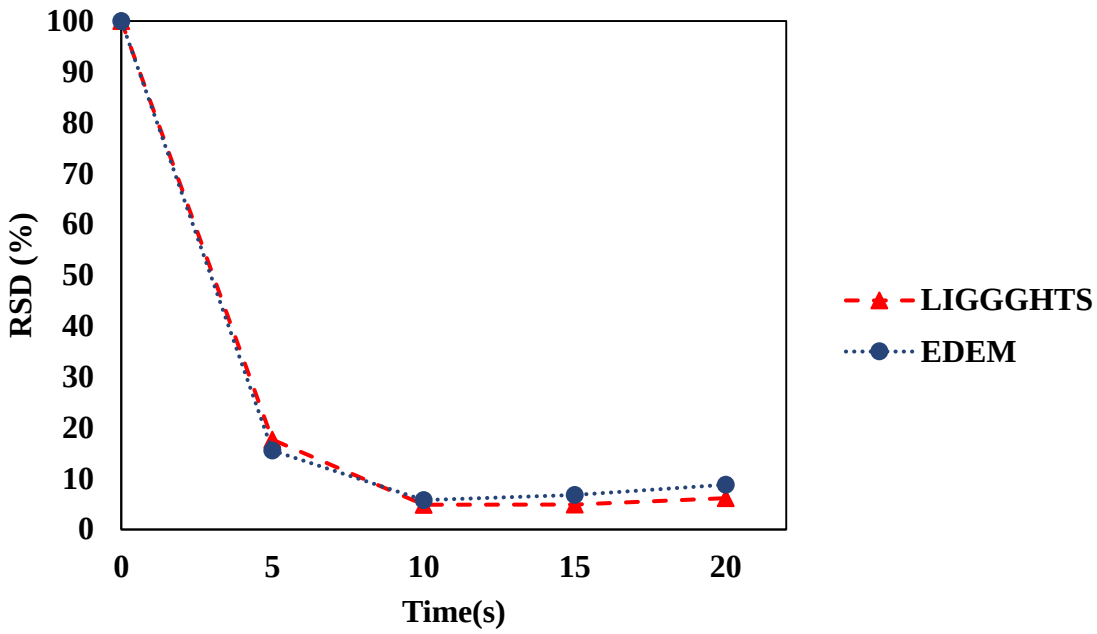


Figure 25: Comparison of simulation results between EDEM and LIGGGHTS software.

### 6.2.2 Mixing kinetics

In this section, initially the effect of impeller rotational speed, vessel fill level, and particle loading arrangement on the mixing kinetics of a bi-disperse mixture was analyzed. Similar to experiments the volume proportionality factor for both types of particles were fixed at 0.5, which corresponded to number composition of 80% of 3 mm and 20% of 5 mm particles inside a horizontal agitated paddle blender. The effect of number composition on the mixing quality will be covered in section 6.2.4.

#### *6.2.2.1 The effect of operating parameters for 80% 3 mm – 20 % 5 mm bi-disperse mixture*

Figure 26 depicts the influence of impeller rotational speed on RSD values for 80% 3-mm and 20% 5-mm bi-disperse mixture. Figure 26 corresponds to the simulation results for the TB arrangement at various vessel fill levels of 40% (~ 146000 particles), 50% (~182400 particles), and 60% (~ 219000 particles), respectively.

(a)

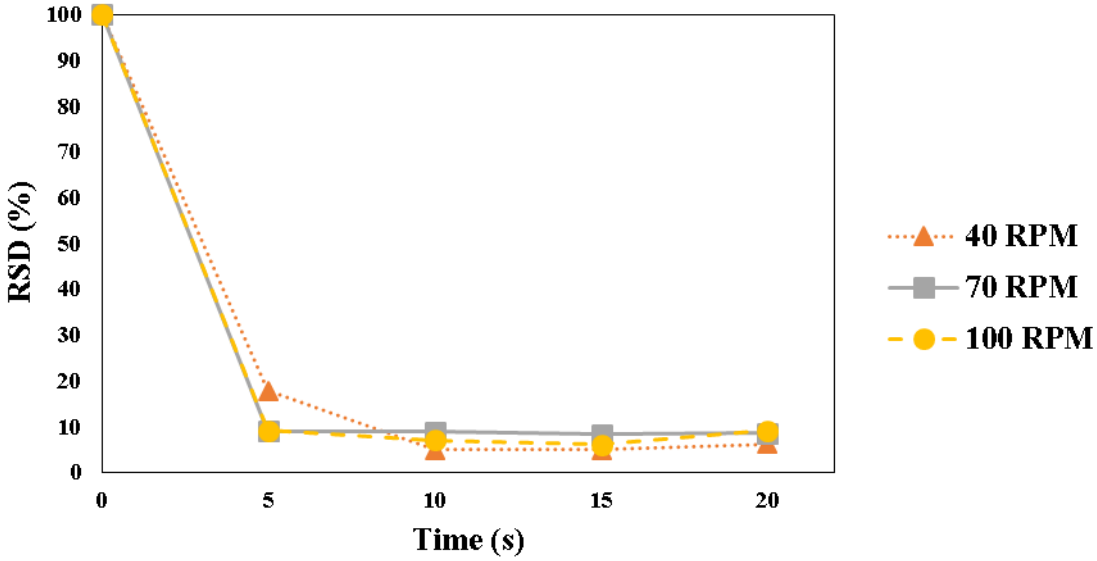
RSD (%)
100
90
80
70
60
50
40
30
20
10
0
0
5
10
15
20
Time (s)
40 RPM
70 RPM
100 RPM

(b)

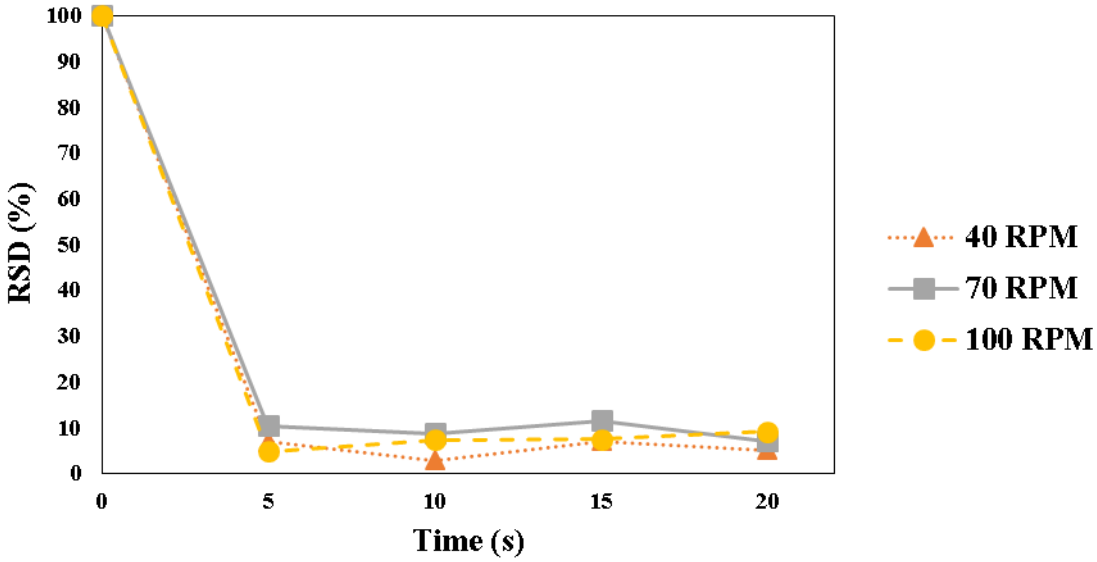
RSD (%)
100
90
80
70
60
50
40
30
20
10
0
0
5
10
15
20
Time (s)
40 RPM
70 RPM
100 RPM

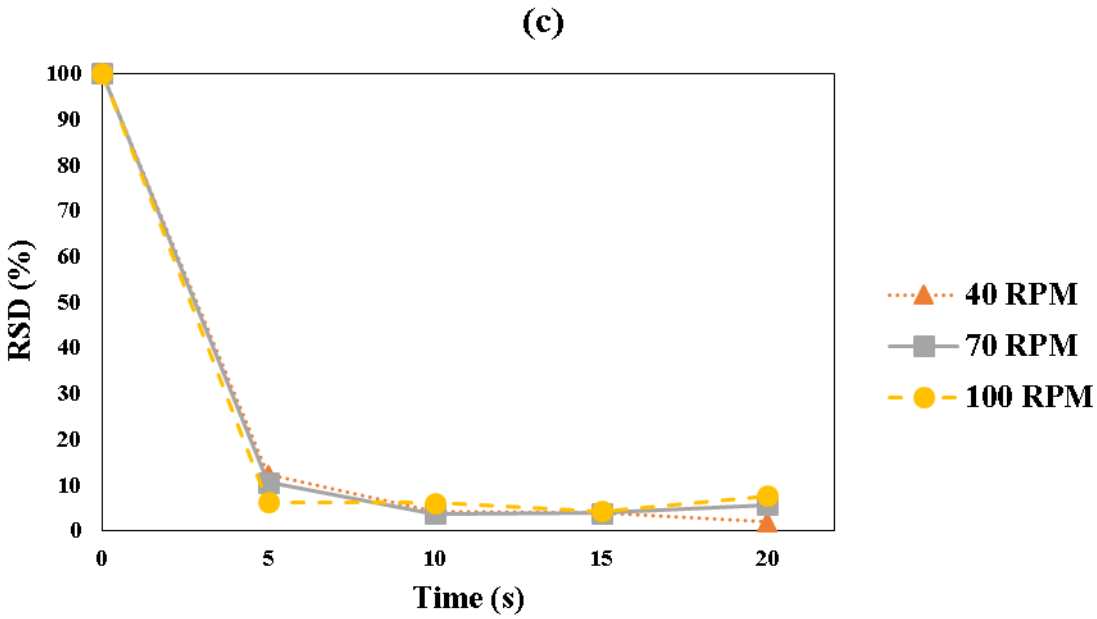


Figure 26: The effect of impeller rotational speed on RSD %, for (a) 40%, (b) 50%, (c) 60% vessel fill level, TB loading arrangement, and 80 % 3 mm – 20 % 5mm bi-disperse mixture.

The results from Figure 26 indicate that regardless of the vessel fill level implemented for the TB loading arrangement as the impeller rotational speed was increased from 40 RPM to 70 RPM and subsequently to 100 RPM the RSD values did not change significantly. Moreover, it can be concluded that the mixing performance observed in Figure 26 is relatively high since the RSD values fall within the ~ 2-12% range. Therefore, indicating that segregation did not occur for this mixture. The same result was also observed for the FB loading arrangement for which the impeller rotational speed did not have a significant impact on the RSD values. However, for the sake of brevity only the TB results were presented for all parametric studies in this section.

Figure 27 depicts the influence of vessel fill level on RSD values for 80% 3-mm and 20% 5-mm bi-disperse mixture. Figure 27 represents the simulation results for the TB arrangement at various impeller rotational speeds of 40, 70, and 100 RPM.

(a)

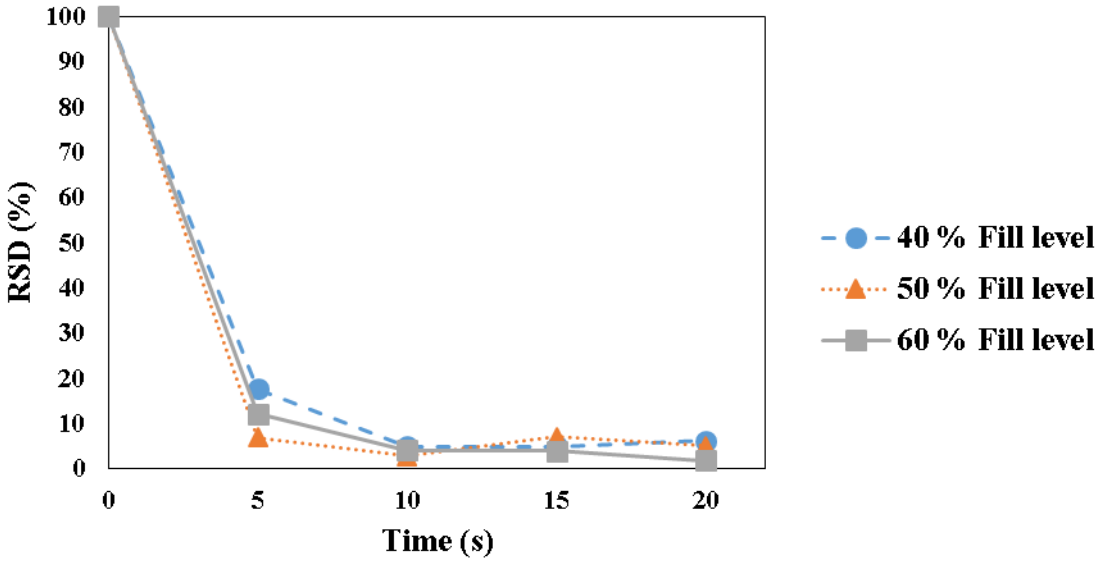
RSD (%)
100
90
80
70
60
50
40
30
20
10
0
0
5
10
15
20
Time (s)
40 % Fill level
50 % Fill level
60 % Fill level

(b)

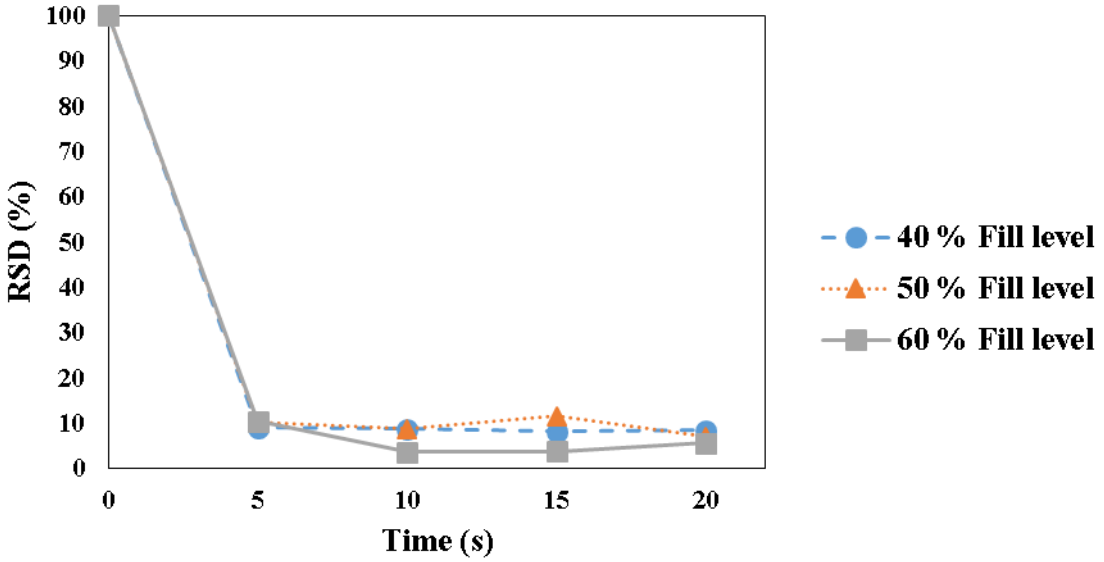
RSD (%)
100
90
80
70
60
50
40
30
20
10
0
0
5
10
15
20
Time (s)
40 % Fill level
50 % Fill level
60 % Fill level

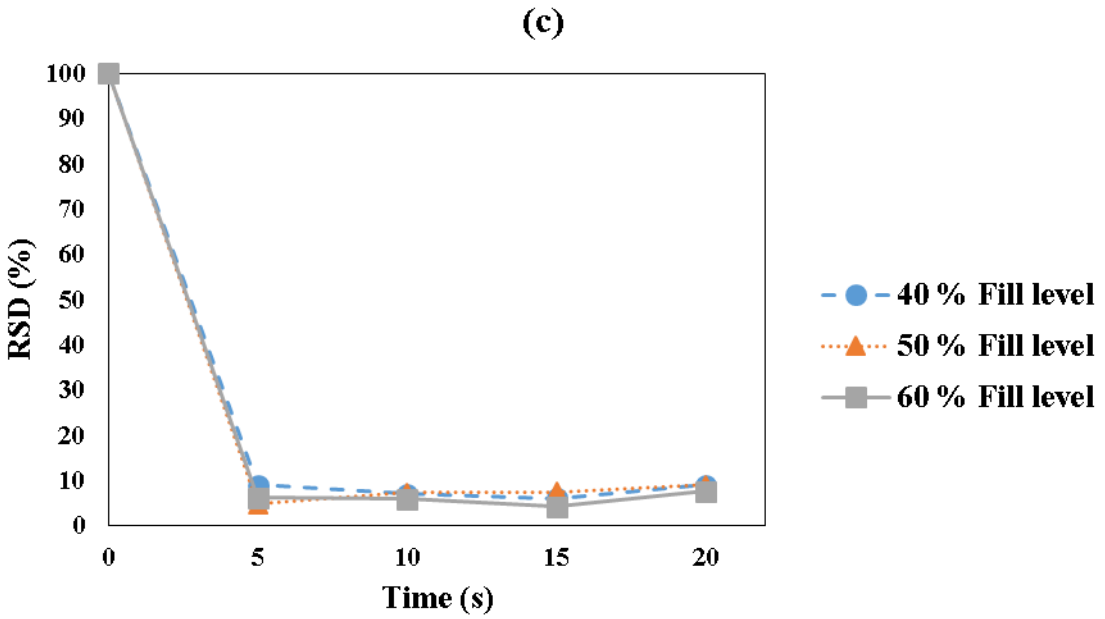


Figure 27: The effect of vessel fill level on RSD %, for (a) 40 RPM, (b) 70 RPM, (c) 100 RPM, TB loading arrangement, and 80 % 3 mm – 20 % 5 mm bi-disperse mixture.

Similar to the results obtained for the previous analysis, the simulation results shown in Figure 27 indicate that for any given impeller rotational speed increasing the vessel fill level from 40% to 50% and subsequently to 60 % did not significantly affect the mixing performance of the blender for the TB loading arrangement. Moreover, the final mixing quality at 20 seconds of mixing in all cases depicted in Figure 27 were found to be uniform and relatively equal to one another.

Initially the RSD results for each mixing time (i.e. 5, 10, 15, 20 seconds) for both TB and FB were thoroughly analyzed to understand the influence of particle loading arrangement on the mixing performance. However, no consistent and conclusive trend was observed. Therefore, illustrating that the particle loading arrangement did not play an instrumental role on the final mixing quality.

From the results presented in this section it can be concluded that, for the studied cases, there must be another dominant parameter, which controls the mixing kinetics rather than impeller rotational

speed, vessel fill level, or particle loading arrangement. Therefore, it was proposed that a possible controlling parameter could be the particle number composition, which was further investigated in section 6.2.4.

### 6.2.3 Qualitative mixing assessment for 80% 3 mm – 20% 5 mm bi-disperse mixture

A qualitative assessment of mixing performance was carried out for the mixing of bi-disperse particles within a horizontal agitated paddle blender. The operating conditions for the selected simulation run consisted of an impeller rotational speed of 40 RPM, vessel fill level of 60%, and the TB particle loading arrangement. The captured images from the simulation results shown in Figure 28 were taken at 5, 10, and 20 seconds of mixing, respectively. The aforementioned mixing times were selected in order to clearly capture the significant mixing trends taking place. Figure 28 represents the qualitative results with respect to the side view of the blender. Images were constructed by slicing the blender on a plane normal to the *x*-direction (refer to Figure 10) at the center of the vessel. Figure 28 shows that as mixing progressed from 5 to 20 seconds, a more uniform mixture was observed. Therefore, indicating that mixing was enhanced. This result also confirms the trend illustrated in Figure 26-c where the RSD result at 5 seconds of mixing was slightly higher than RSD values at 10 seconds, 15 seconds, and 20 seconds of mixing. The aforementioned results show that no segregation took place for this specific bi-disperse system. However, other investigations performed on bi-disperse systems have reported fast segregation mechanisms in various powder blenders [66-67].

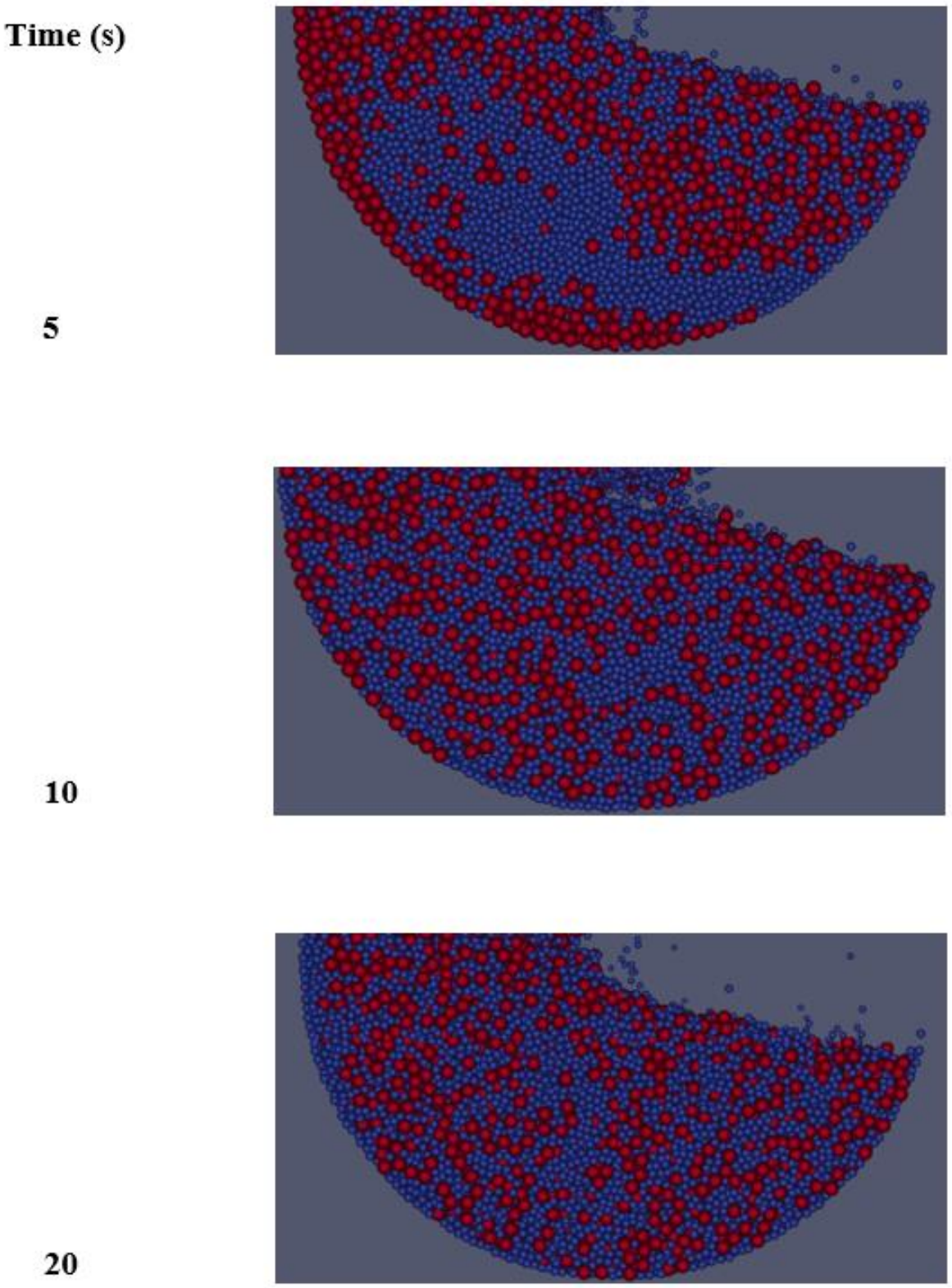


Figure 28: Mixing in bi-disperse system, 3 and 5 mm particles, 60% vessel fill level, 40 RPM impeller rotational speed, and TB particle loading arrangement (side view).

### 6.2.4 The effect of particle number composition

The results from the analysis in section 6.2.2.1 showed that impeller rotational speed, vessel fill level, and particle loading arrangement did not significantly influence the mixing performance of the Paddle blender containing 80% 3 mm – 20% 5 mm bi-disperse mixture. Therefore, in this section the effect of particle number composition on the RSD values was assessed. Figure 29 represents the simulation results for the TB arrangement, and impeller rotational speed of 40 RPM at various particle number compositions. It can be seen that increasing the number of smaller particles (3 mm) or decreasing the number of larger particles (5 mm) significantly enhanced the mixing performances of this blender. From the results obtained in section 6.2.2.1 and Figure 29, one can conclude that the mixing performance for the selected bi-disperse mixture is highly sensitive towards the number composition of the particles. Therefore, to minimize the dominant effect of particle composition on the RSD values, the least unbiased particle number composition (50% 3 mm – 50% 5 mm) was selected to perform a parametric investigation on the mixing performance.

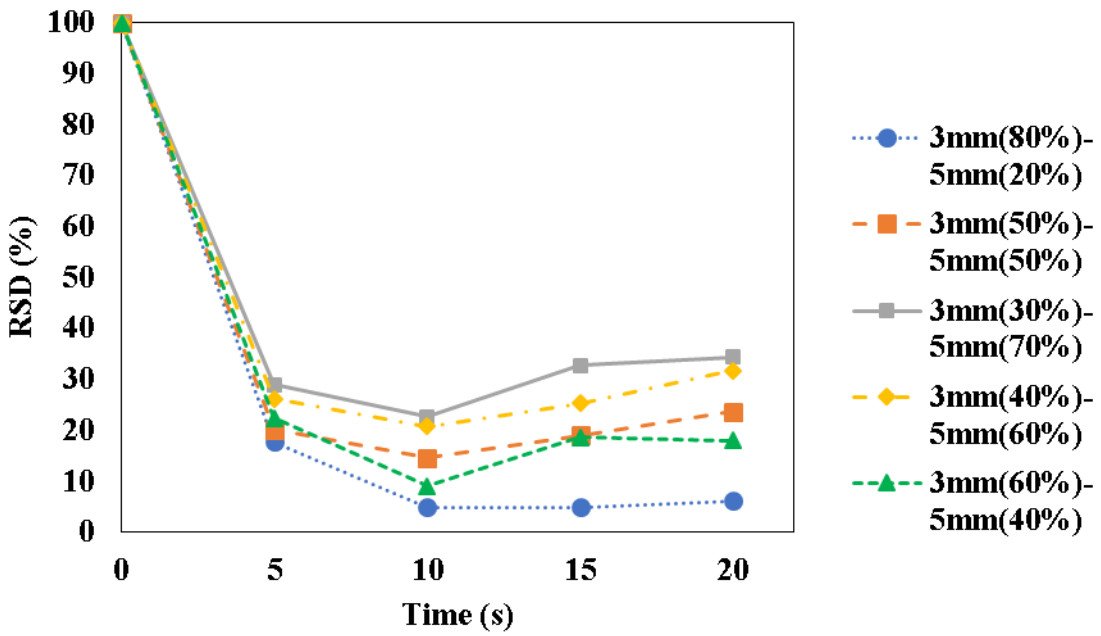


Figure 29: The effect of particle number composition on RSD% for, 3 mm - 5 mm bi-disperse mixture, 40 RPM, 40% vessel fill level, and TB loading arrangement.

### 6.2.5 The effect of operating parameters for 50% 3 mm – 50% 5 mm bi-disperse mixture

Figure 30 illustrates the impact of impeller rotational speed on RSD values for 50% 3 mm – 50% 5 mm bi-disperse mixture. Figure 30 corresponds to the simulation results for the TB arrangement at various vessel fill levels of 40% (~ 85281 particles), 50% (~ 106600 particles), and 60% (~ 127920 particles), respectively. Figure 30 indicates that regardless of the vessel fill level used for the TB particle loading arrangement, implementing an impeller rotational speed of 40 RPM yielded a better overall mixing performance than utilizing an impeller rotational speed of 70 RPM. For an impeller rotational speed of 70 RPM a higher amount of energy was transferred to the particle assembly when compared to 40 RPM. This may have intensified the segregation in the system leading to higher RSD values. The segregation can be seen as a sharp increase in the RSD

values as time progresses for 70 RPM. No conclusive trend has been observed for the effect of 100 RPM on the mixing performance.

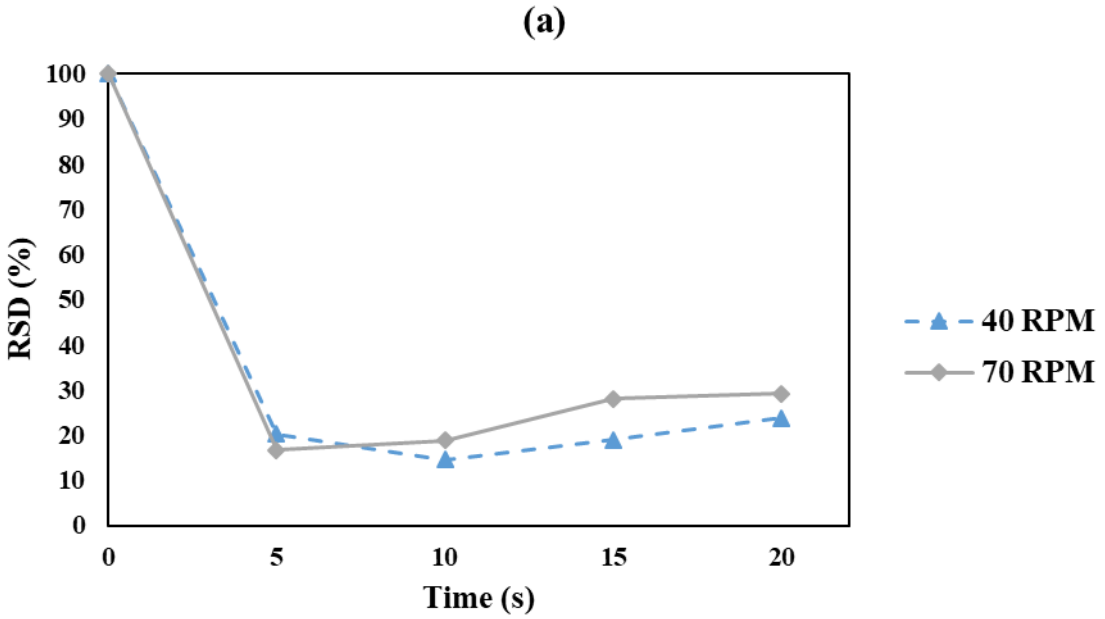


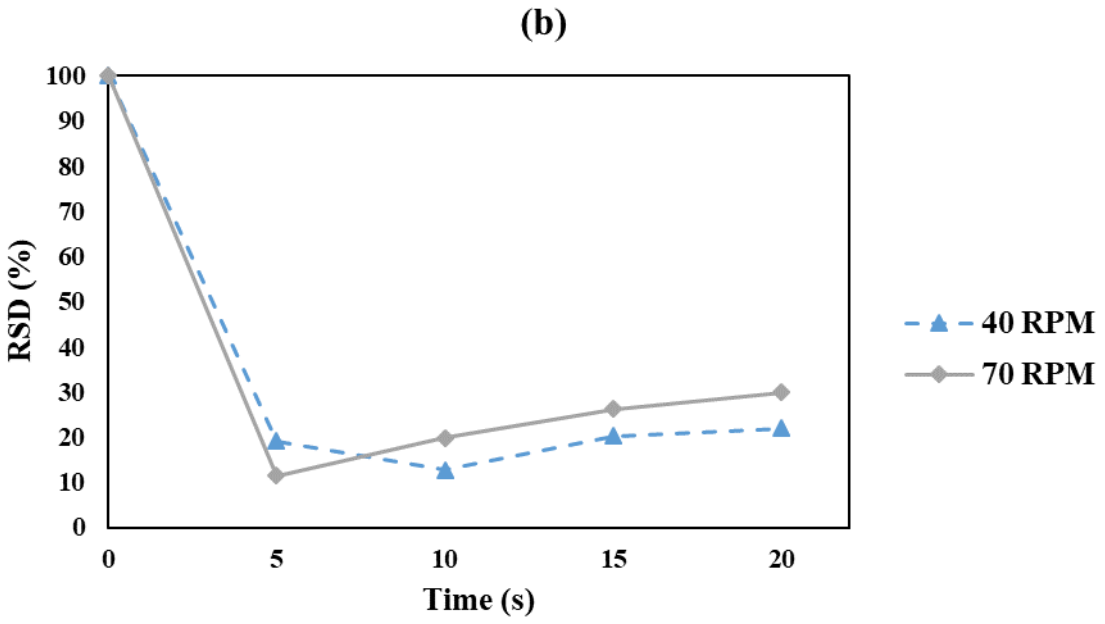

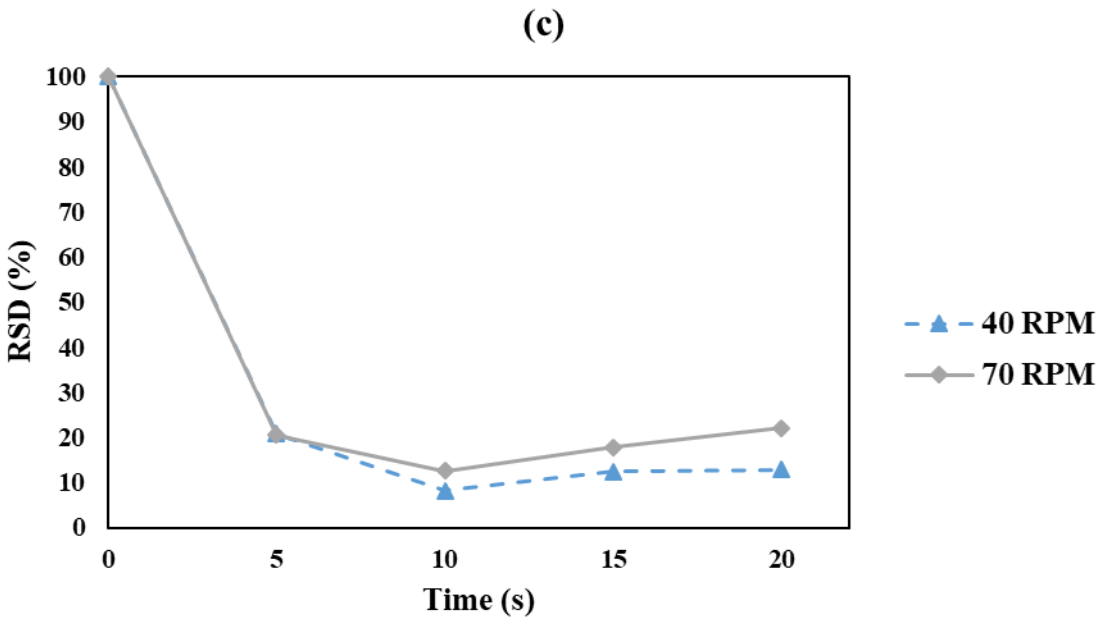


Figure 30: The effect of impeller rotational speed on RSD %, for (a) 40%, (b) 50%, (c) 60% vessel fill level, TB loading arrangement, and 50 % 3mm – 50 % 5mm bi-disperse mixture.

Figure 31 depicts the effect of vessel fill level on RSD values for 50% 3 mm – 50% 5 mm bi-disperse mixture. Figure 31 represents the simulation results for the TB arrangement at various impeller rotational speeds of 40, and 70. Figure 31 indicates that for TB arrangement, and impeller rotational speeds of 40, and 70 RPM increasing the vessel fill level from 40% to 60% enhanced the mixing performance. However, the mixing performance of the system did not change when the vessel fill level was increased from 40% to 50% regardless of the impeller rotational speed applied. Similar to the previous analysis no conclusive trend was observed for studying the effect of vessel fill level when the impeller rotational speed was set to 100 RPM.

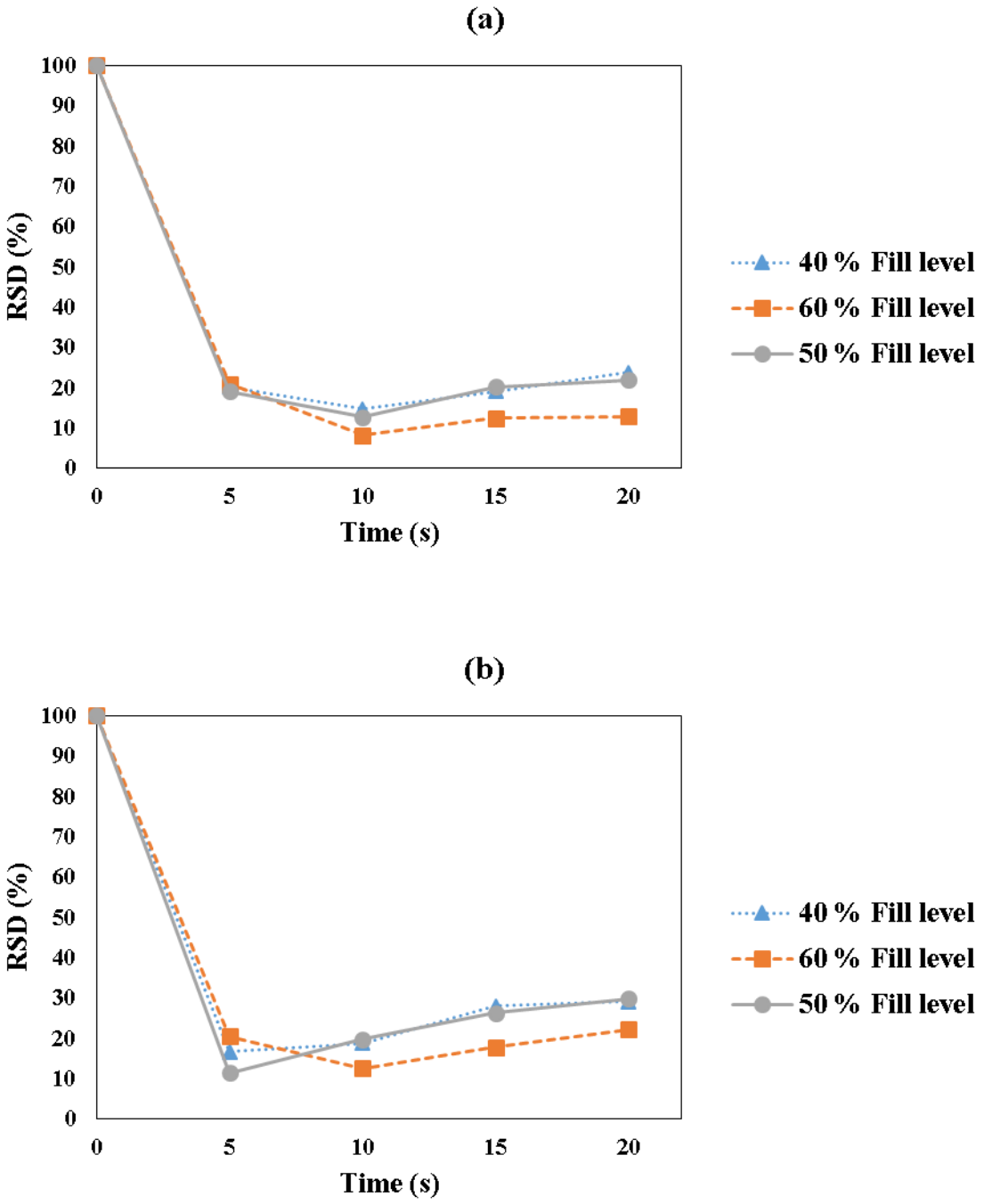


Figure 31: The effect of vessel fill level on RSD %, for (a) 40 RPM, (b) 70 RPM, TB loading arrangement, and 50% 3 mm – 50% 5 mm bi-disperse mixture.

In almost all bi-disperse particle mixtures segregation is highly dependent on the number and position of the mixing components. Therefore, it was decided to investigate the impact of alternative particle placements for the TB loading arrangement on the mixing performance.

### 6.2.6 The effect of alternative TB particle loading arrangements

As mentioned in the previous sections all experimental and simulation runs were performed by incorporating the 3 mm particles on top and the 5 mm particles on bottom for the TB loading arrangements. In this section however, the effect of alternative particle loading arrangements for the TB arrangement is examined on the RSD%. This parameter has also been investigated by Alchikh-Sulaiman et al. (2015). In the alternative particle arrangement, 3 mm particles were loaded at the bottom and 5 mm particles were placed on top. Figure 32 compares the simulation results for the two TB arrangements, where vessel fill level was set to 40% and an impeller rotational speed of 40 was applied. This specific impeller speed was selected since it was concluded from the previous analysis that it provided the highest mixing performance. Figure 32 illustrates that for an impeller rotational speed of 40 RPM, implementing the 3 mm (top) – 5 mm (bottom) loading arrangement provided better mixing when compared to the 3 mm (bottom) – 5 mm (top) alternative pattern. As mentioned previously, due to the sieving phenomenon, the larger particles tend to move toward the top of the mixing system while the smaller particles often mobilize towards the bottom region. As shown in Figure 32 (at 10 and 15 seconds) for the simulation run in which the 5 mm particles were initially loaded on top the mixing performance as expected was significantly lower than the case in which the 5 mm particles were initially loaded on the bottom. This result could be related to the fact that for the arrangement in which the larger 5 mm particles were loaded at the bottom, the initial (10 seconds) movement of the 5 mm particles towards the top region of the bed

improved the mixing performance. However, as mixing progressed (15 seconds) segregation took place. After 20 seconds of mixing both arrangements showed the same RSD values.

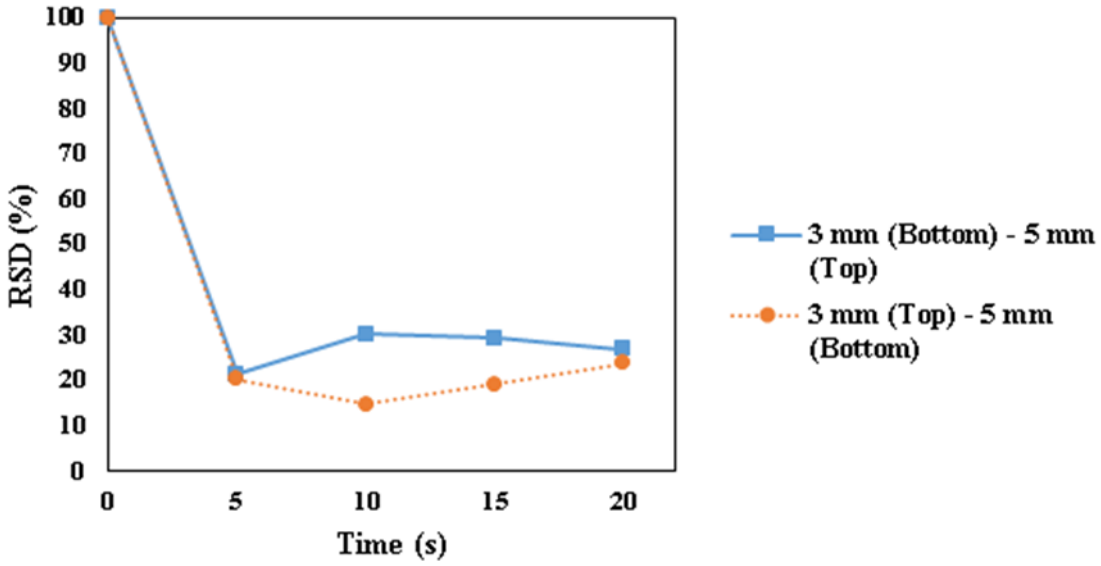


Figure 32: The effect of particle loading pattern on RSD % for 40 RPM, 40 % vessel fill level, TB loading arrangement, and 50% 3 mm – 50% 5 mm bi-disperse mixture.

In addition, a qualitative comparison was performed for the simulation run outlined in Figure 32. Figure 33 depicts captured images at 10, 15, and 20 seconds of mixing at particle loading patterns of 3 mm (top) – 5 mm (bottom). The images were constructed by slicing the blender on a plane normal to the *x*-direction (refer to Figure 10) at the center of the vessel. The results from Figure 33 validates the results from Figure 32 which illustrated that at 10 of mixing segregation occurred where the larger particles mobilized towards the top region of the bed and the smaller particles moved to the bottom region of the bed. This segregation phenomenon intensifies as mixing

progresses (15, 20 seconds) which also validates the increase in RSD values observed in Figure 32.

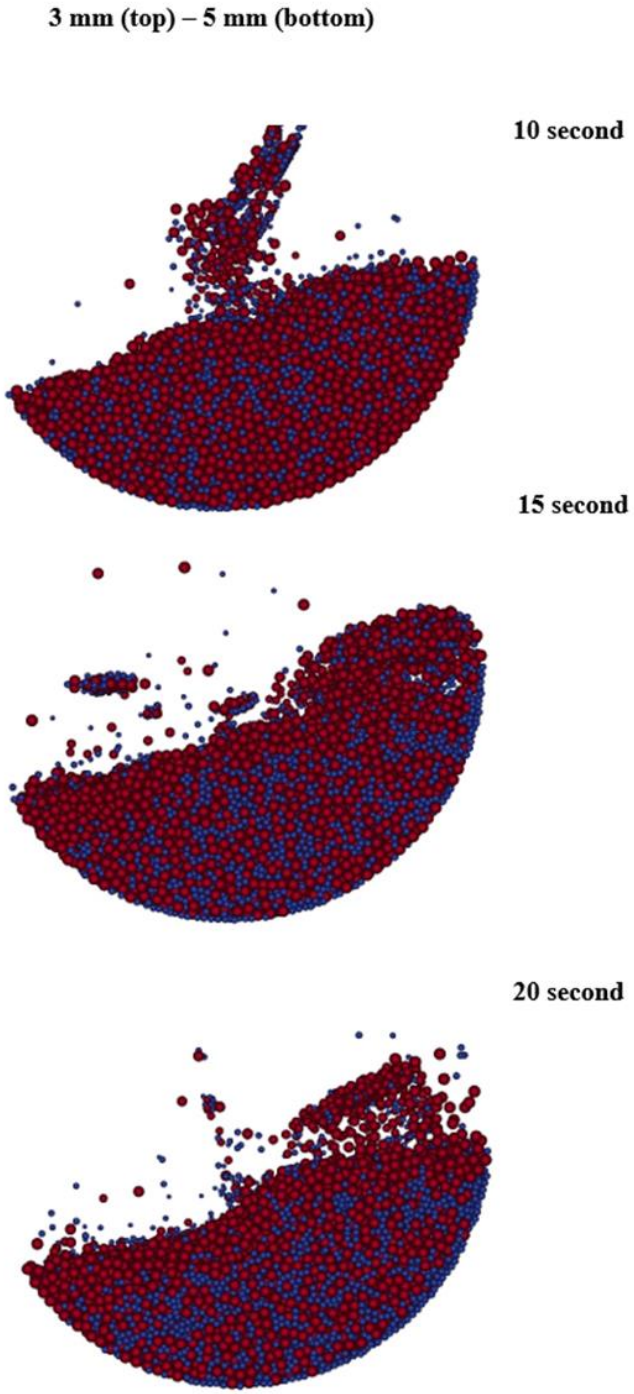


Figure 33: Qualitative assessment of mixing for 40 RPM, 40 % fill level, TB loading arrangement, and 50 % 3mm - 50 % 5 mm bi-disperse mixture.

### 6.2.7 Diffusivity coefficient and Peclet number

The flow of particles can be quantified based on their microscopic properties by determining the particle diffusivities (Remy et al., 2016). Particle diffusivity measures the mass flux rate of particles induced by random motion. This property is defined by:

$$D_{fg} = \frac{\langle \left(\Delta x_f - \overline{\Delta x_f}\right)\left(\Delta x_g - \overline{\Delta x_g}\right)\rangle}{2\Delta t} \tag{19}$$

where, $\Delta x_f$ represents the particle displacement in the $f$ direction relative to particle's initial position, $\overline{\Delta x_f}$ represents the mean particle displacement of all particles in the system during Δt, and $D_{fg}$ represents particle diffusivity in the $f$ direction due to gradient in $g$ direction (Remy et al., 2011). $\Delta t$ of $\frac{1}{4}$ of a revolution was chosen for the diffusivity calculations. This selection was done based on a comprehensive testing procedure where various time intervals were incorporated in order to examine the changes observed on the resulting diffusivity values. As a result, it was determined that reducing the time interval to values less than $\frac{1}{4}$ of a revolution did not affect the calculated diffusivity value. The convective and diffusive contributions to particle motion were evaluated by calculating the Peclet number defined by:

$$Pe_{fg} = \frac{U_f R}{D_{fg}} \tag{20}$$

where $U_f$ is the average particle velocity in the $f$ direction and $R$ is the mixer radius. The operating conditions for the selected simulation runs consisted of 40% vessel fill level, TB particle loading arrangement, and 50% 3 mm – 50% 5 mm bi-disperse mixture. The particle diffusivity and Peclet number results for simulation runs corresponding to 40, and 70 RPM are summarized in Table 18. From Table 18 it becomes clear that for all impeller speeds the dominant mixing mechanism was found to be diffusive mixing (in any given direction). As all Peclet values in Table 18 are less than

unity, which signifies the dominance of the diffusive mechanism over convection. From Table 18 it becomes clear that as the impeller rotational speed was increased from 40 RPM to 70 RPM the diffusivity coefficient values increased accordingly. Therefore, higher diffusivity coefficient values could have intensified the sieving segregation mechanism which explains the inferior mixing performance obtained while using an impeller rotational speed of 70 RPM.

Table 18: Diffusivity coefficient and Peclet number results for 40 RPM, and 70 RPM for 50% 3 mm – 50% 5 mm mixture

| **Impeller rotational speed (RPM)** | $\boldsymbol{D_{xx}}\left(\frac{m^2}{s}\right)$ | $\boldsymbol{D_{yy}}\left(\frac{m^2}{s}\right)$ | $\boldsymbol{D_{zz}}\left(\frac{m^2}{s}\right)$ | $\boldsymbol{Pe_{xx}}$ | $\boldsymbol{Pe_{yy}}$ | $\boldsymbol{Pe_{zz}}$ |
|---|---|---|---|---|---|---|
| **40** | 2.65e-04 | 1.10e-03 | 5.89e-04 | 0.059 | 0.023 | 0.175 |
| **70** | 7.92e-04 | 1.60e-03 | 1.50e-03 | 0.272 | 0.009 | 0.148 |

# Chapter 7: Conclusion and recommendations

The performance of an agitated Paddle blender was investigated for mono-disperse and bi-disperse particles through experiments and DEM simulations. The DEM model was validated using series of experimental data obtained by the thief sampling technique. The results from the experiments and simulations were found to be in good agreement with one another. The performance of the Paddle mixer was then evaluated by studying the influence of impeller rotational speed, vessel fill level, particle loading arrangement, and particle number composition on the RSD index through simulations.

## 7.1 Mono-disperse investigation

The flow pattern of particles was examined and quantified by using granular temperature, diffusivity coefficient and Peclet number. The simulation results indicated that for any given particle loading arrangement, for vessel fill levels of 40% and 50 % as the impeller rotational speed was increased from 10 RPM to 70 RPM the RSD indices were reduced and better mixing was achieved. For vessel fill level of 60%, however, as the impeller rotational speed was increased from 40 RPM to 70 RPM the mixing quality was not affected significantly.

For all impeller rotational speeds and TB arrangement, it was concluded that changing the vessel fill level from 40% to 50% did not significantly affect the mixing quality. However, at 10 RPM, TB arrangement and 60% vessel fill level, RSD values decreased significantly after 10 seconds of mixing. For impeller rotational speeds of 40 RPM, 70 RPM, TB arrangement, and 60% vessel fill level the mixing performance did not change. For the FB arrangement, it was observed that at impeller rotational speeds of 40 RPM and 70 RPM changing the vessel fill level from 40% to 60% did not influence the mixing quality. At 10 RPM on the other hand changing the vessel fill level

from 40% to 50% enhanced the mixing performance during the initial 5 seconds of mixing. In addition, changing the vessel fill level from 50% to 60% resulted in minor changes on the RSD values. For vessel fill levels of 40% and 50 %, generally the FB arrangement produced a higher degree of uniformity within the mixture at 20 seconds of mixing time. In general, for vessel fill level of 60 %, better mixing was obtained through the TB arrangement. The ANOVA showed that impeller rotational speed had the strongest effect on the extent of mixing, followed by the interaction between the vessel fill level and particle loading arrangement, and particle loading arrangement accordingly.

The granular temperature data showed that as the impeller rotational speed increased the chaotic motion of particles increased accordingly. This behaviour was found to be in good agreement with the RSD values where increasing the impeller rotational speeds resulted in improved mixing performance. Maximum granular temperature values were obtained at the corner edges of the paddle blades for impeller rotational speeds of 10 RPM and 40 RPM. For 70 RPM the maximum granular temperature values were reached near the tip of the blades, where the values obtained for the corner edges and the center of the blades did not differ considerably. The Peclet number and diffusivity coefficient calculated from simulations indicated that in almost all cases the dominant mixing mechanism within this system was diffusion. In addition, as the impeller rotational speed was increased the diffusivity coefficients were increased in all directions. This observation is in good agreement with results obtained in the mixing kinetic section. An increase in impeller rotational speed resulted in the amplification of the diffusive mixing mechanism and therefore improved the mixing quality accordingly.

## 7.2 Bi-disperse investigation

The mixing performance of a horizontal agitated paddle blender was investigated for the blending of bi-disperse particles through experiments and DEM simulations. This was done by examining the effects of impeller rotational speed, vessel fill level, particle loading arrangement, and particle number composition on the RSD mixing index. Initially, the simulation model was validated by a test case experiment, where it was shown that the results from both simulation and experiment were in good agreement. Afterwards, the effect of the aforementioned operating parameters on the RSD index of a bi-disperse mixture consisting of a particle number composition of 80% 3 mm and 20% 5 mm particles was investigated. For this system, it was concluded that the selected parameters did not have a significant impact on the mixing performance. Moreover, the final mixture quality (RSD values at 20 seconds) did not change significantly for any given vessel fill level, impeller rotational speed, and particle loading arrangement. In addition, the RSD values and the qualitative assessment showed that segregation did not occur for this specific bi-disperse system. Therefore, the impact of various bi-disperse mixture compositions were studied on the mixing performance. It was concluded that increasing the number of smaller particles (3 mm) enhanced the mixing performance significantly. To offset the dominant influence of particle composition on the RSD values an unbiased particle number composition of 50%, 3 mm – 50%, 5 mm was selected. This mixture was then utilized to examine the impact of impeller rotational speed, vessel fill level, and particle loading arrangement on RSD mixing index. For any given vessel fill level and the TB loading arrangement, utilizing 40 RPM impeller speed provided better mixing when compared to 70 RPM impeller speed. For impeller speeds of 40, 70 RPM, and the TB loading arrangement (Top (3 mm) – Bottom (5 mm)), increasing the vessel fill level from 40% to 60% improved the mixing performance. For the simulation run with 40% vessel fill level, 40

RPM impeller rotational speed, and TB particle loading arrangement, placing the 3 mm particles on top and the 5 mm particles on bottom provided a higher mixing performance during the initial stages of mixing (10, 15 seconds) when compared to the alternative TB arrangement including 5 mm particles on top and the 3 mm particles on bottom. The Peclet number and particle diffusivity values illustrated that mixing was dominated by the diffusive mechanism in all directions.

## 7.3 Recommendations

Based on the results obtained from the mixing assessments performed on mono-disperse and bi-disperse particles in a horizontal paddle blender it was concluded that the DEM model was successful in predicating the experimental data accurately. Therefore, DEM modeling could be implemented in the following recommended investigations:

- Analyzing the effect of particle size on mixing kinetics, mixing mechanism of free-flowing particles in various applicable powder blenders.
- Developing a scale-up procedure for industrially applicable powder blenders.
- Assessing the effect of irregular particle shapes on the mixing kinetics and quality.
- Analyzing the impact of poly-disperse particle mixtures with various particle distributions on the mixing performance of relevant blenders.

# Appendices

## Appendix A: Procedure for installing and operating LIGGGHTS-PUBLIC simulation software, and Paraview visualization software.

Need to install 5 major components in order to execute and visualize particle simulations via LIGGGHTS numerical software:

1. Install the GNU C and GNU C++ compilers.
2. Install openmpi: parallel computation.
3. Install Paraview: post-processing visualization.
4. Install the LIGGHTS-PUBLIC software.
5. Install LPP: conversion of raw LIGGGHTS files to vtk format).
6. Load Point Sprite plugin: visualize realistic particle size in Paraview.

### Installing the GNU compiler and GNU C++ compiler

To install the gcc and g++ compilers, you will need the build-essential package. This will also install GNU make. Build-essential contains a list of packages which are essential for building Ubuntu packages including gcc compiler, make and other required tools.

Type the following commands in the terminal on UBUNTU:

*sudo apt-get update*

*sudo apt-get upgrade*

*sudo apt-get install build-essential*

*gcc -v*

*make -v*

Now, you should be able to compile software using C / C++ compilers.

### Installing openmpi

1. Make a directory and go into it by typing the following command in the terminal

    a. *mkdir openmpi*
    b. *cd openmpi*

2. Download OpenMPI from the openmpi website from the download section

a. Download the file name “openmpi-1.8.7.tar.gz” and save file.

3. Copy tar.gz file into the created folder by typing the following commands in the terminal under the *~/openmpi directory*:

    a. *cp ~/Downloads/openmpi-1.8.7.tar.gz .*

4. Now extract the file and go into it by typing the following commands in the terminal under the *~/openmpi directory*:

    a. *tar -xzvf openmpi-1.8.7.tar.gz*

5. go into the installed version directory by typing the following commands in the terminal under the *~/openmpi directory*:

    a. *cd openmpi-1.8.7/*

6. Configure and compile the files by typing the following commands in the terminal under the *~/openmpi/openmpi-1.8.7$ directory*:

    a. *./configure --prefix=$HOME/openmpi*

7. Type the following commands in the terminal under the *~/openmpi/openmpi-1.8.7$ directory*:

    a. *make all*

8. Type the following commands in the terminal under the *~/openmpi/openmpi-1.8.7$ directory to install*

    a. *make install*

9. Add OpenMPI to your PATH and LD_LIBRARY_PATH environment variable
   To do this type the following command in the terminal

   *gedit ~/.bashrc*

   Then add the two following commands to your .bashrc:

   *export PATH=$PATH:$HOME/openmpi/bin*

   *export LD_LIBRARY_PATH=$LD_LIBRARY_PATH:$HOME/openmpi/lib*

   Then type the following command in the terminal:

   *source ~/.bashrc*

10. Refer to the YouTube link for step by step instruction on how to install openmpi: https://www.youtube.com/watch?v=QIMAu_o_5V8

    You can also refer to the following link for a step by step written procedure on how to install openmpi:

    http://www.simunano.com/2015/07/how-to-install-openmpi.html

**Installing Paraview**

1. Type the following command in the terminal
    a. *Sudo apt-get install paraview*

2. If Point Sprite isn't working properly (radius of particles are not represented correctly). Need to update the graphics card driver. This is done by performing the following tasks

    a. go to <*system settings*> then <*software & Updates*> then <*Additional drivers*> then select proprietary driver then <*Apply changes*> then <*close*> restart computer.

**Installing LIGGGHTS-PUBLIC**

3. Type the following command line in the terminal

    b. *sudo apt-get install git*

    c. *git clone https://github.com/CFDEMproject/LIGGGHTS-PUBLIC.git $HOME/LIGGGHTS-PUBLIC*

4. If got clone does not work go to github and download the LIGGGHTS file manually, create a LIGGGHTS directory under home and place the downloaded zip file in there. Next unzip the file by typing the following command in the directory which contains the zip file. This action will unzip all zip files within the current folder.

    a. *unzip *.zip*

5. Install LIGGGHTS by typing the following commands in the terminal

    a. *sudo apt-get install liggghts*

    b. In the /src directory, type *make clean-all*, then *make fedora*

c. Type *gedit ~/.bashrc* in the terminal. Afterwards the bashrc file will open. Then type and add the following lines at the bottom of the file

*export PATH=$PATH:$HOME/bin*
*export PATH=/home/Ubuntu user name/LIGGGHTS/src/:$PATH*

d. Ubuntu user name: for example, when you open the terminal window the first name that appears before the @ sign is your corresponding Ubuntu user name.

6. Execute a simulation example for the paddle blender by performing the following tasks.

a. Create a directory called *paddleblender* within the following directory *~/LIGGGHTS-PUBLIC/examples/LIGGGHTS/Tutorials_public*

b. Create two directories called *Meshes and Post* within the following directory *~/LIGGGHTS-PUBLIC/examples/LIGGGHTS/Tutorials_public/paddleblender*

*c.* Place geometry CAD files in the *Meshes* directory. Make sure geometry files are in ASCII STL format. Binary STL formats are not compatible with LIGGGHTS. It is recommended to convert CAD files to ASCII STL format using *SALOME* software.

*d.* The CSV formatted simulation results are dumped in the *Post* directory. Make sure all previous dump files are deleted from the *Post* directory before executing a new simulation run.

*e.* Create a new document called *in.paddleblender* within the following directory.

*~/LIGGGHTS-PUBLIC/examples/LIGGGHTS/Tutorials_public/paddleblender*

This is the input script for the simulation to be carried out. Refer to appendix B. for detail description of the contents within the input script.

*f.* Execute the input script for the specified simulation by right clicking on the *paddleblender* directory and clicking on "*Open in Terminal".* This should take you to the following directory

*~/LIGGGHTS-PUBLIC/examples/LIGGGHTS/Tutorials_public/paddleblender*

*g.* Type the following command in the terminal
*mpirun –np 10 liggghts –in in.paddleblender*

- 10 corresponds to the number of processors declared for communication between processors which enables parallel computation. Refer to

LIGGGHTS manual for detail explanation of selecting the optimum number of processors.

**Installing LPP**

1. Create a directory called "*bin*" under the home directory.
2. Download lpp by typing the following command in the terminal.
    a. *sudo apt-get install python-numpy*
    b. *sudo git clone https://github.com/CFDEMproject/LPP.git $HOME/LPP*
    c. *gedit ~/.bashrc*
    d. *alias lpp="python $HOME/LPP/src/lpp.py"*
3. Install lpp by typing the following commands in the terminal.
    a. *cd LPP/*
    b. *./install.sh*

**Loading the PointSprite plugin for visualizing actual particle size in paraview**

1. Open Paraview.
2. Go to <*Tools*> then <*Manage plugins*>.
3. Select the PointSprite plugin and click on <*Load selected*> also check off the <*Auto Load*> box.
4. Close the plugin manager.
5. Initially you will need to execute your simulation, once before you can apply the PointSprite plugin to your particles.
6. Open the desired vtk files for the simulation under investigation in Paraview.
7. Select the file that corresponds to the **particle** simulation result under the pipeline browser.

8. Select <*Point Sprite*> under the <*Representation*> tab in the <*Properties*> section.

9. Click on <*Constant Radius*> tab under the <*Point Sprite section*> and change to <*radius*>.

10. Click on <*Edit Radius Transfer Function*> then check off the < *Proportional*> box.

Note: All procedures were accessed in the year of 2016.

## Appendix B: Sample LIGGGHTS input script for executing a simulation run

```
units           si
atom_style      sphere
atom_modify     map array sort 0 0
newton          off
communicate     single vel yes
processors      5 2 1

neighbor        0.012 bin
neigh_modify    delay 0

boundary    m m m
region          reg block -0.290 0.290 -0.109 0.109 -0.109 0.109 units box
create_box      3 reg

fix     1 all nve/sphere
fix     gravi all gravity 9.81 vector 0.0 0.0 -1.0

pair_style gran model hertz tangential history rolling_friction cdt
pair_coeff      * *

fix             m1 all property/global youngsModulus peratomtype 5.2e6 7.8e9 5.2e6
fix             m2 all property/global poissonsRatio peratomtype 0.3 0.3 0.3
fix             m3 all property/global coefficientRestitution peratomtypepair 3 0.75 0.75 0.75 0.75
0.75 0.75 0.75 0.75 0.75
fix             m4 all property/global coefficientFriction peratomtypepair 3 0.2 0.35 0.2 0.35 0.2
0.35 0.2 0.35 0.2
fix             m5 all property/global coefficientRollingFriction peratomtypepair 3 0.01 0.005
0.01 0.005 0.01 0.005 0.01 0.005 0.01

fix             impeller all mesh/surface file Meshes/Impellerreza.stl type 2 heal
auto_remove_duplicates scale 1.0  curvature 1e-05
fix             vessel all mesh/surface file Meshes/Vesselreza.stl type 2 heal
auto_remove_duplicates scale 1.0  curvature 1e-05
```

```
timestep        0.0000288664

fix             pts1 all particletemplate/sphere 1 atom_type 1 density constant 2500 radius constant 0.0025
fix             pts2 all particletemplate/sphere 1 atom_type 3 density constant 2500 radius constant 0.0015

fix             pdd1 all particledistribution/discrete 1.  1 pts1 1.0
fix             pdd2 all particledistribution/discrete 1.  1 pts2 1.0

fix     granwall all wall/gran model hertz tangential history rolling_friction cdt mesh n_meshes 2 meshes impeller vessel


region  fact1 cylinder x -0.05 -0.025 0.025 -0.24 0.24 units box
region  fact2 cylinder x 0.05 -0.025 0.025 -0.24 0.24 units box


fix    inj1 all insert/rate/region seed 1234 distributiontemplate pdd1 &
       maxattempt 10 nparticles 12963.0 massrate 2.12 all_in yes &
       insert_every 1000 overlapcheck yes  &
       vel constant 0.0 0.0 -0.1 omega constant 0.0 0.0 0.0  region fact1 ntry_mc 10000

fix    inj2 all insert/rate/region seed 1234 distributiontemplate pdd1 &
       maxattempt 10 nparticles 12963.0 massrate 2.12 all_in yes &
       insert_every 1000 overlapcheck yes  &
       vel constant 0.0 0.0 -0.1 omega constant 0.0 0.0 0.0  region fact2 ntry_mc 10000



fix                             ts all check/timestep/gran 10000 0.1 0.1
compute                         rke all erotate/sphere
thermo_style    custom step atoms ke c_rke f_ts[1] f_ts[2] vol time cpu
thermo                  100000
thermo_modify           lost ignore norm no
compute_modify          thermo_temp dynamic yes

dump            dmp_geom1 all mesh/vtk 1733 Post/vessel_*.vtk id vessel
dump            dmp_geom2 all mesh/vtk 1733 Post/impeller_*.vtk id impeller
dump            dmp all custom 1733 Post/dump*.paddleblender id x y z vx vy vz fx fy fz radius

run 86625

fix    inj3 all insert/rate/region seed 1234 distributiontemplate pdd2 &
       maxattempt 10 nparticles 60013.0 massrate 2.12 all_in yes &
```

```
        insert_every 1000 overlapcheck yes  &
        vel constant 0.0 0.0 -0.1 omega constant 0.0 0.0 0.0  region fact1 ntry_mc 10000

fix     inj4 all insert/rate/region seed 1234 distributiontemplate pdd2 &
        maxattempt 10 nparticles 60013.0 massrate 2.12 all_in yes &
        insert_every 1000 overlapcheck yes  &
        vel constant 0.0 0.0 -0.1 omega constant 0.0 0.0 0.0  region fact2 ntry_mc 10000
run 69300

fix  movecad1 all move/mesh mesh impeller rotate origin 0.0 0.0 0.0 axis 1.0 0.0 0.0 period 1.5


run 693000
unfix movecad1

run 1
```

## Appendix C: Post-processing MATLAB script for obtaining the RSD index from LIGGGHTS Simulations

```
numfiles = 4; % Number of data points for RSD calculations (5 s, 10 s, 15 s, 20 s of mixing).

for k = 1:numfiles % Initializing loop calculations for each mixing time.

        dir time ; % Define a directory called "time" in the MATLAB folder.

        mydirinfo = dir('time'); % Extracts information regarding the files in the "time" directory.

        xlRange = 'c10:f145961'; % Defines the excel spreadsheet range to be read within each file
        in the time directory. This range corresponds to the x, y, and z position of particles within
        the system. This range depends on the vessel fill level (number of particles) and number of
        parameters required.

        matrix_data = xlsread(mydirinfo(k+2).name,xlRange);% Reads the defined spreadsheet
        range for the file name within the time directory and places it into "matrix_data" matrix.

        d = mydirinfo(k+2).name; % Tracker for filename or mixing time.

        x_min = [-0.248 -0.169 -0.089 -0.0095 0.073 0.15]; % Lower boundary sample (6 samples)
        coordinates for x direction with reference to the origin of vessel.

        x_max = [-0.231 -0.152 -0.072 0.0075 0.09 0.167]; % Upper boundary sample (6samples)
        coordinates for x direction with reference to the origin of vessel.
```

```
y_min = 0.0335; % Lower boundary sample coordinates. Fixed location in y-direction for all 6 samples.

y_max = 0.0505; % Upper boundary sample coordinates. Fixed location in y-direction for all 6 samples.

z_min = -0.06; % Lower boundary sample coordinates. Fixed location in z-direction for all 6 samples.

z_max = -0.04; % Upper boundary sample coordinates. Fixed location in z-direction for all 6 samples.

[r,c] = size(x_min); % Returns the size of "x-min" matrix.

numbersamples = c; % Column size of x-min matrix which gives the number of samples.

type_1 = zeros(1,numbersamples); % Initialize a zero matrix for the number of 5 mm particles.

type_3 = zeros(1,numbersamples); % Initialize a zero matrix for the number of 3 mm particles.

[m,n] = size(matrix_data); % Reruns the size of "matrix_data" matrix.

for i=1:m % initializes the loop calculations for each particle (m).

    X_P = matrix_data(i,1);% x position, index must be determined based on the output.

    Y_P = matrix_data(i,2);% y position, index must be determined based on the output.

    Z_P = matrix_data(i,3);% z position , index must be determined based on the output.

    T_P = matrix_data(i,4);% Particle radius, index must be determined based on the output.

    for j = 1:numbersamples % Initializes the loop calculations for determining # of particles of 5 mm and 3 mm in each sample.

        if (x_min(1,j) <= X_P) && (X_P <= x_max(1,j))&&(y_min <= Y_P) && (Y_P <= y_max)&&(z_min <= Z_P) && (Z_P <= z_max)&&(T_P ==0.0025)
```

```
                type_1(1,j) = type_1(1,j)+1; % if conditions are met add one integer to the
                initial number of 5 mm particles declared for each sample.

                elseif (x_min(1,j) <= X_P) && (X_P <= x_max(1,j))&&(y_min <= Y_P)
                && (Y_P <= y_max)&&(z_min <= Z_P) && (Z_P <= z_max)&&(T_P
                ==0.0015)

                type_3(1,j) = type_3(1,j)+1; % if conditions are met add one integer to the
                initial number of 3 mm particles declared for each sample.
            end

            end

        end
    display (d)
    Bp= type_1; % Number of red particles (3 mm).
    Rp= type_3 % Number of black particles (5 mm).
    Tp = Rp + Bp % Total number of particles.
End
```

## Appendix D: Post-processing MATLAB scripts for obtaining Granular temperature from EDEM results

```
numfiles = 39; % number of files extracted from EDEM which corresponds to the numebr of bins
defined for granular temperature calculations in the x-direction.

mycell = cell (numfiles,1)

for k = 1:numfiles % initiates loop calculations for each bin

    dir Grantemp ; % define a directory called "Grantemp" in MATLAB folder. This line will
    access that directory

    mydirinfo = dir ('Grantemp'); % Extracts information regarding the files in the "Grantemp"
    directory.

    xlRange = 'B12:ZZ132'; % Defines the excel spreadsheet range to be read within each file
    in the Grantemp directory. This range depends on the number of time-steps, impeller
    rotational speed, number of parameters needed, and vessel fill level (total number of
    particles).

    out = xlsread(mydirinfo(k+2).name,xlRange); % Reads the defined spreadsheet range for
    the file name within the Grantemp directory and places it into "out" matrix.

    d = mydirinfo(k+2).name; % Tracker for filename or bin #.
```

```
out1 = out(1:3:end,:); % Every third  rows is read for each time-step which correspond to the average velocities for all particles(each column)in the specified bin. The reading sequence is defined in a way to skip empty rows between each time-step. The results are then placed within "out1" matrix.

y = nanmean(out1,2);% Row average is performed to calculate the average  velocities for all particles, after removing NaN values for each time-step.

N = sum(~isnan(out1),2); % Counts the total number of particles within the specified bin.

NN = sum(~isnan(y),1); % Counts the total number of time-steps.

C = bsxfun(@minus, out1, y); % Mean of each row is subtracted from the initial matrix, column by column to calculate the fluctuation velocity of particles within the specified bin. Refer to granular temperature equation.

D = C.^2; % Refer to granular temperature equation.

E = D ./ 2; % Evaluates the granular temperature value for the specified bin. Refer to granular temperature equation.

S = sum(E,2, 'omitnan'); % Evaluates the summation of granular temperature values for each row.

T = bsxfun(@rdivide, S, N); % Evaluates the average granular temperature values for each row which corresponds to a single value for all particles in the specified time-step.

Tcv = nansum(T); % Evaluates the summation of granular temperature values for all time-steps.

display (d)% Displays bin number.

TcvF = Tcv / NN % Evaluates the temporal average of granular temperature values for all times-steps

mycell {k,1} = TcvF; % Places granular temperature value for each bin in a cell with k rows corresponding to specific bin number.

end
mycell
```

## Appendix E: Post-processing MATLAB scripts for obtaining particle diffusivity and Peclet number from LIGGGHTs results

### E.1 40 RPM impeller rotational speed

```
xlRange = 'a10:g145961'; % provides the range for the cells needed to be post-processed from the excel spreadsheet containing the raw data obtained from LIGGGHTS. 7 columns (A-G) corresponds to the Particle ID, x, y, z positions, vx, vy, vz velocities for each particle. number of rows (10-145961) correspond to the total number of particles (40% fill level for this case).

out1 = xlsread('time1',xlRange); % Reads the given spreadsheet range provided within the excel file "time1" which corresponds to the file for the first time-step. afterwards the read files are placed within the matrix "out1".

[T1,I1] = sort (out1(:,1)); % sorts the "out1" matrix based on the data in the first column which corresponds to the particle ID.

T1 = out1(I1,:); % places the sorted data in matrix "T1" which is for the first time-step.

% This step is repeated for every time-step.
% The total number of time-steps required are determined by the impeller
% rotational speed (40 RPM) and the data capturing rate which was taken as
% a fraction of each impeller revolution (0.25 of a revolution).
% For 40 RPM the total number of time-steps required was determined to be
% 50.


xlRange = 'a10:g145961';
out2 = xlsread('time2',xlRange);
[T2,I2] = sort (out2(:,1));
T2 = out1(I2,:);

xlRange = 'a10:g145961';
out3 = xlsread('time3',xlRange);
[T3,I3] = sort (out3(:,1));
T3 = out3(I3,:);

xlRange = 'a10:g145961';
out4 = xlsread('time4',xlRange);
[T4,I4] = sort (out4(:,1));
T4 = out4(I4,:);

xlRange = 'a10:g145961';
out5 = xlsread('time5',xlRange);
[T5,I5] = sort (out5(:,1));
```

```
T5 = out5(I5,:);

xlRange = 'a10:g145961';
out6 = xlsread('time6',xlRange);
[T6,I6] = sort (out6(:,1));
T6 = out6(I6,:);

xlRange = 'a10:g145961';
out7 = xlsread('time7',xlRange);
[T7,I7] = sort (out7(:,1));
T7 = out7(I7,:);

xlRange = 'a10:g145961';
out8 = xlsread('time8',xlRange);
[T8,I8] = sort (out8(:,1));
T8 = out8(I8,:);

xlRange = 'a10:g145961';
out9 = xlsread('time9',xlRange);
[T9,I9] = sort (out9(:,1));
T9 = out9(I9,:);

xlRange = 'a10:g145961';
out10 = xlsread('time10',xlRange);
[T10,I10] = sort (out10(:,1));
T10 = out10(I10,:);

xlRange = 'a10:g145961';
out11 = xlsread('time11',xlRange);
[T11,I11] = sort (out11(:,1));
T11 = out11(I11,:);

xlRange = 'a10:g145961';
out12 = xlsread('time12',xlRange);
[T12,I12] = sort (out12(:,1));
T12 = out12(I12,:);

xlRange = 'a10:g145961';
out13 = xlsread('time13',xlRange);
[T13,I13] = sort (out13(:,1));
T13 = out13(I13,:);

xlRange = 'a10:g145961';
out14 = xlsread('time14',xlRange);
[T14,I14] = sort (out14(:,1));
T14 = out14(I14,:);
```

```
xlRange = 'a10:g145961';
out15 = xlsread('time15',xlRange);
[T15,I15] = sort (out15(:,1));
T15 = out15(I15,:);

xlRange = 'a10:g145961';
out16 = xlsread('time16',xlRange);
[T16,I16] = sort (out16(:,1));
T16 = out16(I16,:);

xlRange = 'a10:g145961';
out17 = xlsread('time17',xlRange);
[T17,I17] = sort (out17(:,1));
T17 = out17(I17,:);

xlRange = 'a10:g145961';
out18 = xlsread('time18',xlRange);
[T18,I18] = sort (out18(:,1));
T18 = out18(I18,:);

xlRange = 'a10:g145961';
out19 = xlsread('time19',xlRange);
[T19,I19] = sort (out19(:,1));
T19 = out19(I19,:);

xlRange = 'a10:g145961';
out20 = xlsread('time20',xlRange);
[T20,I20] = sort (out20(:,1));
T20 = out20(I20,:);

xlRange = 'a10:g145961';
out21 = xlsread('time21',xlRange);
[T21,I21] = sort (out21(:,1));
T21 = out21(I21,:);

xlRange = 'a10:g145961';
out22 = xlsread('time22',xlRange);
[T22,I22] = sort (out22(:,1));
T22 = out22(I22,:);

xlRange = 'a10:g145961';
out23 = xlsread('time23',xlRange);
[T23,I23] = sort (out23(:,1));
T23 = out23(I23,:);
```

```
xlRange = 'a10:g145961';
out24 = xlsread('time24',xlRange);
[T24,I24] = sort (out24(:,1));
T24 = out24(I24,:);

xlRange = 'a10:g145961';
out25 = xlsread('time25',xlRange);
[T25,I25] = sort (out25(:,1));
T25 = out25(I25,:);

xlRange = 'a10:g145961';
out26 = xlsread('time26',xlRange);
[T26,I26] = sort (out26(:,1));
T26 = out26(I26,:);

xlRange = 'a10:g145961';
out27 = xlsread('time27',xlRange);
[T27,I27] = sort (out27(:,1));
T27 = out27(I27,:);

xlRange = 'a10:g145961';
out28 = xlsread('time28',xlRange);
[T28,I28] = sort (out28(:,1));
T28 = out28(I28,:);

xlRange = 'a10:g145961';
out29 = xlsread('time29',xlRange);
[T29,I29] = sort (out29(:,1));
T29 = out29(I29,:);

xlRange = 'a10:g145961';
out30 = xlsread('time30',xlRange);
[T30,I30] = sort (out30(:,1));
T30 = out30(I30,:);

xlRange = 'a10:g145961';
out31 = xlsread('time31',xlRange);
[T31,I31] = sort (out31(:,1));
T31 = out31(I31,:);

xlRange = 'a10:g145961';
out32 = xlsread('time32',xlRange);
[T32,I32] = sort (out32(:,1));
T32 = out32(I32,:);

xlRange = 'a10:g145961';
```

```
out33 = xlsread('time33',xlRange);
[T33,I33] = sort (out33(:,1));
T33 = out33(I33,:);

xlRange = 'a10:g145961';
out34 = xlsread('time34',xlRange);
[T34,I34] = sort (out34(:,1));
T34 = out34(I34,:);

xlRange = 'a10:g145961';
out35 = xlsread('time35',xlRange);
[T35,I35] = sort (out35(:,1));
T35 = out35(I35,:);

xlRange = 'a10:g145961';
out36 = xlsread('time36',xlRange);
[T36,I36] = sort (out36(:,1));
T36 = out36(I36,:);

xlRange = 'a10:g145961';
out37 = xlsread('time37',xlRange);
[T37,I37] = sort (out37(:,1));
T37 = out37(I37,:);

xlRange = 'a10:g145961';
out38 = xlsread('time38',xlRange);
[T38,I38] = sort (out38(:,1));
T38 = out38(I38,:);

xlRange = 'a10:g145961';
out39 = xlsread('time39',xlRange);
[T39,I39] = sort (out39(:,1));
T39 = out39(I39,:);

xlRange = 'a10:g145961';
out40 = xlsread('time40',xlRange);
[T40,I40] = sort (out40(:,1));
T40 = out40(I40,:);

xlRange = 'a10:g145961';
out41 = xlsread('time41',xlRange);
[T41,I41] = sort (out41(:,1));
T41 = out41(I41,:);

xlRange = 'a10:g145961';
out42 = xlsread('time42',xlRange);
```

```
[T42,I42] = sort (out42(:,1));
T42 = out42(I42,:);

xlRange = 'a10:g145961';
out43 = xlsread('time43',xlRange);
[T43,I43] = sort (out43(:,1));
T43 = out43(I43,:);

xlRange = 'a10:g145961';
out44 = xlsread('time44',xlRange);
[T44,I44] = sort (out44(:,1));
T44 = out44(I44,:);

xlRange = 'a10:g145961';
out45 = xlsread('time45',xlRange);
[T45,I45] = sort (out45(:,1));
T45 = out45(I45,:);

xlRange = 'a10:g145961';
out46 = xlsread('time46',xlRange);
[T46,I46] = sort (out46(:,1));
T46 = out46(I46,:);

xlRange = 'a10:g145961';
out47 = xlsread('time47',xlRange);
[T47,I47] = sort (out47(:,1));
T47 = out47(I47,:);

xlRange = 'a10:g145961';
out48 = xlsread('time48',xlRange);
[T48,I48] = sort (out48(:,1));
T48 = out48(I48,:);

xlRange = 'a10:g145961';
out49 = xlsread('time49',xlRange);
[T49,I49] = sort (out49(:,1));
T49 = out49(I49,:);

xlRange = 'a10:g145961';
out50 = xlsread('time50',xlRange);
[T50,I50] = sort (out50(:,1));
T50 = out50(I50,:);

delt1 = T2(:,1:4) - T1(:,1:4); % subtracts the position of each particle within each time-step from
the position of the same particles within the next time-step.
% Procedure is repeated for all time-steps to obtain 49 (50 timesteps - 1 )
```

```
% matrices.

delt2 = T3(:,1:4) - T2(:,1:4);
delt3 = T4(:,1:4) - T3(:,1:4);
delt4 = T5(:,1:4) - T4(:,1:4);
delt5 = T6(:,1:4) - T5(:,1:4);
delt6 = T7(:,1:4) - T6(:,1:4);
delt7 = T8(:,1:4) - T7(:,1:4);
delt8 = T9(:,1:4) - T8(:,1:4);
delt9 = T10(:,1:4) - T9(:,1:4);
delt10 = T11(:,1:4) - T10(:,1:4);
delt11 = T12(:,1:4) - T11(:,1:4);
delt12 = T13(:,1:4) - T12(:,1:4);
delt13 = T14(:,1:4) - T13(:,1:4);
delt14 = T15(:,1:4) - T14(:,1:4);
delt15 = T16(:,1:4) - T15(:,1:4);
delt16 = T17(:,1:4) - T16(:,1:4);
delt17 = T18(:,1:4) - T17(:,1:4);
delt18 = T19(:,1:4) - T18(:,1:4);
delt19 = T20(:,1:4) - T19(:,1:4);
delt20 = T21(:,1:4) - T20(:,1:4);
delt21 = T22(:,1:4) - T21(:,1:4);
delt22 = T23(:,1:4) - T22(:,1:4);
delt23 = T24(:,1:4) - T23(:,1:4);
delt24 = T25(:,1:4) - T24(:,1:4);
delt25 = T26(:,1:4) - T25(:,1:4);
delt26 = T27(:,1:4) - T26(:,1:4);
delt27 = T28(:,1:4) - T27(:,1:4);
delt28 = T29(:,1:4) - T28(:,1:4);
delt29 = T30(:,1:4) - T29(:,1:4);
delt30 = T31(:,1:4) - T30(:,1:4);
delt31 = T32(:,1:4) - T31(:,1:4);
delt32 = T33(:,1:4) - T32(:,1:4);
delt33 = T34(:,1:4) - T33(:,1:4);
delt34 = T35(:,1:4) - T34(:,1:4);
delt35 = T36(:,1:4) - T35(:,1:4);
delt36 = T37(:,1:4) - T36(:,1:4);
delt37 = T38(:,1:4) - T37(:,1:4);
delt38 = T39(:,1:4) - T38(:,1:4);
delt39 = T40(:,1:4) - T39(:,1:4);
delt40 = T41(:,1:4) - T40(:,1:4);
delt41 = T42(:,1:4) - T41(:,1:4);
delt42 = T43(:,1:4) - T42(:,1:4);
delt43 = T44(:,1:4) - T43(:,1:4);
delt44 = T45(:,1:4) - T44(:,1:4);
delt45 = T46(:,1:4) - T45(:,1:4);
```

```
delt46 = T47(:,1:4) - T46(:,1:4);
delt47 = T48(:,1:4) - T47(:,1:4);
delt48 = T49(:,1:4) - T48(:,1:4);
delt49 = T50(:,1:4) - T49(:,1:4);

deltavg1 = mean(delt1,1); % Takes the column average of delta matrix. this is the average of each
ID, and position (column) ID, x, y, z within each delta matrix.
% This procedure is repeated for all time-steps.

deltavg2 = mean(delt2,1);
deltavg3 = mean(delt3,1);
deltavg4 = mean(delt4,1);
deltavg5 = mean(delt5,1);
deltavg6 = mean(delt6,1);
deltavg7 = mean(delt7,1);
deltavg8 = mean(delt8,1);
deltavg9 = mean(delt9,1);
deltavg10 = mean(delt10,1);
deltavg11 = mean(delt11,1);
deltavg12 = mean(delt12,1);
deltavg13 = mean(delt13,1);
deltavg14 = mean(delt14,1);
deltavg15 = mean(delt15,1);
deltavg16 = mean(delt16,1);
deltavg17 = mean(delt17,1);
deltavg18 = mean(delt18,1);
deltavg19 = mean(delt19,1);
deltavg20 = mean(delt20,1);
deltavg21 = mean(delt21,1);
deltavg22 = mean(delt22,1);
deltavg23 = mean(delt23,1);
deltavg24 = mean(delt24,1);
deltavg25 = mean(delt25,1);
deltavg26 = mean(delt26,1);
deltavg27 = mean(delt27,1);
deltavg28 = mean(delt28,1);
deltavg29 = mean(delt29,1);
deltavg30 = mean(delt30,1);
deltavg31 = mean(delt31,1);
deltavg32 = mean(delt32,1);
deltavg33 = mean(delt33,1);
deltavg34 = mean(delt34,1);
deltavg35 = mean(delt35,1);
deltavg36 = mean(delt36,1);
deltavg37 = mean(delt37,1);
deltavg38 = mean(delt38,1);
```

```
deltavg39 = mean(delt39,1);
deltavg40 = mean(delt40,1);
deltavg41 = mean(delt41,1);
deltavg42 = mean(delt42,1);
deltavg43 = mean(delt43,1);
deltavg44 = mean(delt44,1);
deltavg45 = mean(delt45,1);
deltavg46 = mean(delt46,1);
deltavg47 = mean(delt47,1);
deltavg48 = mean(delt48,1);
deltavg49 = mean(delt49,1);


deltsub1 = (bsxfun(@minus, delt1, deltavg1)).^2; % refer to equation used for calculating particle diffusivities. this line corresponds to the calculation of the numerator component excluding the "<>" temporal averaging.
% This procedure is repeated for all time-steps.

deltsub2 = (bsxfun(@minus, delt2, deltavg2)).^2;
deltsub3 = (bsxfun(@minus, delt3, deltavg3)).^2;
deltsub4 = (bsxfun(@minus, delt4, deltavg4)).^2;
deltsub5 = (bsxfun(@minus, delt5, deltavg5)).^2;
deltsub6 = (bsxfun(@minus, delt6, deltavg6)).^2;
deltsub7 = (bsxfun(@minus, delt7, deltavg7)).^2;
deltsub8 = (bsxfun(@minus, delt8, deltavg8)).^2;
deltsub9 = (bsxfun(@minus, delt9, deltavg9)).^2;
deltsub10 = (bsxfun(@minus, delt10, deltavg10)).^2;
deltsub11 = (bsxfun(@minus, delt11, deltavg11)).^2;
deltsub12 = (bsxfun(@minus, delt12, deltavg12)).^2;
deltsub13 = (bsxfun(@minus, delt13, deltavg13)).^2;
deltsub14 = (bsxfun(@minus, delt14, deltavg14)).^2;
deltsub15 = (bsxfun(@minus, delt15, deltavg15)).^2;
deltsub16 = (bsxfun(@minus, delt16, deltavg16)).^2;
deltsub17 = (bsxfun(@minus, delt17, deltavg17)).^2;
deltsub18 = (bsxfun(@minus, delt18, deltavg18)).^2;
deltsub19 = (bsxfun(@minus, delt19, deltavg19)).^2;
deltsub20 = (bsxfun(@minus, delt20, deltavg20)).^2;
deltsub21 = (bsxfun(@minus, delt21, deltavg21)).^2;
deltsub22 = (bsxfun(@minus, delt22, deltavg22)).^2;
deltsub23 = (bsxfun(@minus, delt23, deltavg23)).^2;
deltsub24 = (bsxfun(@minus, delt24, deltavg24)).^2;
deltsub25 = (bsxfun(@minus, delt25, deltavg25)).^2;
deltsub26 = (bsxfun(@minus, delt26, deltavg26)).^2;
deltsub27 = (bsxfun(@minus, delt27, deltavg27)).^2;
deltsub28 = (bsxfun(@minus, delt28, deltavg28)).^2;
deltsub29 = (bsxfun(@minus, delt29, deltavg29)).^2;
```

```
deltsub30 = (bsxfun(@minus, delt30, deltavg30)).^2;
deltsub31 = (bsxfun(@minus, delt31, deltavg31)).^2;
deltsub32 = (bsxfun(@minus, delt32, deltavg32)).^2;
deltsub33 = (bsxfun(@minus, delt33, deltavg33)).^2;
deltsub34 = (bsxfun(@minus, delt34, deltavg34)).^2;
deltsub35 = (bsxfun(@minus, delt35, deltavg35)).^2;
deltsub36 = (bsxfun(@minus, delt36, deltavg36)).^2;
deltsub37 = (bsxfun(@minus, delt37, deltavg37)).^2;
deltsub38 = (bsxfun(@minus, delt38, deltavg38)).^2;
deltsub39 = (bsxfun(@minus, delt39, deltavg39)).^2;
deltsub40 = (bsxfun(@minus, delt40, deltavg40)).^2;
deltsub41 = (bsxfun(@minus, delt41, deltavg41)).^2;
deltsub42 = (bsxfun(@minus, delt42, deltavg42)).^2;
deltsub43 = (bsxfun(@minus, delt43, deltavg43)).^2;
deltsub44 = (bsxfun(@minus, delt44, deltavg44)).^2;
deltsub45 = (bsxfun(@minus, delt45, deltavg45)).^2;
deltsub46 = (bsxfun(@minus, delt46, deltavg46)).^2;
deltsub47 = (bsxfun(@minus, delt47, deltavg47)).^2;
deltsub48 = (bsxfun(@minus, delt48, deltavg48)).^2;
deltsub49 = (bsxfun(@minus, delt49, deltavg49)).^2;

diffavg1 = mean(deltsub1,1); % takes the average of particle diffusivities for all three directions
within in each time-step.
% Average particle diffusivity values are evaluated for x, y, z direction for all time-steps.

diffavg2 = mean(deltsub2,1);
diffavg3 = mean(deltsub3,1);
diffavg4 = mean(deltsub4,1);
diffavg5 = mean(deltsub5,1);
diffavg6 = mean(deltsub6,1);
diffavg7 = mean(deltsub7,1);
diffavg8 = mean(deltsub8,1);
diffavg9 = mean(deltsub9,1);
diffavg10 = mean(deltsub10,1);
diffavg11 = mean(deltsub11,1);
diffavg12 = mean(deltsub12,1);
diffavg13 = mean(deltsub13,1);
diffavg14 = mean(deltsub14,1);
diffavg15 = mean(deltsub15,1);
diffavg16 = mean(deltsub16,1);
diffavg17 = mean(deltsub17,1);
diffavg18 = mean(deltsub18,1);
diffavg19 = mean(deltsub19,1);
diffavg20 = mean(deltsub20,1);
diffavg21 = mean(deltsub21,1);
diffavg22 = mean(deltsub22,1);
```

```
diffavg23 = mean(deltsub23,1);
diffavg24 = mean(deltsub24,1);
diffavg25 = mean(deltsub25,1);
diffavg26 = mean(deltsub26,1);
diffavg27 = mean(deltsub27,1);
diffavg28 = mean(deltsub28,1);
diffavg29 = mean(deltsub29,1);
diffavg30 = mean(deltsub30,1);
diffavg31 = mean(deltsub31,1);
diffavg32 = mean(deltsub32,1);
diffavg33 = mean(deltsub33,1);
diffavg34 = mean(deltsub34,1);
diffavg35 = mean(deltsub35,1);
diffavg36 = mean(deltsub36,1);
diffavg37 = mean(deltsub37,1);
diffavg38 = mean(deltsub38,1);
diffavg39 = mean(deltsub39,1);
diffavg40 = mean(deltsub40,1);
diffavg41 = mean(deltsub41,1);
diffavg42 = mean(deltsub42,1);
diffavg43 = mean(deltsub43,1);
diffavg44 = mean(deltsub44,1);
diffavg45 = mean(deltsub45,1);
diffavg46 = mean(deltsub46,1);
diffavg47 = mean(deltsub47,1);
diffavg48 = mean(deltsub48,1);
diffavg49 = mean(deltsub49,1);

deltsubtimeavg = (diffavg1 + diffavg2 + diffavg3 + diffavg4 + diffavg5 + diffavg6 + diffavg7 +
diffavg8 + diffavg9 + diffavg10 + diffavg11 + diffavg12 + diffavg13 + diffavg14 + diffavg15 +
diffavg16 + diffavg17 + diffavg18 + diffavg19 + diffavg20 + diffavg21 + diffavg22 + diffavg23
+ diffavg24 + diffavg25 + diffavg26 + diffavg27 + diffavg28 + diffavg29 + diffavg30 + diffavg31
+ diffavg32 + diffavg33 + diffavg34 + diffavg35 + diffavg36 + diffavg37 + diffavg38 + diffavg39
+ diffavg40 + diffavg41 + diffavg42 + diffavg43 + diffavg44 + diffavg45 + diffavg46 + diffavg47
+ diffavg48 + diffavg49)/49; % This line evaluates the average of all diffusivity values obtained
for all time-steps. This line accounts for the "<>" temporal averaging symbol indicated in the
numerator component of the diffusivity equation.

Diff = deltsubtimeavg/(2*0.4); % Evaluates the diffusivity values in three directions, x, y, and z.
Refer to particle diffusivity equation. Time-step value in the equation must be changed depending
on the impeller rotational speed used (40 RPM = 0.4 seconds).

Diff = Diff(2:end); % Converts column vector to row vector.

Tv1 = T1(:,5:7); % places particle velocities, vx, vy, vz for all particles within the specified time-
step in "Tv1" matrix
```

```
% This procedure is repeated for all time-steps.

Tv2 = T2(:,5:7);
Tv3 = T3(:,5:7);
Tv4 = T4(:,5:7);
Tv5 = T5(:,5:7);
Tv6 = T6(:,5:7);
Tv7 = T7(:,5:7);
Tv8 = T8(:,5:7);
Tv9 = T9(:,5:7);
Tv10 = T10(:,5:7);
Tv11 = T11(:,5:7);
Tv12 = T12(:,5:7);
Tv13 = T13(:,5:7);
Tv14 = T14(:,5:7);
Tv15 = T15(:,5:7);
Tv16 = T16(:,5:7);
Tv17 = T17(:,5:7);
Tv18 = T18(:,5:7);
Tv19 = T19(:,5:7);
Tv20 = T20(:,5:7);
Tv21 = T21(:,5:7);
Tv22 = T22(:,5:7);
Tv23 = T23(:,5:7);
Tv24 = T24(:,5:7);
Tv25 = T25(:,5:7);
Tv26 = T26(:,5:7);
Tv27 = T27(:,5:7);
Tv28 = T28(:,5:7);
Tv29 = T29(:,5:7);
Tv30 = T30(:,5:7);
Tv31 = T31(:,5:7);
Tv32 = T32(:,5:7);
Tv33 = T33(:,5:7);
Tv34 = T34(:,5:7);
Tv35 = T35(:,5:7);
Tv36 = T36(:,5:7);
Tv37 = T37(:,5:7);
Tv38 = T38(:,5:7);
Tv39 = T39(:,5:7);
Tv40 = T40(:,5:7);
Tv41 = T41(:,5:7);
Tv42 = T42(:,5:7);
Tv43 = T43(:,5:7);
Tv44 = T44(:,5:7);
Tv45 = T45(:,5:7);
```

```
Tv46 = T46(:,5:7);
Tv47 = T47(:,5:7);
Tv48 = T48(:,5:7);
Tv49 = T49(:,5:7);
Tv50 = T50(:,5:7);

deltvavg1 = mean(Tv1,1); % Evaluates the average velocities for each particle within the specified time-step for all three directions.
% This procedure is repeated for all time-steps.

deltvavg2 = mean(Tv2,1);
deltvavg3 = mean(Tv3,1);
deltvavg4 = mean(Tv4,1);
deltvavg5 = mean(Tv5,1);
deltvavg6 = mean(Tv6,1);
deltvavg7 = mean(Tv7,1);
deltvavg8 = mean(Tv8,1);
deltvavg9 = mean(Tv9,1);
deltvavg10 = mean(Tv10,1);
deltvavg11 = mean(Tv11,1);
deltvavg12 = mean(Tv12,1);
deltvavg13 = mean(Tv13,1);
deltvavg14 = mean(Tv14,1);
deltvavg15 = mean(Tv15,1);
deltvavg16 = mean(Tv16,1);
deltvavg17 = mean(Tv17,1);
deltvavg18 = mean(Tv18,1);
deltvavg19 = mean(Tv19,1);
deltvavg20 = mean(Tv20,1);
deltvavg21 = mean(Tv21,1);
deltvavg22 = mean(Tv22,1);
deltvavg23 = mean(Tv23,1);
deltvavg24 = mean(Tv24,1);
deltvavg25 = mean(Tv25,1);
deltvavg26 = mean(Tv26,1);
deltvavg27 = mean(Tv27,1);
deltvavg28 = mean(Tv28,1);
deltvavg29 = mean(Tv29,1);
deltvavg30 = mean(Tv30,1);
deltvavg31 = mean(Tv31,1);
deltvavg32 = mean(Tv32,1);
deltvavg33 = mean(Tv33,1);
deltvavg34 = mean(Tv34,1);
deltvavg35 = mean(Tv35,1);
deltvavg36 = mean(Tv36,1);
deltvavg37 = mean(Tv37,1);
```

```
deltvavg38 = mean(Tv38,1);
deltvavg39 = mean(Tv39,1);
deltvavg40 = mean(Tv40,1);
deltvavg41 = mean(Tv41,1);
deltvavg42 = mean(Tv42,1);
deltvavg43 = mean(Tv43,1);
deltvavg44 = mean(Tv44,1);
deltvavg45 = mean(Tv45,1);
deltvavg46 = mean(Tv46,1);
deltvavg47 = mean(Tv47,1);
deltvavg48 = mean(Tv48,1);
deltvavg49 = mean(Tv49,1);
deltvavg50 = mean(Tv50,1);


avgvel = (deltvavg1 + deltvavg2 + deltvavg3 + deltvavg4 + deltvavg5 + deltvavg6 + deltvavg7 +
deltvavg8 + deltvavg9 + deltvavg10 + deltvavg11 + deltvavg12 + deltvavg13 + deltvavg14 +
deltvavg15 + deltvavg16 + deltvavg17 + deltvavg18 + deltvavg19 + deltvavg20 + deltvavg21 +
deltvavg22 + deltvavg23 + deltvavg24 + deltvavg25 + deltvavg26 + deltvavg27 + deltvavg28 +
deltvavg29 + deltvavg30 + deltvavg31 + deltvavg32 + deltvavg33 + deltvavg34 + deltvavg35 +
deltvavg36 + deltvavg37 + deltvavg38 + deltvavg39 + deltvavg40 + deltvavg41 + deltvavg42 +
deltvavg43 + deltvavg44 + deltvavg45 + deltvavg46 + deltvavg47 + deltvavg48 + deltvavg49 +
deltvavg50)/50 ; % evaluates the temporal average of average velocities obtained for all three
directions.

Radius = 0.108; % Raidus of vessel

Peclet = (avgvel*Radius)./Diff % Evaluates Peclet number for all three directions. Refer to Peclet
number equation.
```

# References


1. Alexander, A., Goodridge, C., Muzzio, F. J., Shen, E., & Shinbrot, T. (2004). Solid mixing. In E. L. Paul, V. A. Atiemo-Obeng, & S. M. Kresta (Eds.), *Handbook of Industrial mixing - Science and Practice* (pp. 887 - 923). Hoboken: John Wiley & Sons.
2. Ortega-Rivas, E. (2011). Mixing. In E. Ortega-Rivas, *Unit Operations of Particulate Solids: Theory and Practice* (pp. 229 - 247). Boca Raton: CRC Press.
3. Bridgwater, J. (1976). Fundamental Powder Mixing Mechanisms. *Powder Technology*, 15, 215 - 236.
4. Holdich, R. G. (2002). Solid/solid mixing. In R. G. Holdich, *Fundamentals of Particle Technology*. Leicestershire: Midland Information Technology.
5. Harnby, N., Edwards, M. F., & Nienow, A. W. (1997). *Mixing in the Process Industries*. Oxford: Butterworth-Heinemann.
6. Williams, J. C. (1968). The Mixing of Dry Powders. *Powder Technology,* 2, 13 - 20.
7. Hogg, R. (2009). Mixing and Segregation in Powders: Evaluation, Mechanisms and Processes. *KONA Powder and Particle Journal*, 27, 3 - 17.
8. Mosby, J., de Silva, S. R., & Enstad, G. G. (1996). Segregation and Particulate Materials Mechanisms and Testers. *KONA Powder and Particle Journal*, 14, 31 - 43.
9. Dickey, D. S. (2009). Equipment design. In P. J. Cullen, *Food Mixing: Principles and Applications* (pp. 73 - 89). Hoboken: John Wiley & Sons.
10. Berk, Z. (2009). *Food Process Engineering and Technology*. Burlington: Academic Press.
11. Moakher, M., Shinbrot, T., & Muzzio, F. J. (2000). Experimentally validated computations of flow, mixing and segregation of non-cohesive grains in 3D tumbling blenders. *Powder Technology*, 109, 58 - 71.
12. Lemieux, M., Bertrand, F., Chaouki, J., & Gosseling, P. (2007). Comparative study of the mixing of free-flowing particles in a V-blender and a Bin-belnder. *Chemical Engineering Science*, 62, 1783 - 1802.
13. Tahvildarian, P., Ein-Mozaffari, F., & Upreti, S. R. (2013). Circulation intensity and axial dispersion of non-cohesive solid particles in a V-blender via DEM simulation. *Particuology*, 11, 619 - 626.

14. Chandratilleke, G. R., Yu, A. B., Stewart, R. L., & Bridgwater, J. (2009). Effects of blade rake angle and gap on particle mixing in a cylindrical mixer. *Powder Technology, 193,* 303 - 311.
15. Hassanpour, A., Tan, H., Bayly, A., Gopalkrishnan, P., Ng, B., & Ghadiri, M. (2011). Analysis of particle motion in a paddle mixer using Discrete Element Method (DEM). *Powder Technology, 206,* 189 - 194.
16. Beitzel, H., Charonnat, Y., & Beitzel, M. (2003). Assessment and classification of performance mixers. *Materials and Structures, 36,* 250 - 264.
17. Shinbrot, T., Alexander, A., Moakher, M., & Muzzio, F. J. (1999). Chaotic granular mixing. *Chaos,* 9, 611 - 620.
18. Van den Bergh, W. (1994). Removing the uncertainty in solids mixer selection. *Chemical engineering; ProQuest Science Journals,* 101, 70 - 77.
19. Nakamura, H., Miyazaki, Y., Sato, Y., Iwasaki, T., & Watano, S. (2009). Numerical analysis of similarities of particle behavior in high shear mixer granulators with different vessel sizes. *Advanced Powder Technology,* 20, 493 - 501.
20. Bertrand, F., Leclaire, L. A., & Levecque, G. (2005). DEM-based models for mixing of granular materials. *Chemical Engineering Science,* 60, 2517 - 2531.
21. Alian, M., Ein-Mozaffari, F., & Upreti, S. R. (2015a). Analysis of the mixing of solid particles in a plowsharemixer via discrete. *Powder Technology,* 274, 77 - 87.
22. Smith, J. L. (1997). Mechanically fluidized bed Plough mixers: fast intense processing without high shear. *Powder Bulk Eng.,* 11, 45 - 57.
23. Forberg, H. (1992). Short note on modern mixing: theory and practice. *Powder Handl. Process,* 4, 318 - 320.
24. Ramponi, S., Negrini, D., & Passerini, M. (2002). Mixer selection for powders. *Powder Handl*. Process, 14, 30 - 39.
25. Tang, P., & Puri, V. M. (2004). Methods for Minimizing Segregation: A Review. *Particulate Science and Technology, 22,* 321 - 337.
26. Fitzpatrick, J. J. (2009). Particulate and powder mixing. In P. J. Cullen, *Food Mixing: Principles and Applications* (pp. 269 - 287). Hoboken: John Wiley & Sons.
27. Khakhar, D. V., McCarthy, J. J., Gilchrist, J. F., & Ottino, J. M. (1999). Chaotic mixing of granular materials in two-dimensional tumbling mixers. *Chaos,* 9, 195 - 205.

28. Cleary, P. W., & Sinnott, M. D. (2008). Assessing mixing characteristics of particle-mixing and granulation devices. *Particuology, 6*, 419 - 444.
29. Alizadeh, E., Bertrand, F., & Chaouki, J. (2014). Discrete element simulation of particle mixing and segregation in a tetrapodal blender. *Computers & Chemical Engineering*, 64, 1 - 12.
30. Jones, J. R., & Bridgwater, J. (1998). A case study of particle mixing in a ploughshare mixer using Positron Emission Particle Tracking. *International Journal of mineral processing*, 53, 29 - 38.
31. Jones, J. R., Parker, D. J., & Bridgwater, J. (2007). Axial mixing in a ploughshare mixer. *Powder Technology*, 178, 73 - 86.
32. Laurent, B. C., & Bridgwater, J. (2002). Performance of single and six-bladed powder mixers. *Chemical Engineering Science*, 57, 1695 - 1709.
33. Stewart, R. L., Bridgwater, J., & Parker, D. J. (2001a). Granular flow over a flat-bladed stirrer. *Chemical Engineering Science*, 56, 4257 - 4271.
34. Stewart, R. L., Bridgwater, J., Zhou, Y. C., & Yu, A. B. (2001b). Simulated and measured flow of granules in a bladed mixer- a detailed comparison. *Chemical Engineering Science*, 56, 5457 - 5471.
35. Conway, S. L., Lekhal, A., Khinast, J. G., & Glasser, B. J. (2005). Granular flow and segregation in a four-bladed mixer. *Chemical Engineering Science*, 60, 7091 - 7107.
36. Remy, B., Canty, T. M., Khinast, J. G., & Glasser, B. J. (2010a). Experiments and simulations of cohesionless particles with varying roughness in a bladed mixer. *Chemical Engineering Science*, 65, 4557 - 4571.
37. Blanco, M., Bano, R. G., & Bertran, E. (2002). Monitoring powder blending in pharmaceutical processes by use of near infrared spectroscopy. *Talanta*, 56, 203 - 212.
38. Berntsson, O., Danielsson, L. G., Lagerholm, B., & Folestad, S. (2002). Quantitative in-line monitoring of powder blending by near infrared reflection spectroscopy. *Powder Technology*, 123, 185 - 193.
39. Muzzio, F. J., Robinson, P., Wightman, C., & Brone, D. (1997). Sampling practices in powder blending. *International Journal of Pharmaceutics, 155*, 153 - 178.
40. Simons, T. A., Bensmann, S., Zigan, S., Feise, H. J., & Kwade, A. (2016). Characterization of granular mixing in a helical ribbon blade blender. *Powder Technology*, 293, 15 - 25.

41. Deen, N. G., Willem, G., Sander, G., & Kuipers, J. A. (2010). Numerical Analysis of Solids Mixing in Pressurized Fluidized Beds. *I&EC research*, 49, 5246 - 5253.
42. Wen, Y., Liu, M., Liu, B., & Shao, Y. (2015). Comparative study on the characterization method of particle Mixing Index Using DEM Method. *Procedia Engineering*, 102, 1630 - 1642.
43. Zhu, H. P., Zhou, Z. Y., Yang, R. Y., & Yu, A. B. (2007). Discrete particle simulation of particulate systems: Theoretical developments. *Chemical Engineering Science*, 62, 3378 - 3396.
44. Aca, J., Lato, P., Sanja, S., Nenad, K., & Ljubinko, L. (2015). Discrete element modelling of screw conveyor-mixers. *Hemijska industrija*, 69, 95 - 101.
45. Cleary, P. W. (2004). Large scale industrial DEM modelling. *Engineering Computations*, 21, 169 - 204.
46. Abbaaspour-Fard, M. H. (2000). *Discrete element modeling of the dynamic behaviour of non-spherical particulate materials* (doctoral thesis). University of Newcastle, Newcastle, United Kingdom.
47. Ketterhagen, W. R., Am Ende, M. T., & Hancock, B. C. (2009). Process Modeling in the Pharmaceutical Industry using the discrete element method. *Journal of Pharmaceutical Sciences*, 98, 442 - 470.
48. Zhu, H. P., Zhou, Z. Y., Yang, R. Y., & Yu, A. B. (2008). Discrete particle simulation of particulate systems: A review of major applications and findings. *Chemical Engineering Science, 63*, 5728 - 5770.
49. Kwan, C., Mio, H., Chen, Y., Ding, Y., Saito, F., Papadopoulos, D. G., Ghadiri, M. (2005). Analysis of the milling rate of pharmaceutical powders using the Distinct Element Method (DEM). *Chemical Engineering Science*, 60, 1441 - 1448.
50. Wu, C.-Y. (2008). DEM simulations of die filling during pharmaceutical tabletting. *Particuology*, 6, 412 - 418.
51. Cleary, P. W. (2000). DEM simulation of industrial particle flows: case studies of dragline excavators, mixing in tumblers and centrifugal mills. *Powder Technology*, 109, 83 - 104.
52. Tan, Y., Yang, D., & Sheng, Y. (2009). Discrete element method (DEM) modeling of fracture and damage in the machining process of polycrystalline SiC. *Journal of the European Ceramic Society*, 29, 1029 - 1037.

53. Manickam, S. S., Shah, R., Tomei, J., Bergman, T. L., & Chaudhuri, B. (2010). Investigating mixing in a multi-dimensional rotary mixer: Experiments and simulations. *Powder Technology*, 201, 83 - 92.
54. Luding, s. (1998). Collisions and contacts between two particles. In H. J. Herrmann, J. -P. Hovi, & S. Luding (Eds.), *Physics of Dry Granular Media* (Vol. 350, pp. 285 - 304). Stuttgart: Springer Netherlands.
55. Basinskas, G., & Sakai, M. (2016). Numerical study of the mixing efficiency of a ribbon mixer using the discrete element method. *Powder Technology*, 287, 380 - 394.
56. Golshan, S., Zarghami, R., Norouzi, H., & Mostoufi, N. (2017). Granular mixing in nauta blenders. *Powder Technology*, 305, 279 - 288.
57. Sakai, M., Shigeto, Y., Basinskas, G., Hosokawa, A., & Fuji, M. (2015). Discrete element simulation for the evaluation of solid mixing in an industrial blender. *Chemical Engineering Journal*, 279, 821 - 839.
58. Kaneko, Y., Shiojima, T., & Horio, M. (2000). Numerical analysis of particle mixing characteristics in a single helical ribbon agitator using DEM simulation. Powder Technology, 108, 55 - 64.
59. Remy, B., Boonkanokwong, V., Khinast, J. G., & Glasser, B. J. (2016). The effect of the number of impeller blades on granular flow in a bladed mixer. *Powder Technology*, 302, 333 - 349.
60. Remy, B., Glasser, B. J., & Khinast, J. G. (2010b). The Effect of Mixer Properties and Fill Level on Granular Flow in a Bladed Mixer. *AIChE*, 56, 336 - 353.
61. Portillo, P. M., Ierapetritou, M. G., & Muzzio, F. J. (2009). Effects of rotation rate, mixing angle, and cohesion in two continous powder mixers- A statistical approach. *Powder Technology*, 194, 217 - 227.
62. Just, S., Toschkoff, G., Funke, A., Djuric, D., Scharrer, G., Khinast, J., Kleinebudde, P. (2013). Optimization of the inter-tablet coating uniformity for an active coating process at lab and pilot scale. *International journal of Pharmaceutics*, 457, 1 - 8.
63. Pakzad, L., Ein-Mozaffari, F., Upreti, S. R., & Lohi, A. (2013). Evaluation of the mixing of non-Newtonian biopolymer solutions in the reactors equipped with the coaxial mixers through tomography and CFD. *Chemical Engineering Journal*, 215 - 216, 279 - 296.

64. Radl, S., Kalvoda, E., Glasser, B. J., & Khinast, G. J. (2010). Mixing characteristics of wet granular matter in a bladed mixer. *Powder Technology*, 200, 171 - 189.

65. Abouzeid, A.-Z. M., & Fuerstenau, D. W. (2010). Mixing–demixing of particulate solids in rotating drums. *International Journal of Mineral Processing, 95*, 40 - 46.

66. Remy, B., Khinast, J. G., & Glasser, B. J. (2011). Polydisperse granular flows in a bladed mixer: Experiments and simulations of cohesionless spheres. *Chemical Engineering Science*, 66, 1811 - 1824.

67. Zhou, Y., Yu, A., & Bridgwater, J. (2003). Segregation of binary mixture of particles in a bladed mixer. *Journal of Chemical Technology and Biotechnology, 78*, 187 - 193.

68. Alchikh-Sulaiman, B., Ein-Mozaffari, F., & Lohi, A. (2015). Evaluation of poly-disperse solid particles mixing in a slant cone mixer using discrete element method. *Chemical Engineering Research and Design, 96*, 196 - 213.

69. Arratia, P. E., Duong, N.-h., Muzzio, F. J., Godbole, P., & Reynolds, S. (2006). A study of the mixing and segregation mechanisms in the Bohle. *Powder Technology, 164*, 50 - 57.

70. Lemieux, M., Leonard, G., Doucet, J., Leclaire, L. A., Viens, F., Chaouki, J., & Bertrand, F. (2008). Large-scale numerical investigation of solids mixing in a V-blender using the discrete element method. *Powder Technology*, 181, 205 - 216.

71. Hassanpour, A., & Pasha, M. (2014). Discrete Element Method Applications in Process Engineering. In M. M. Martin, *Introduction to Software for Chemical Engineers* (pp. 245 - 286). Boca Raton: CRC Press.

72. Kloss, C., Goniva, C., Hager, A., Amberger, S., & Pirker, S. (2012). Models, algorithms and validation for opensource DEM and CFD-DEM. *Progress in Computational Fluid Dynamics, An Int. J., 12*, 140 - 152.

73. Margio, M., Cairns, D. L., Davies, M., Ingram, A., & Stitt, E. H. (2012). A numerical comparison of mixing efficiencies of solids in a cylindrical vessel subject to a range of motions. *Powder Technology*, 217, 540 - 547.